STUDIES ON THERMAL SHOCK AND CRACK HEALING BEHAVIOR FOR POLYCRYSTALLINE YTTRIUM IRON GARNET (YIG)

By

HSIEN-MING (JACK) CHOU

A DISSERTATION

Submitted to
MICHIGAN STATE UNIVERSITY
in Partial Fulfillment of the Requirements
for the Degree of

DOCTOR OF PHILOSOPHY

in

Materials Science

Department of Metallurgy, Mechanics and Materials Science
1988

ABSTRACT

STUDIES OF THERMAL SHOCK AND CRACK HEALING OF POLYCRYSTALLINE YTTRIUM IRON GARNET (YIG)

By

Hsien-Ming (Jack) Chou

Thermal shock damage can occur for ceramic materials which are subjected to high heat flux. The thermal shock induced thermo-mechanical stress may cause microcracking or mechanical failure, which may significantly limit the usefulness of ceramic materials.

Thermal shock damage is typically characterized by "single quench-fracture tests", in which a specimen is quenched a single time into a water bath then fractured. But technical ceramics, such as engine components, solar collectors, ceramic seals and ceramic computer memory substrates must tolerate repeated thermal shocks under in-service conditions. Therefore, the understanding of damage induced by multiple thermal shocks is very important. In this study, thermal shock damage caused by repeated thermal shock in polycrystalline yttrium iron garnet (YIG) microwave substrate was monitored by nondestructive techniques, such as the elasticity measurements and the internal friction measurements.

The internal friction of the air quenched yttrium iron garnet specimens significantly increased due to thermal fatigue. The Young's modulus, on the other hand, decreased by a few percent relative to the undamaged specimens. The change of internal friction was much more

sensitive than the change of Young's modulus when the specimen subjected to repeated thermal shock. Thus, the change of internal friction could be a powerful technique to assess the crack damage. The temperature-time profile in a thermal shock process was measured by a thin film thermocouple to aid the understanding of the heat transfer and stress distribution of the thermally shocked specimen.

Secondly, for a relatively low level of thermal shock-induced damage, an unexpected time-dependent recovery in elastic modulus at room temperature was observed, and successfully characterized by a nonhomogeneous, linear, first order differential equation. A hydrate formed on the crack surfaces was assumed to assist the crack healing (closure). In order to investigate the mechanism of the modulus recovery, various quenching media such as oil and liquid nitrogen were used in thermal shock process. The time-dependent Young' modulus recovery for a water quenched specimen was also measured in a vacuum environment.

To the Lord my Heavenly Father

who endows the heart with wisdom

and

gives understanding to the mind.

ACKNOWLEDGEMENTS

I would like to express my sincere appreciation to my advisor, Professor Eldon D. Case for his continuous guidance and support throughout this work. As the first graduate student of Dr. Case, I enjoyed the time closely working with him and the opportunity to gain some extra experiences in establishing a new laboratory. I also like to thank my colleagues, C. C. Chiu, W. J. Lee, N. Dahotre, S. White and C. S. Lee for their generous advise and helpful discussions about this work. Grateful thanks are extended to the other members of the guidance committee, Professors Harry Eick, Kalinath Mukherjee, Frederick T. Fink.

Special thanks are given to T. Negas and L. Dominques of Trans-Tech, Inc., Adamstown, MD, for supplying the polycrystalline YIG microwave substrate material, from which we subsequently machined the specimens for this study.

The support of the teaching assistantship awarded by the Department of Metallurgy, Mechanics and Materials Science and the research assistantship supported jointly by Michigan State University through an All-University Research Initiation Grant and the National Science Foundation under grant MSM-8706915 are grateful acknowledged.

A final note of appreciation should go to my wife Miao-Sze (Olivia) for her stimulated discussions to this work and the assistance in most of the typing work. Without her endurance and continuous encouragement to me, the accomplishment of my graduate studies may not be possible.

TABLE OF CONTENTS

LIST OF FIGURES

LIST OF TABLES

1. INTRODUCTION

Rapid change in ambient temperature (thermal shock) induces thermomechanical stress in a material [1]. For brittle ceramic components, these stresses can result in microcracking or mechanical failure [2-7].

1.1 Applications of Ceramics That Involved Thermal Shock

Ceramics, because of their excellent chemical inertness, dielectric and insulating properties, and superior high temperature mechanical behavior are widely used in advanced technology, serving as high temperature refractories and electronic materials, as well as engine components. However, most of these applications involve high heat flux during operational conditions. Thermal shocks, though in different levels, always happen. Therefore, the endurance to thermal shock damage is important in many industrial applications of technical ceramics. For example, alumina substrates used in large-scale computer memories suffer thermal shock due to cyclic Joule heating by imposed circuit elements [8]. Ceramic coatings on metal heat engine components need to overcome the residual stresses arising during the application of the coating on the substrate and the repeated operational thermal stress [9]. Glass-to-metal hermetic seals in microelectronics packaging can experience temperature transients either during the manufacture of the component or in-service due to

Joule heating [10 and 11]. Cermet-to-metal seals developed for reflood instrument sensors, which introduce cooling water to a simulated loss-of-coolant accident in a pressurized water nuclear core, must endure repeated loading to high temperature steam and water, and severe thermal shock transient estimated maximum up to 300°C/sec [12]. In general, the susceptibility of ceramics to thermal stress and thermal shock failure is a major factor limiting their usefulness.

1.2 Thermal Shock Characterization

The study of the characterization of thermal shock in ceramic materials has been very active for the last two decades. Most of the efforts involved can be summarized into two areas:

1. Factors affecting thermal shock resistance,
2. Thermal shock damage evaluation.

These intensive studies help ceramists/materials scientists to understand thermal shock and guide the development of better thermal shock resistant materials to reach a high performance requirement. Both areas are reviewed in this study.

1.2.1 Thermal Shock Damage Parameters R, R′, R′′′, and R′′′′

Factors affecting the thermal stress resistance of ceramic materials are one of the important features in thermal shock testing. Kingery [13] proposed that thermal shock resistance depends on

five different material properties: strength (S_t), Young's modulus (E), thermal conductivity (k), thermal expansion coefficient (α), and Poisson's ratio (ν). Kingery defined the thermal shock resistance parameters R and R' [13], where

$$R = S_t(1-\nu)/\alpha E \qquad \text{or} \qquad (1a)$$

$$R' = kS_t(1-\nu)/\alpha E \qquad (1b)$$

In order to have high R and R', materials should have high values of S_t and k, and low values of E, α, and ν. Materials with high thermal shock resistance parameters, R and R', minimize the initiation of cracks during thermal shock. The application of equations (1a) and (1b) depend on the heat-flow condition and the specimen geometry. For a rapid quench, for example, the specimen is cooled so fast that the surface temperature reaches its final value before the average temperature of the specimen changes, the fracture ΔT_f is defined [14]

$$\Delta T_f = S_t\ (1-\nu)/(E\alpha)\ S = RS \qquad (2a)$$

where S is a shape factor. Equation (2a) will be a good approximation for the thick specimens. On the other hand, when the cooling rate is not so high, Kingery defined fracture ΔT_f as [14]

$$\Delta T_f = kS_t (1 - \nu)/E\alpha \cdot 1/(0.3\, r_m h) = R'S \quad (2b)$$

where r_m = the half-thickness of the specimen,

h = Surface-heat-transfer coefficient.

Here the thermal conductivity is included, and the size of the specimen also affects ΔT_f. This situation is somewhat more complicated and a more careful analysis of the cooling conditions is needed [14].

On the other hand, the "thermal shock damage resistance" parameters R''' and R'''' defined as [14 and 15]

$$R''' = E/[S_t^2(1-\nu)] \quad \text{or} \quad (3a)$$

$$R'''' = Er_f/[S_t^2(1-\nu)] \quad (3b)$$

where, r_f = the fracture surface energy.

R''' = the minimum available elastic strain energy at fracture,

R''''= the minimum crack propagation after the initiation of cracks.

To avoid crack propagation which can cause macrocracks and failure in ceramic components , high R''' and R'''' are necessary, which means high values of E and r_f and low values of S_t and ν are needed. A comparison of equations (1a) and (3b) shows that the two resistance parameters are affected by the material properties in an opposite manner. It is therefore impossible to provide a material with both

high values of R and R''''. The choice of R and R'''' to characterize thermal shock effect depends on whether crack initiation or crack propagation is the dominant problem for a giving in-service condition.

1.2.2 Survey of Material Properties Affecting Thermal Shock

Buessem [16] pointed out that the thermal shock resistivity is not an instrinsic material property. The five material properties, S_t, E, ν, α, and k are all temperature dependent. Buessem commented [16] that even when the thermal shock data are available and correct, they are often incomplete and are difficult to use under conditions different from the thermal shock test. In order to obtain reliable thermal shock parameters the temperature dependence of the five instrinsic material properties should be determined by separate standard tests.

These five properties can depend on geometry, initial flaws, and specimen history. For ceramic materials, the strength measured reflects only the maximum flaw existing in the specimen. The larger the specimen the more likely it is that it includes a large flaw which will lower the strength. The strength and Young's modulus are also specimen history dependent. Surface damage which resulted from manufacturing, handling, and improper storage might significantly reduce the strength. The same kind of surface damage might also reduce the Young's modulus, though not as significantly.

Furthermore, the effect of grain size on thermal shock resistance was studied empirically [4 and 17]. Typically, residual strength of

thermally shocked materials decreases as ΔT increases. Studies of polycrystalline Al_2O_3 [4] and B_4C [17] (figures 1 and 2) have shown that the larger grain sizes inhibit catastrophic strength degradation. For example, the retained strength of the thermally shocked alumina specimens remains constant at furnace temperatures up to 200 degrees Celsius, and then decreases due to crack propagation. The difference of temperature at which the initial crack propagation (initial thermal fracture) occurs is defined as the critical quenching temperature ΔT_c. For alumina and boron carbide quenched in water, the critical temperature is approximately 200 degrees Celsius. After the initial thermal fracture, the retained strength of the alumina specimens with smaller grain size (i.e. 10 microns) drops instantaneously as the quenching temperature increases (figure 1a). The retained strength of the alumina specimens with larger grain size (i.e. 85 microns), on the other hand, decreases gradually after the initial thermal fracture (figure 1b). The initial strength of the alumina with an average grain size of 10 microns is larger by a factor of two than the alumina with the average grain size of 85 microns. This difference can be explained by the Hall-Petch relation which states that the strength of a polycrystalline material is proportional to the inverse of the square root of the average grain size [18 and 19]. According to the strength data of the pre-shocked alumina specimens that Gupta [4] gave for the 10 microns, 34 microns, 40 microns and 85 microns specimens, the author plotted the relationship between the strength and the average grain size (figure 3). This figure shows that the Hall-Petch relation fit relatively well for Gupta's strength-grain size

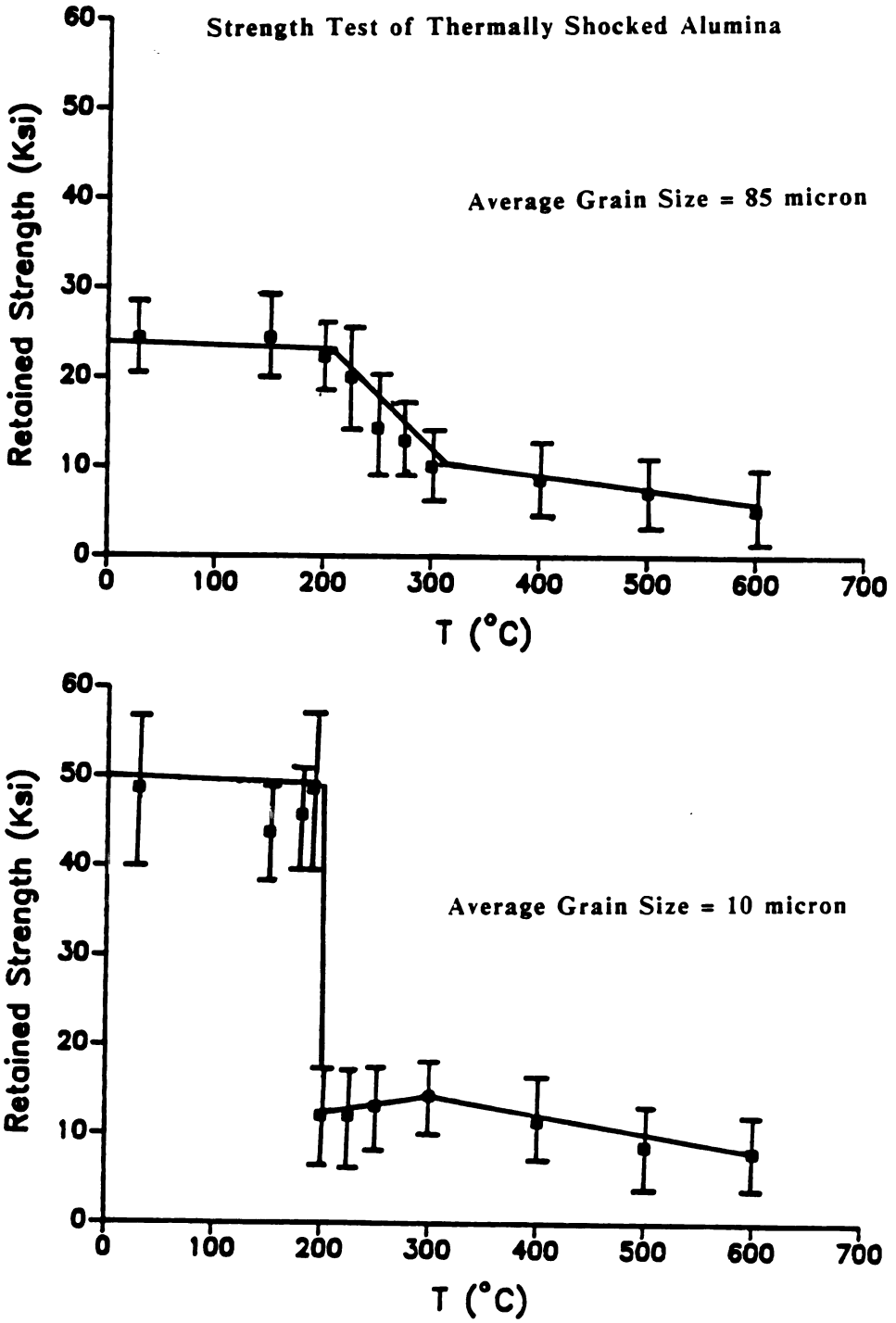

Figure 1. Room-temperature strength of thermally shocked polycrystalline Al_2O_3 (after Gupta, 1972, [4])

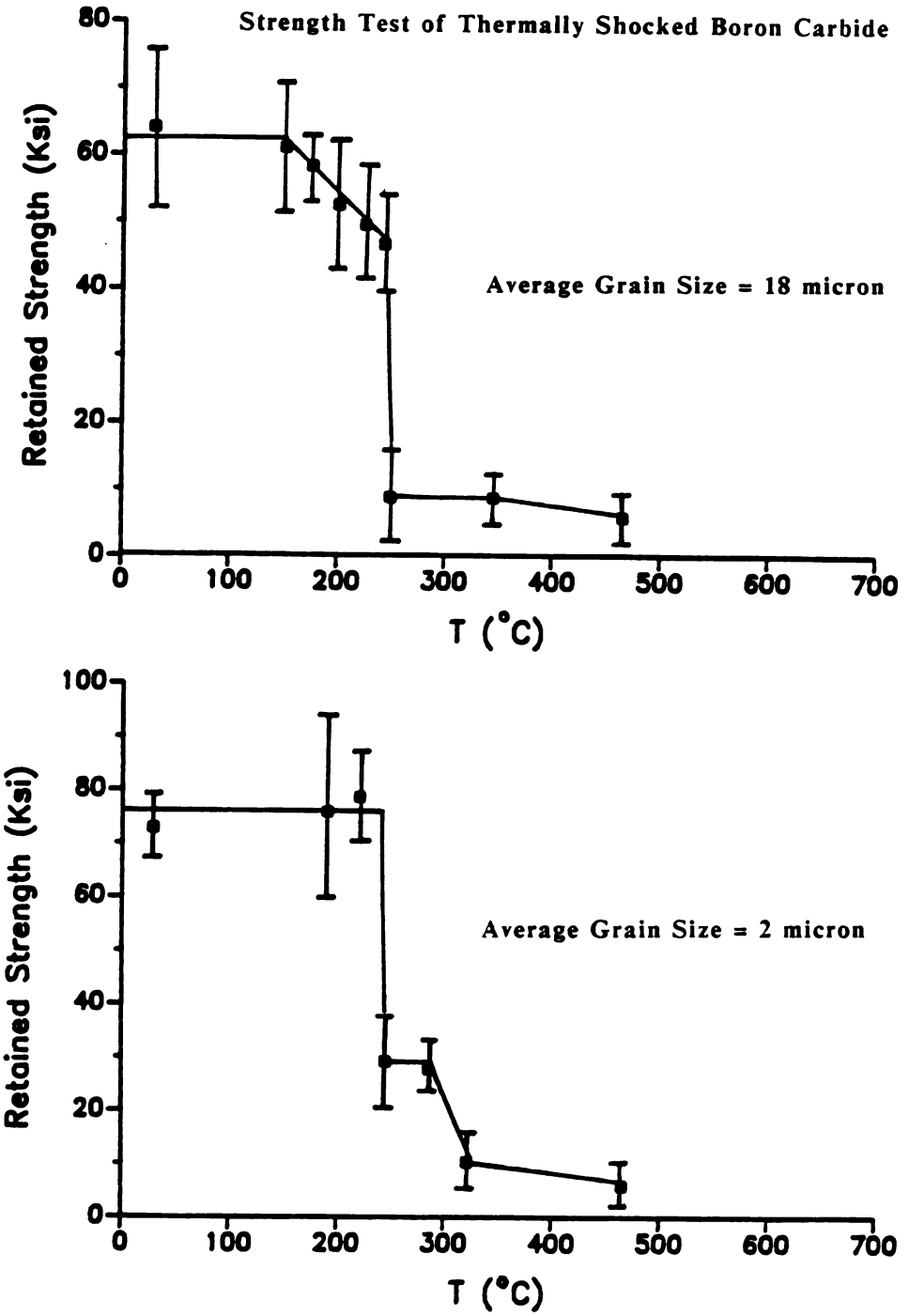

Figure 2. Room-temperature strength of thermally shocked polycrystalline B_4C (after Seaton, 1974, [17])

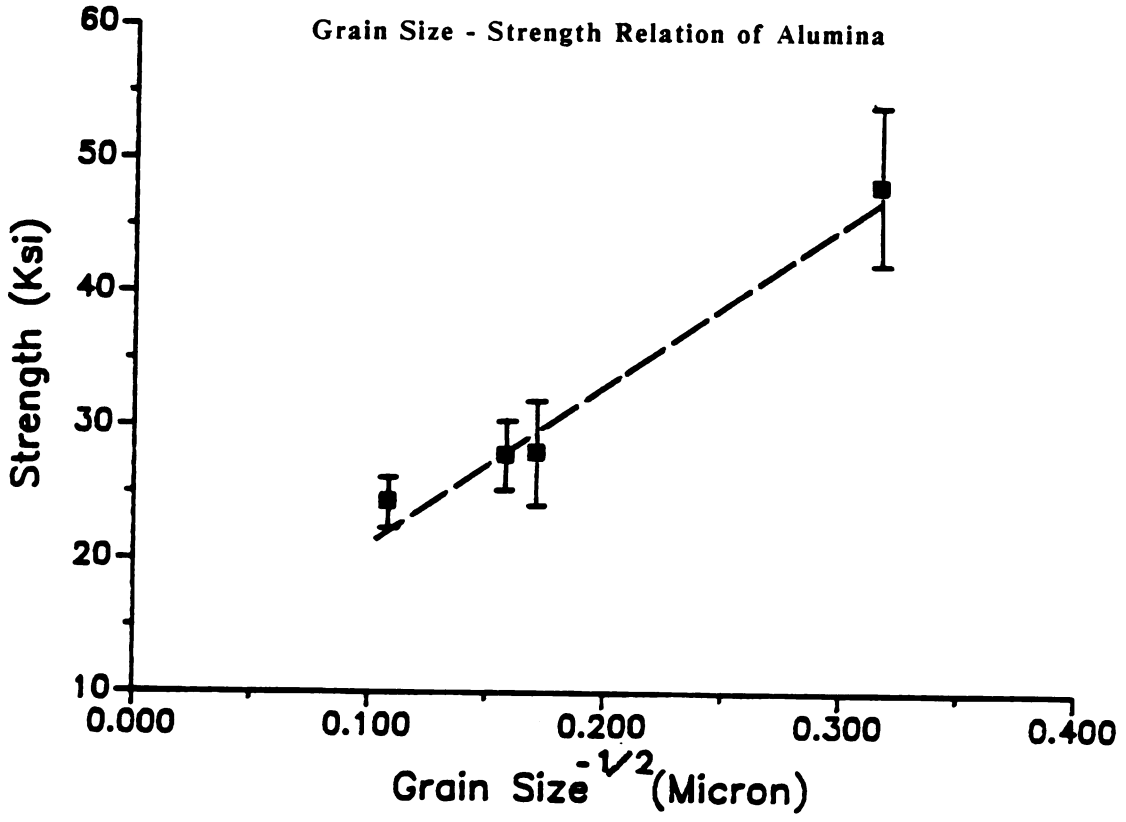

Figure 3. The average grain size-strength data of alumina [4]. The dashed line is fitted the Hall-Petch relationship.

experimental result. The regression line based on the four data point yields $\sigma_{th} = A + B/(G.S)^{1/2}$, where parameter A = 9.58 ksi and parameter B = 119.22 ksi•(micron)$^{1/2}$. The correlation coefficient of the regression is 0.98.

Polycrystalline boron carbide is another example that shows the grain-size effect on strength degradation of thermally shocked specimen. The retained strength of the 2 microns specimens instantaneously decreased as the quench temperature increased to 250 degrees Celsius (figure 2a). Increasing the grain size from 2 microns to 16 microns increased the resistance of B_4C [17] to the kinetic propagation of thermally induced cracks [17]. This increase in resistance to kinetic crack propagation resulted in the quasi-static behavior observed following the initial thermal fracture (figure 2b).

Addition of a second phase to the matrix [17 and 20] can improve thermal shock resistance (figures 4 and 5). Due to thermal expansion anisotropy*, microcracks formed in boron nitride as the polycrystalline alumina-based specimens were cooled from the sintering temperature. These thermal expansion anisotropy induced microcracks have been observed to limit crack growth resulting from thermal shock [17]. An addition of a boron nitride second phase thus may improve the thermal shock resistance of alumina materials. Addition of zirconia to β-alumina shows an increase in the critical quenching temperature, ΔT_c, from 180 degrees Celsius to 300 degrees Celsius, and the retained strength is also improved (figure 5).

---

* The expansion coefficients of each crystal lattice orientation are different enough to cause microcracking in a thermal treatment.

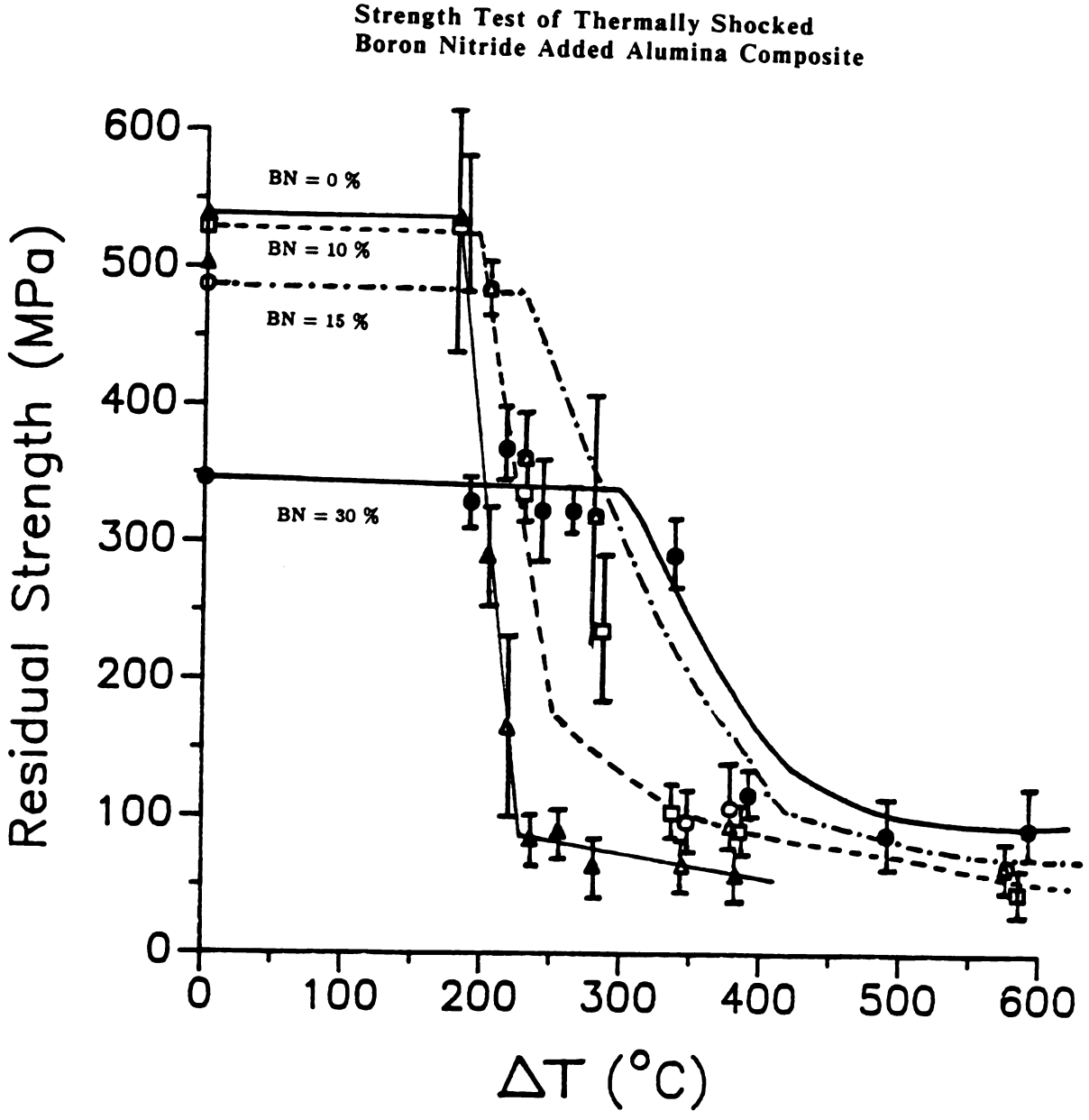

Figure 4. The thermal shock resistance of boron nitride added alumina-base ceramic composite (after Goeuriot-Launay, 1986, [20]). BN = (▲), 0 %, (△) 5 %, (□) 10 %, (○) 15 %, (●) 30 %.

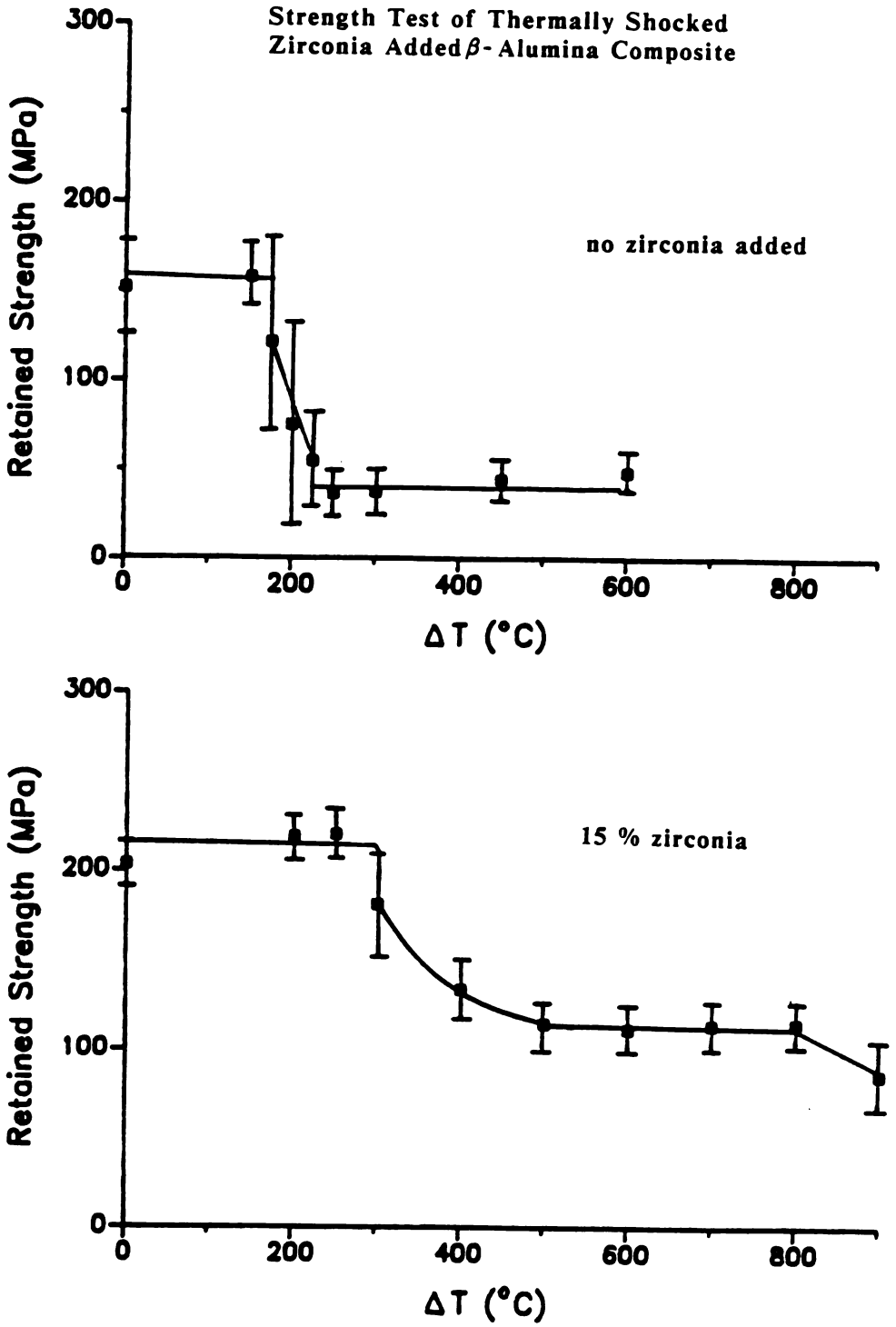

Figure 5. Thermal shock of β - alumina with zirconia addition (after Evans et al., 1984 [24]).

1.3 Evaluation of Thermal Shock Damage

The second important feature of thermal shock testing is the evaluation of thermal shock induced damage. The experimental evaluation techniques used to monitor and quantify specimen degradation caused by thermal shock damage include: 1) modulus of rupture σ, 2) dynamic modulus of elasticity E, 3) ultrasonic velocity V_1, 4) fracture toughness K_{IC}, 5) fracture surface energy γ, 6) internal friction Q^{-1}, 7) weight loss.

The evaluation techniques listed above can be determined via a number of destructive and non-destructive methods. The destructive tests require comparison of the before- and after- shock properties by using the equivalent sized specimens, whereas the nondestructive tests may use a single specimen to measure the property changes before, during and after shock. An example of a correlation between the results of nondestructive and destructive testing on a given material is provided by the relationship between the modulus of rupture (MOR) measurements and the nondestructive modulus of elasticity (MOE) measurements in a fire clay refractory brick [21] (see figure 6). Establishing such a relationship allows the prediction of the strength of fire clay refractory specimens by a non-destructive test. However, refractory bricks tend to be relatively porous, and such pores act as crack nuclei when the bricks are stressed. The elasticity modulus-strength relationship observed for the refractory bricks would not be observed for dense, monolithic ceramics where, for example, changes in

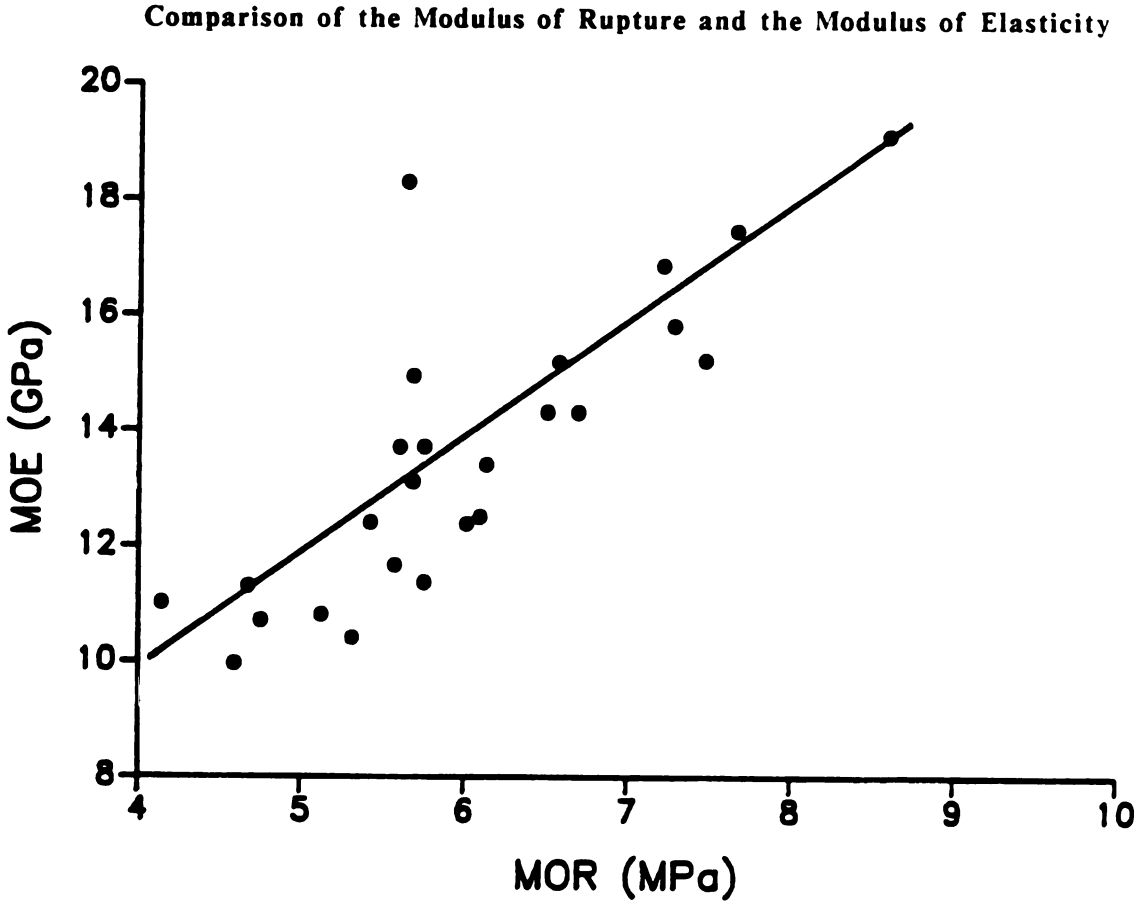

Figure 6. Relation between the modulus of rupture and the modulus of elasticity for a high duty fireclay brick (after Semler et al., 1980, [21]).

surface flaw length dominate the measured fracture strength. Therefore, the elastic modulus-strength relationship observed in dense alumina [22] and silicon carbide [23] subjected to thermal shock damage was not the same as the elastic modulus strength relationship observed for the refractory bricks. Further explanation will be given under the Results and Discussion section 3.2.

Destructive assessment of thermal shock damage typically included [2-7, 20 and 24-26]:

1. Measurement of residual strength of the thermal shock damaged specimen. Usually, the residual strength was determined by a four-point bend test performed at room temperature, in air, on the thermal shocked specimen. A typical plot of the residual strength versus temperature difference is given in figure 7.

2. The specimen was usually subjected to a single quench prior to damage assessment.

For nondestructive tests, thermal shock damage has been evaluated by weight loss [27 and 28], decrease in elastic moduli [22, 23, 29 and 30], and increase of internal friction [22 and 23] after a specified treatment or cyclic thermal shock treatments. The severity of treatment (ΔT_{max}) necessary to significantly reduce the weight and the elasticity, or increase the internal friction also was evaluated as the thermal shock resistant parameter. For high density sintered ceramics, the measurement of weight loss after thermal shock treatment is not practical and is generally not accurate [31]. As an alternative (or as a supplement) to residual strength testing, several authors [22, 23, 29 and 30] assessed thermal shock by measuring

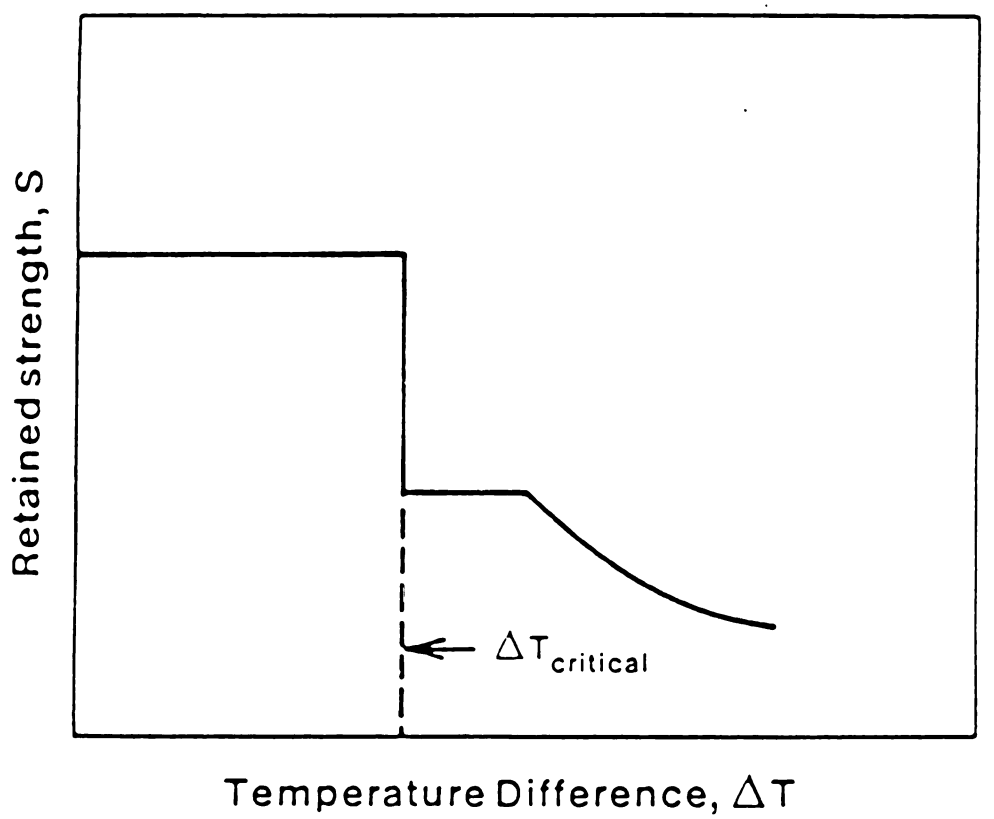

Figure 7. Schematic of residual strength versus temperature difference for a thermally shocked brittle material. (See, for example, references [2] and [4]).

elastic moduli and internal friction using nondestructive techniques.

1.3.1 Comparison of Destructive and Nondestructive Techniques for Thermal Shock Damage Evaluation

The evaluation of thermal shock damage based only on fracture testing is somewhat problematic as brittle fracture is a stochastic process which depends on the details of the length and spatial distributions of maximal flaws in the test specimen [23], as well as the details of the stress distribution. The scatter in strength data can be considerable for brittle specimens. For examples, given a mean fracture strength S, scatter of $\geq 0.1S$ is not uncommon [2,4,17], even if five, ten or even more specimens are tested at a fixed quench temperature. The probabilistic nature of brittle fracture thus can impart considerable uncertainty to a given experimental strength value.

In addition to the scatter in the data, there are statistical questions inherent in the interpretation of strength data. For residual strength testing, as for any destructive test, one must account for statistical fluctuations in the measured property (strength) among the many individual specimens measured. Ceramics can exhibit significant specimen to specimen variations in strength for specimens taken from a single billet, and even more significant variations between different batches of a given material.

Internal friction also has been used to characterize thermal shock damage for single quench silicon carbide and alumina specimens

[22, 23 and 30]. The sensitivity of the internal friction increase is relatively higher than that of the decrement of Young's modulus. However, the strength losses do not necessarily correlate with the change observed in damping and modulus [23]. The changes of Young's modulus and internal friction reflect the total damage over the entire specimen, whereas the strength changes result from the "maximum flaws."

1.3.2 Multiple Thermal Shock Cycles for a Given Specimen

One of the advantages of a "single quench-fracture test" protocol is that it directly gives a key physical property (fracture strength) as a function of quench temperature. However, instead of a single quench, many applications involve repeated thermal loadings (i.e. computer circuit substrates [8], or turbine components). When repeated or cyclic thermal loads are applied to a specimen, the evolution of damage as a function of the cycle number becomes an important aspect of the problem. D. Lewis III [32] and several authors [33-36] studied the effects of repeated thermal shocks on strength of various ceramics and ceramic composites. The progressive degradation of the ceramics under repeated thermal stress, sometimes referred to as thermal fatigue, is typically characterized in terms of the residual fracture strength [32-37].

Hence, not only the testing technique itself but also the testing methodology determine the reliability of the thermal shock evaluation. Regardless of the testing technique used (fracture test or elasticity

measurement), the ranking of thermal shock resistance in a group of materials depends on whether it was evaluated after the first thermal shock or after several thermal shock cycles [21 and 30]. The author would like to emphasize that the "single quench-fracture test" (or elasticity measurement) for thermal shock damage evaluation may be misleading if the ceramic materials experience repeated thermal shock in actual application.

1.3.3 Various Quenching Media Used for Thermal Shock

Water is the quenching media usually used in thermal shock studies. Typically, the quench is performed into a water bath held at room temperature or 100 degrees Celsius. Very few researchers use other quenching media, such as air [36], oil [38], liquid metals [38], and liquid nitrogen [39]. These quenching media offer a wide range of available thermal transfer coefficients as well as the temperatures which enable the researchers to control the desired shock severity. However, some quenching media may also chemically react with the quenching materials. Since the heat transfer coefficients of liquids are viscosity dependent, a constant liquid temperature is important. In order to fully characterize the thermal shock conditions, the quenching media and the rate of temperature change versus time in a thermal shock process need to be determined carefully.

1.4 Overview of the Present Thermal Shock Damage Study

This study utilizes elasticity and internal friction measurements to characterize crack damage induced by the repeated thermal shock of a polycrystalline ceramic material. In this study, specimens were quenched by four different media: water, oil, static air and forced air. The plots of the temperature on the specimen surface versus time during a typical thermal shock in different quenching media were obtained. The materials used in this study were Yttrium Iron Garnet (YIG) and Gd-doped YIG microwave substrates.

For a relatively low level of shock-induced damage, an unexpected time-dependent recovery in elastic modulus at room temperature was observed and successfully characterized by a nonhomogeneous, linear, first order differential equation (see Appendix A).

2: EXPERIMENTAL PROCEDURE

2.1 Materials Selection and Specimen Preparation

Using a low speed diamond saw, the elastic modulus specimens were cut from commercial polycrystalline yttrium iron garnet (YIG) microwave substrate material (Trans-Tech Corporation, Adamstown, MD). The as-received specimens were initially in the form of plates of dimension 5.08cm × 5.08cm × 0.1cm. The resulting as-cut modulus specimens were prismatic bars approximately 5.08cm × 0.9cm × 0.1cm.

The theoretical density of yttrium iron garnet, as determined by x-ray analysis, is 5.17 gm/cm^3 [40]. The mass density of the polycrystalline YIG specimens used in this study, determined from the specimen dimensions and mass, ranged from 5.01 g/cm^3 to 5.09 g/cm^3, corresponding to a volume fraction porosity of approximately 0.004 to 0.024 (detail in Appendix B).

Specimens having as-received surfaces were etched for 30 minutes in a 37 percent concentrated HCl acid bath at a temperature of 84 degrees Celsius. Using a correction factor of 1.5 [41], an average grain size of 13.6 microns was determined by the linear intercept technique on optical micrographs taken from as-etched specimen surfaces.

For the modulus measurements, the larger, uncut specimen surfaces (the 5.08 cm × 0.9 cm faces of the specimen) were left in the as-received condition. The edges of selected specimens were slightly

beveled using 1000 grit SiC polishing powder, to an approximate radius of 0.6 ± 0.2 mm. In order to measure the radius of the beveled curve, the curve of the bevel was assumed to be a part of a circle. The radius lines were constructed normal to the arc and the intersection of the normal lines was the center of the circle. Five normal lines were drawn on the micrograph which was taken from the beveled edge of the YIG specimen. The center of the circle was found by drawing the normal lines to get the intersection. The distance between the center and the beveled curve was taken as the curve radius.

In this study, the specimen geometry was that of prismatic bars. The sonic resonance method also can accommodate rod-shaped or disc-shaped specimen geometries.

2.2 Thermal Shock Treatment and Elastic Modulus Measurements

The measurement of elasticity was done by the sonic resonance technique [42-49]. A schematic of the sonic resonance apparatus is given in figure 8. The specimens were suspended by cotton threads. One thread was attached to a driving transducer which induces a mechanical vibration in the thread and consequently in the specimen. The second thread was attached to a pick-up transducer, which in turn was connected to an electronic circuit that allows one to determine the maximum amplitude (mechanical resonance) for the specimen as a function of frequency.

The flexural and torsional resonance frequencies of prismatic specimens were used to calculate the Young's and shear moduli,

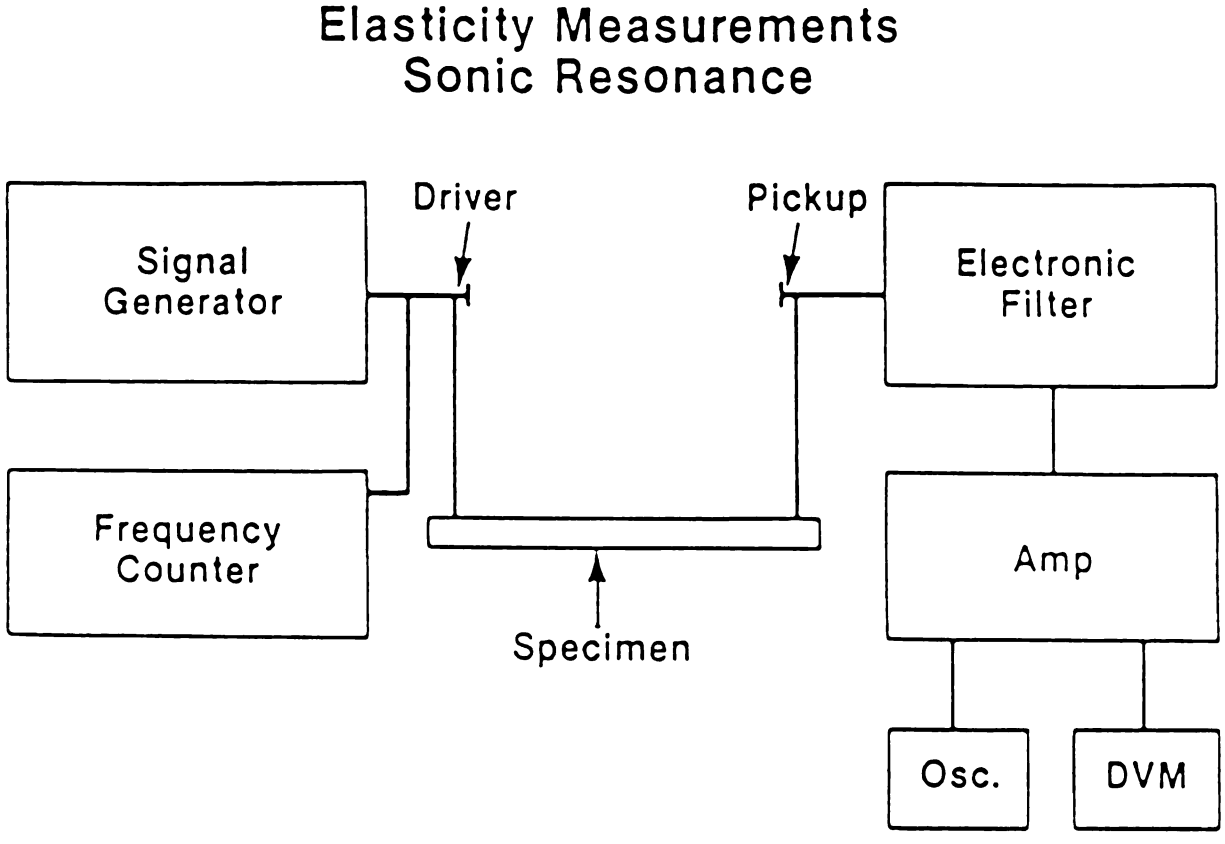

Figure 8. Sonic resonance apparatus diagram.

according to a theory developed by Pickett [44] and Hasselman [45]. The relationship between crack damage and elastic moduli will be discussed further in the following section of this study.

Small changes in the position of the support strings can result in small changes in the calculated elastic moduli. For example, the flexural resonance frequency of the particular YIG specimens used in this study was about 2000 Hz, while small changes in the position, such as 0.2 mm suspension position change, of the support threads can change the resonance frequency by as much as 0.5 Hz. This maximum uncertainty of approximately 2.5 parts in 10^4 in the flexural resonance frequency results in an uncertainty of 5 parts in 10^4 for the calculated Young's modulus (see appendix C for detail.) The calculated Young's modulus is in turn a function of a geometric shape factor and the square of the specimen's flexural resonance frequency. In order to eliminate uncertainties in the elasticity measurements due to possible shifts in the position of the suspension threads, the threads were attached to the specimens via small amounts of high temperature adhesive (M-bond 610, Measurements Group, Inc. Raleigh, NC). Small amounts of glue, about 10^{-3} ml in volume, were placed by a needle at the edges of the specimen. This glue can tolerate temperatures as high as 260 degrees Celsius. Thus, for the water-quench thermal shock treatments, where the furnace temperature was maintained below 260 degrees Celsius, the suspension threads were retained in position by the glue. However, glue was not applied to every specimen. Specimens thermally shocked by quenching in air from 300 degrees Celsius were not glued because the threads were moved to

measure internal friction at several different positions. Also, the temperature used for air quench was so high that the glue and threads would have been oxidized.

The sonic resonance system was calibrated using a standard resonance bar obtained from the National Bureau of Standards (Standard Reference Material 718, polycrystalline alumina resonance bar, NBS serial number C8). The resonant frequencies published by NBS for standard bar C8, measured at 25 degrees Celsius in vacuum were 2002.42 Hz and 11075.3 Hz for the flexural and torsional frequencies, respectively [50]. To convert to resonant frequencies in air, one should subtract 0.99 Hz from the resonant flexural frequency and 2.25 Hz from the torsional frequency, giving "in-air" resonant frequencies of 2001.43 Hz and 11073.1 Hz for the flexural and torsional frequencies, respectively [50]. The resonance frequencies of the alumina standard resonance bar measured in air at 27 degrees Celsius by the sonic resonance system were 2001.40 ± 0.30 HZ for the flexural frequency, and 11073.0 ± 0.5 HZ for the torsional frequency. Thus, the resonant frequencies published by NBS for standard bar C8 confirmed the accuracy of the sonic resonance measurements in this study.

A "working reference" bar of unshocked YIG, of the same dimensions as the thermal shock specimens, was used to check the calibration of the apparatus on a routine basis. Such calibration is advisable since a transducer might possibly be damaged by a slight mechanical bending during the repeated loading and unloading of the specimens and threads. The transducers were replaced whenever the

flexural frequency measured by the YIG reference bar was not within 2270 ± 0.5 HZ, which is the reference frequency measured for the YIG working reference bar. According to the author's experimental experiences, the transducers were replaced every 4 to 6 weeks, or after 200 to 300 measurements.

In order to determine the elastic moduli of specimens prior to thermal shock damage, the flexural and torsional frequencies of the unshocked specimens were measured in air at room temperature. The specimens were subsequently thermally shocked by heating in air in an electric resistance furnace and then quenched in a room-temperature water bath. The water bath consisted of about 4000 ml of water contained in a styrofoam hemispherical cup 30 cm in diameter. The water bath temperature was measured by a mercury-in-glass thermometer (NO. 14-985E, Fisher Scientific) with minimum and maximum temperature markings of −10 to 110 degrees Celsius, respectively, and 1 degree Celsius interval between markings. An electronic timer (Model CO-803, Optimec Co., Taiwan) with 6 digits in readout (hour, minute, second) and accurate to 1 second was used to monitor the elapsed time, beginning from the moment the specimen entered the quenching bath and ending when the final elasticity measurements were made.

Typically the series of modulus-time measurements on an individual specimen continued for 24 hours following a given thermal shock. All specimens were removed from the water bath following a total immersion time of 30 ± 3 seconds. Specimens were then blotted dry using paper towel and attached to the modulus apparatus (via the suspension threads). The subsequent modulus measurements were

performed at room temperature in air.

The typical time interval between the removal of the specimen from the water bath and the commencement of the modulus measurements was two to three minutes as measured by the electronic timer. Flexural and torsional resonant frequencies of the specimens were recorded at time intervals of from 4 to 10 minutes for the first hour, from 20 to 40 minutes for the next 3 hours, and from about 60 to 90 minutes for the subsequent several hours.

2.3 Cyclic Thermal Shock in Air

The thermal cycling in air was performed in a furnace designed and assembled at Michigan State University. The electrical resistance furnace was composed of CM heating elements (KR 3-4, CM Co.) and insulated by high temperature alumina insulating cylinder (Type ALC, Zircar, Florida, NY) and refractory blanket (Kaowool 2600, 6 lb density, Babcock & Wilcox, Augusta, GA). Digital temperature controller-model and vendor furnace was cylindrical, 30.5 cm in length, with a 7.6 cm diameter muffle tube along the cylinder axis of the furnace, mounted so that the muffle was horizontal. The specimen was placed horizontally on a fused silica boat which was designed to minimize the contact area between the specimen edges and the inside wall of the silica boat. The inside wall of the silica boat is a hemicycle. The contact between the rectangular shaped specimen and the tube wall is only along the two bottom longitudinal edges of the specimen that are supported by the tube wall (figure 9A). The boat

Cyclic Thermal Shock Apparatus

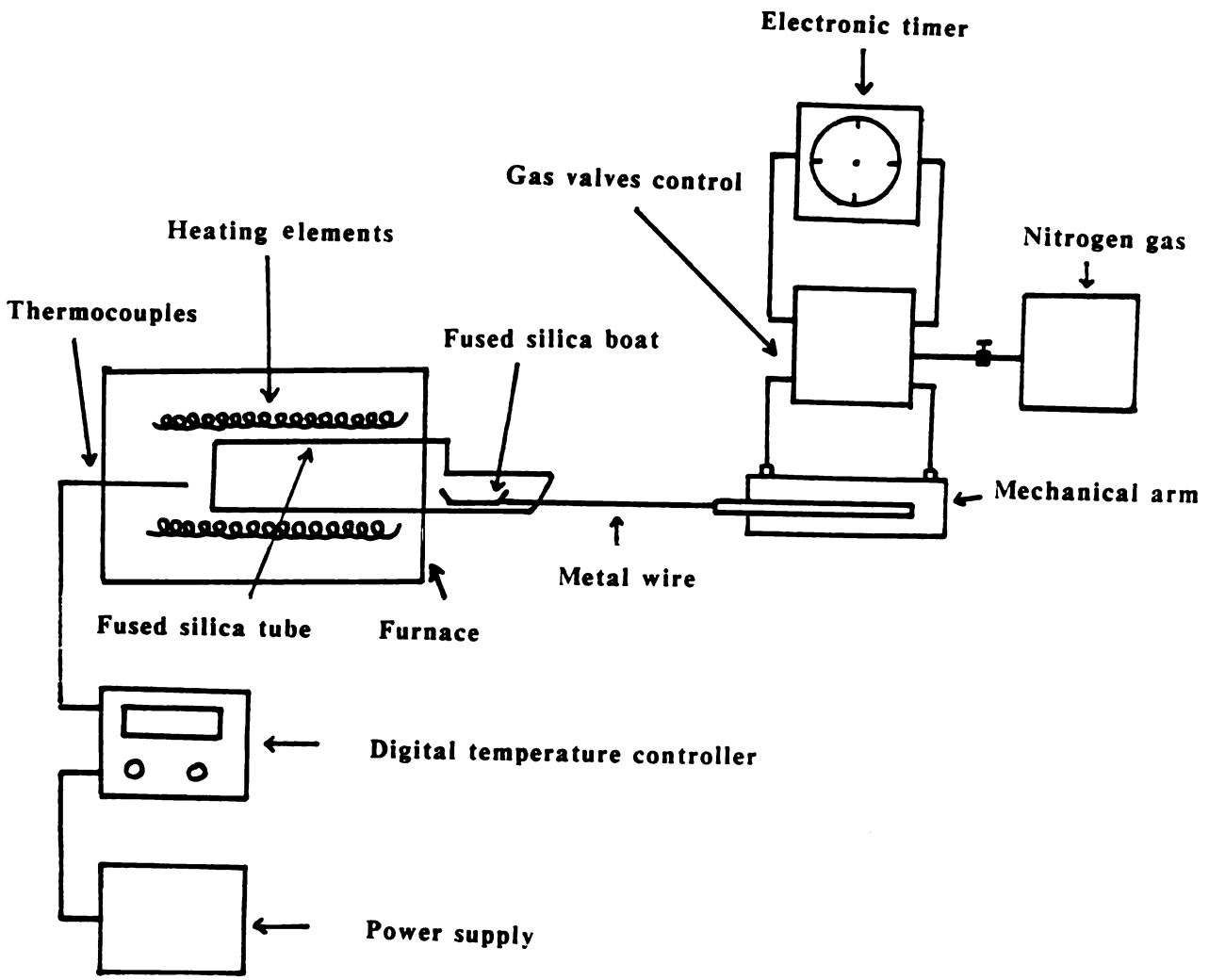

Figure 9A. Diagram of cyclic thermal shock apparatus.

material takes advantage of silica's excellent thermal shock resistance which may help to avoid thermal shock fracture during cyclic thermal shock treatment of the YIG specimens (figure 9B). The major route for heat transfer during cooling is presumably between the forced (or static) air and the ceramic sample. Heat transfer between the fused silica boat and test specimen probably can be ignored.

A timer-controlled mechanical-pressure arm was used to transport the YIG specimen in a typical thermal shock procedure (figure 9A). The mechanical arm (Type C, 7/8 × 10, Allenair Corp., Mineola, NY) was driven by nitrogen gas regulated at 15-20 psi. The pushing and drawing time for the total length of the mechanical arm was adjusted to about 3.0 and 1.0 seconds, respectively.

A gas valve control (Model E11C-PM-111AA-152, MAC Co., Wixom, MI) attached to a timer (Model H3BA, Omron Tateisi Co., Japan) released and introduced adequate pressure to push and draw the mechanical arm in a preselected time interval. The timer was set to 12.5 minutes for each half cycle, which means the specimen stayed in the furnace for 12.5 minutes and stayed outside the furnace to cool for another 12.5 minutes. The 12.5 minutes interval allowed the YIG specimens to reach thermal equilibrium. The fused silica boat was connected to the stainless steel arm by a thin corrosion resistant Cr based alloy metallic rod 30 cm long and 0.15 cm in diameter.

In order to heat the specimen uniformly in the furnace hot zone, the mechanical arm was arranged so that the specimen was located at the midpoint of the furnace hot zone during heating. The specimen and silica boat were placed in a 4.0 cm diameter silica tube, 30 cm in

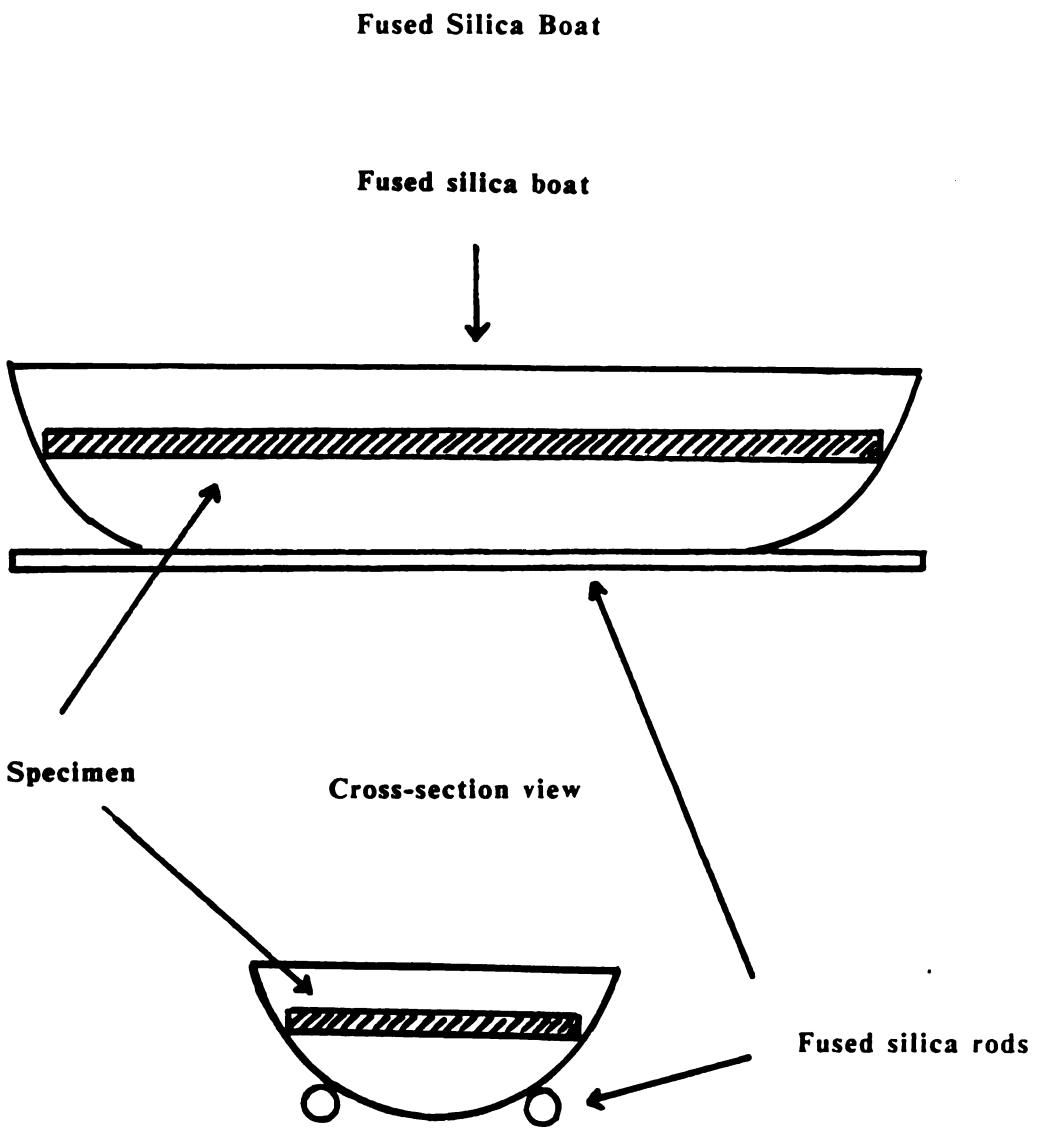

Figure 9B. Fused silica boat used in thermal shock measurement.

length. The silica boat and the tube assembly were centered in the furnace muffle. The specimen thus moved within the silica tube in order to allow the smooth movement of the boat. The silica tube also enhanced the cleanliness of the furnace environment.

A 15.0 cm diameter compact fan (Model Dayton 4C800, Grainger Inc., Chicago, IL) with a capacity of 100 CFM (Cubic Feet volume air per Minute) was placed 15 cm above the fused silica boat to provide the forced cooling air. The elastic modulus and internal friction were measured for a preselected number of thermal shock cycles.

2.4 Temperature Versus Time Measurement

The specimen's surface temperature was measured by attaching a thin-film "Cement-on" K type thermocouple 1.905 × 0.940 × 0.013 cm in dimension (MODEL CO-1K, Omega Co., Stamford, CT). This thermocouple can withstand temperatures to 370 degrees Celsius. The response time of this thin-film thermocouple when cemented in place is 10 to 20 milliseconds.

The thermocouple was connected to an ice-point reference junction to provide a zero. The cement (high temperature cement, Omega Co., Stamford, CT) was applied by a small brush provided with the cement kit to a cleaned YIG specimen surface to form a uniform thin layer estimated thickness about 0.2 mm. Immediately after the cement was applied to the specimen, the thermocouple was clamped by two paper clips parallel with each other on the longitudinal direction of the cemented surface. The cemented thermocouple was allowed to dry for at

least 30 minutes and a final curing time of 18 to 24 hours at room temperature was recommended by the manufacture (Omega). The clips were removed after the drying procedure and the specimen was allow to cure overnight.

The specimen with the cement-on thermocouple attached was set on the fused silica boat as in a typical shock test. The other end of the thermocouple was connected to a chart recorder (Hewlett Packard, Model 7128 A). The voltage signal induced by the thermocouple during a thermal shock cycle was recorded. The voltage signal recorded was converted to temperature based on the ASTM reference [51]. In the air quench process, the specimen remained on the fused silica boat at all times. In the liquid quench process, the specimen with thermocouple attached was immersed into the liquid bath immediately after the specimen was removed from the furnace. Three individual transient temperature measurements were taken for each of the four quench media: static air, forced air, quenching oil and water (figures 10-13). The result of the three runs were then averaged to give the time-temperature history for the YIG specimens as quenched by each of the media.

2.5 Internal Friction Measurement

Internal friction Q^{-1} was measured by both the forced resonant method and free decay method using Forster's method [42].

The equipment required for the forced resonant method is identical to that used in elastic modulus measurement described in

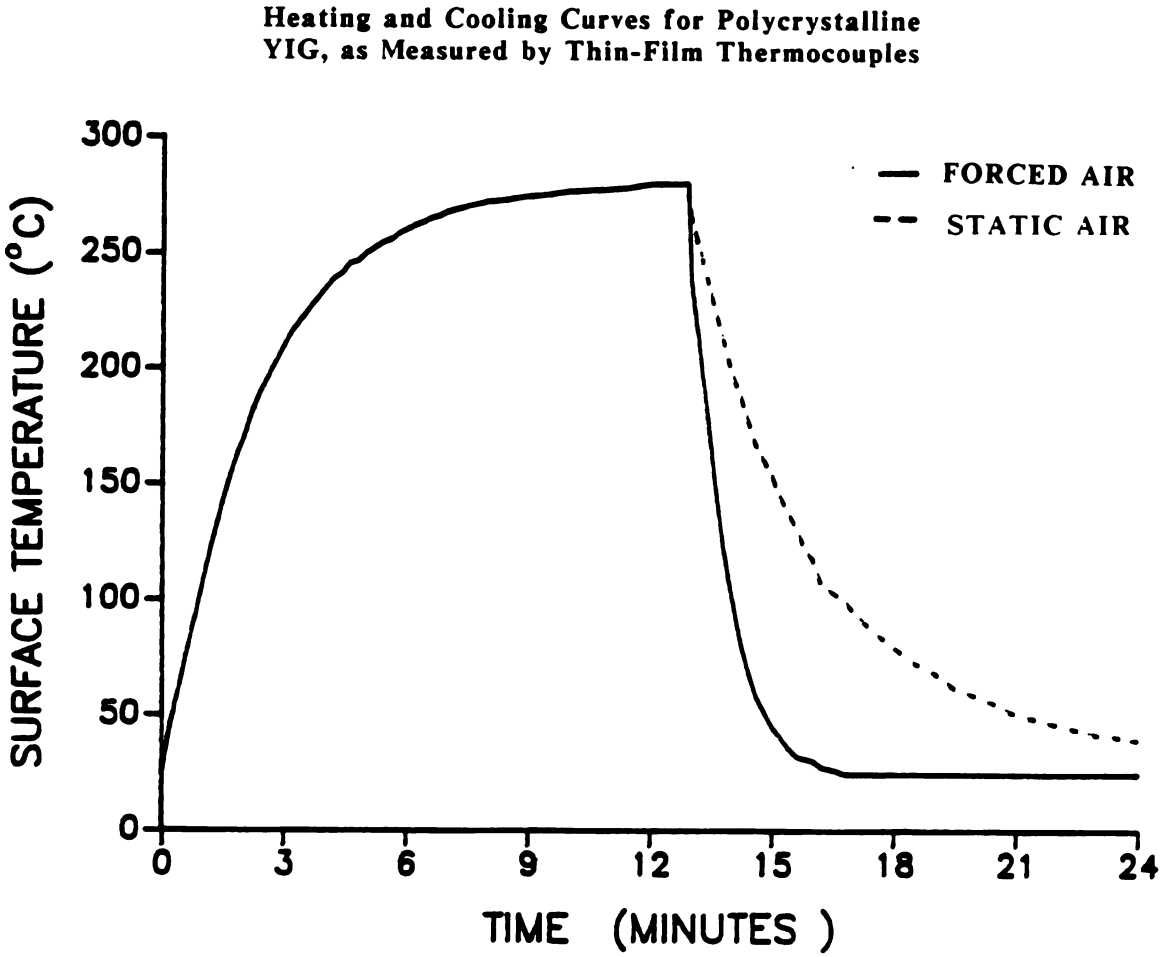

Figure 10. For the YIG specimens included in this study, the complete heating and cooling curves for (1) forced air and (2) static air as the quench medium were recorded using a thin-film type K thermocouple cemented to the specimen. The maximum temperature is 280 degrees Celsius.

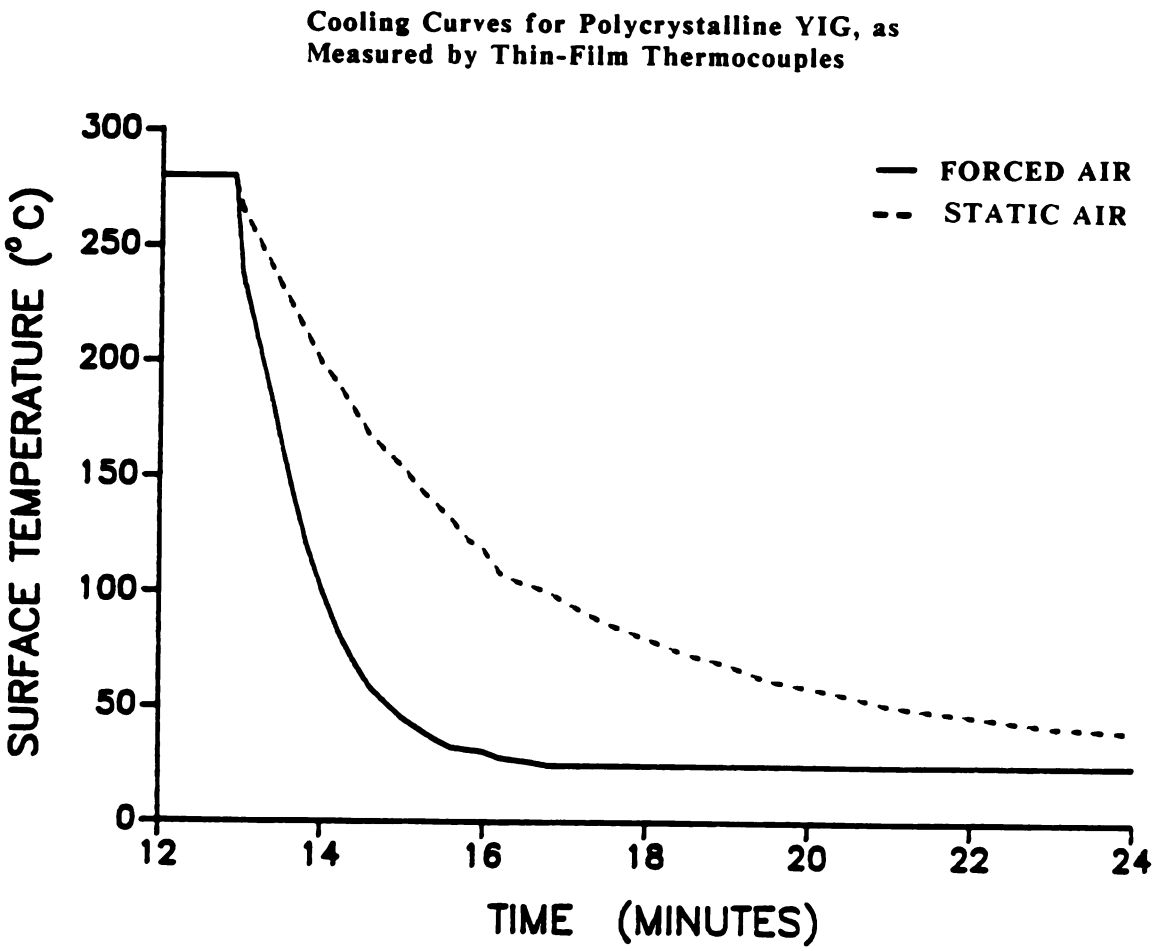

Figure 11. The cooling portion of the curves in Figure 9, which use (1) forced air (2) static air as the quench medium.

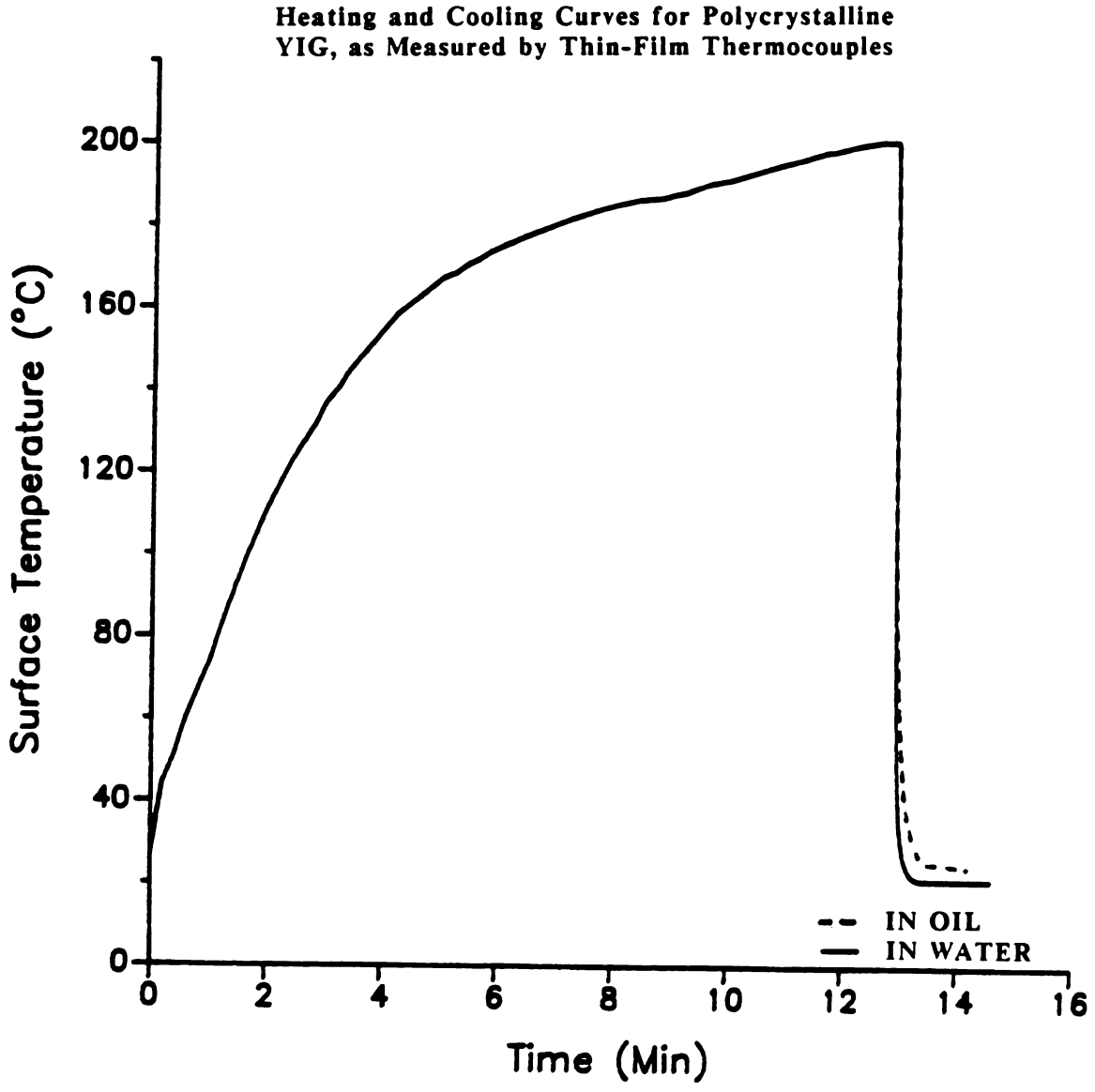

Figure 12. For the YIG specimens included in this study, the complete heating and cooling curves for (1) water and (2) oil as the quench medium were recorded using a thin-film type K thermocouple cemented to the specimen. The maximum temperature is 200 degrees Celsius.

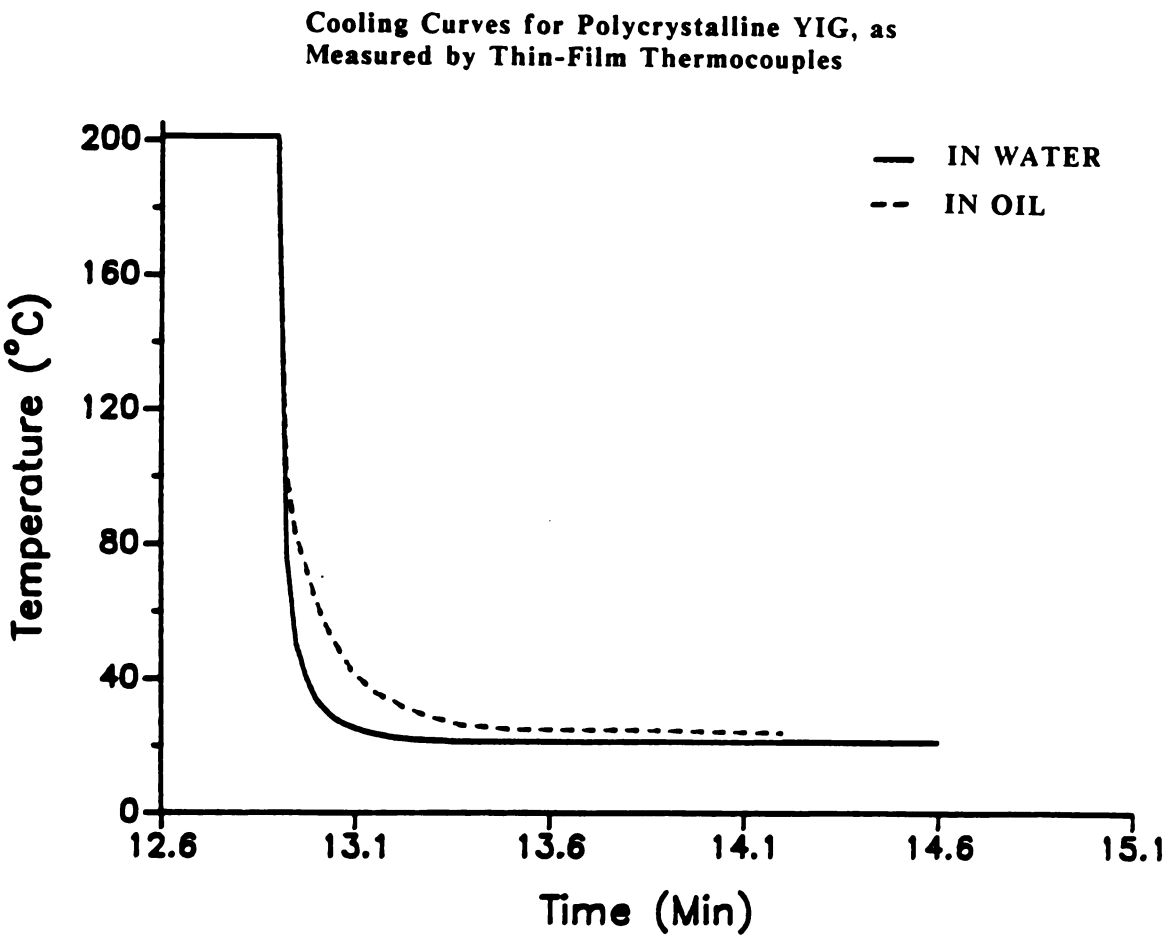

Figure 13. The cooling portion of the curves in Figure 11, for (1) water and (2) oil as the quench medium.

section 2.2. Two frequencies, whose amplitudes are one-half of the flexural resonance amplitude, are located on each side of the central resonant frequency. The peak width, Δf, is defined as the difference between these two frequencies. The formula employed for the calculation of Q_m^{-1} by the forced resonant method is

$$Q_m^{-1} = 0.5773 \times \Delta f / f_r \qquad (4)$$

where f_r is the flexural frequency of the test specimen. The forced resonant method is widely used to measure high internal friction samples whose Q^{-1} are larger than 1×10^{-3}. Some refractories, polymers and composites materials exhibit internal values of this magnitude.

The free decay method, on the other hand, is more appropriate for low internal friction samples, such as dense monolithic ceramics. In this study the internal friction was measured by the free decay method unless indicated otherwise. The specimen was driven at the flexural resonance frequency. The sonic driving force applied to the specimen was abruptly shut off in order to allow the amplitude of the specimen's mechanical vibration to freely decay. The amplitude of the voltage when the specimen is driven at the flexural resonance frequency is V_1. Another voltage amplitude, V_2, was selected such that V_2 was smaller than $V_1/2$, and much larger than the background amplitude. The vibration cycles that the vibration amplitude of the free decay specimen decreases from V_1 to V_2 is N, which could be read from a electronic counter. Therefore, the vibration cycles, N, will

be relatively small and give larger uncertainty if the selected V_2 is very close to V_1. On the other hand, the counter may receive significant noise if the selected V_2 is very close to the peak background. This is the consideration to choose a proper V_2. The internal friction measured by this method is given as [52]

$$Q_m^{-1} = \ln (V_1 / V_2) / \pi \times N \qquad (5)$$

The free decay apparatus includes one trigger and electronic counter added to the elastic apparatus modulus (figure 14). The free decay method used in this study was compared with another technique. The free amplitude decay of the specimen vibration was recorded using a storage oscilloscope. The internal friction was then calculated from equation 4 and the V_1 and V_2 measured from the photograph of the oscilloscope trace. N was calculated by the product of the frequency of the signal and the elapsed time. The Q^{-1} obtained from the free decay curve taken from the storage oscilloscope was consistent with the internal friction measured from the trigger and counter.

The measured internal friction, Q_m^{-1}, by either method included both the contribution from the specimen, Q_s^{-1}, and the contribution from the apparatus, Q_a^{-1}. The internal friction of the specimen was suspension position dependent. Wachtman and Tefft [47] proposed an equation which yields the Q_s^{-1} and Q_a^{-1} separately

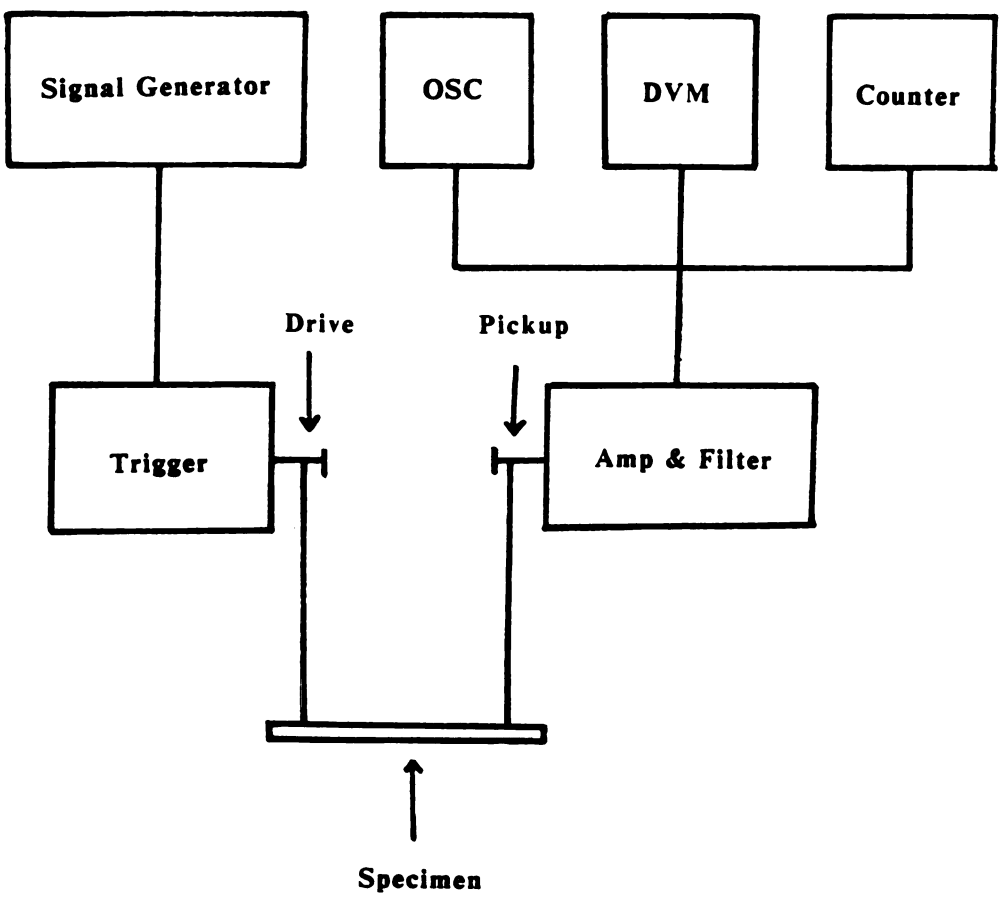

Figure 14. Block diagram of sonic resonance apparatus used for internal friction measurement.

$$Q_m^{-1} = [Q_s^{-1} + k\, Q_a^{-1}\, (Y / Y_0)^2 / [1 + k\, (Y/Y_0)^2] \qquad (6)$$

where Q_s = the internal friction of the specimen

Q_a = the internal friction of the apparatus

k = an empirical constant

Y = the vertical displacement of the suspension position from equilibrium

Y_0 = the vertical displacement of the end of the specimen

The ratio Y/Y_0 can be expressed in terms of the distance, x, from the suspension position to the ends of the specimen by using the equation given by Rayleigh [53] for the transverse vibration of an elastic bar,

$$Y/Y_0 = [1.018\, (\cosh 4.730\, x/L + \cos 4.730\, x/L) - (\sinh 4.730\, x/L + \sin 4.730\, x/L)] / 2.036 \qquad (7)$$

where x = distance, measured from the end of the specimen, where vertical displacement Y was measured,

L = length of the specimen

The non-linear least-squares best fit program used in this study was developed by E. D. Case based on these equations.

The internal friction is typically measured during the free decay of the fundamental flexural excitation of a prismatic bar. (In this study, all free decay measurements were done in this way.) At the node, the vertical displacement is zero, so that Y/Y_0 is zero at the

node for both equationS (6) and (7). In equation (6), which describes the suspension position dependence of the measured internal friction Q_m^{-1}, if Y/Y_0 is zero, then Q_m^{-1} is equal to Q_s^{-1}. Since Y/Y_0 is zero only at the nodes, Q_m^{-1} equals Q_s^{-1} only when the bar is suspended exactly at the nodal positions, for example, the minimum in the Q_m^{-1} versus relation suspension position X/L in figure 15 corresponds to the nodal position for the fundamental flexural frequency.

The distance of suspension from the end of the specimen, x, was measured by metric caliper. The accuracy of the measurement of x can influence the computation of Q_s^{-1} based on experimental experiences on the YIG system. With fixed V_1 and V_2 values, N was measured at least five times for each suspension position, when the specimen was driven at its flexural vibration mode. In order to determine the specimen internal friction, Q_s^{-1}, the empirical internal friction, Q_m^{-1}, was measured for eight to ten suspension positions for a specimen at each thermal shock damage condition. The internal friction Q_m^{-1}, and suspension position x were input to the program to calculate the Q_s^{-1}, Q_a^{-1}, and k. For about ninety percent of the experimental trials the least-squares best fit correlation coefficient for the YIG specimens was equal to or greater than 0.98. For a given set of Q_m^{-1} and x (position) data, the computed values of Q_s^{-1} using the least-squares procedure on equation (6) were slightly different depending on which subset of the data was used to perform the fitting. For example the specimen internal friction, Q_s^{-1}, of a thermally shocked YIG specimen were 26.90, 26.64, 26.72, 27.16, 28.14 $\times 10^{-5}$ when the number of the Q_m^{-1} and x data pairs taken were 10, 9, 8, 7, 6, respectively. The

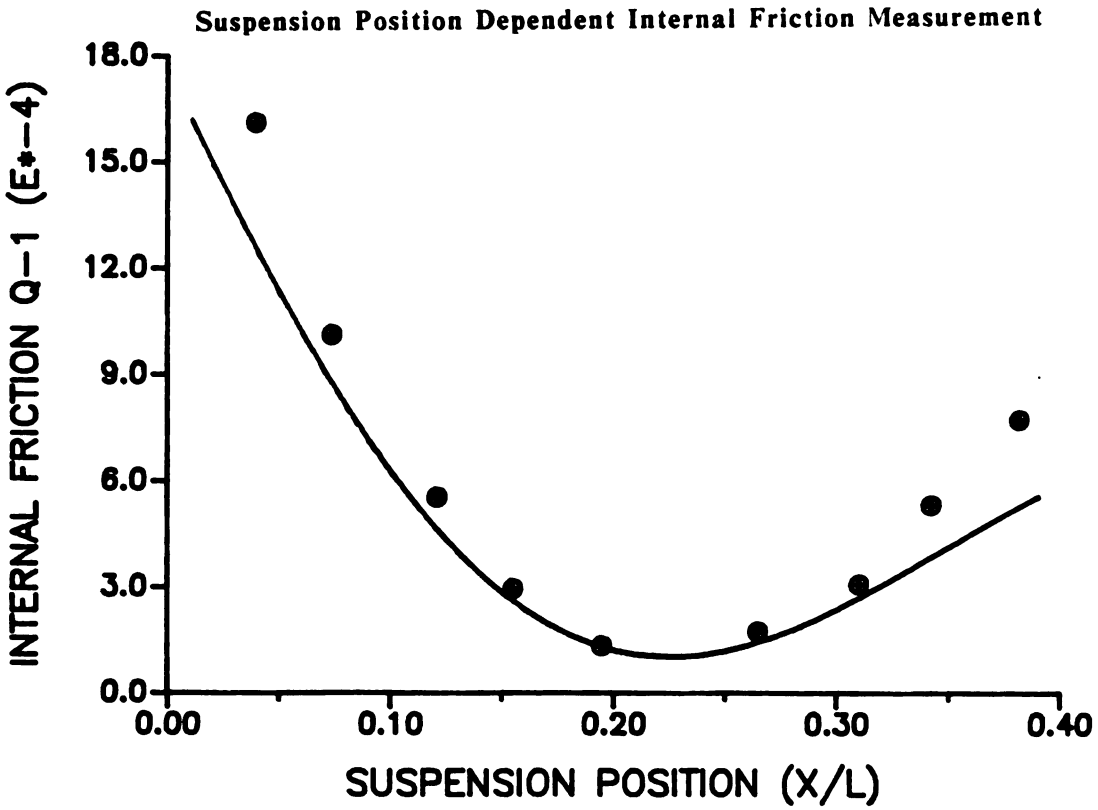

Figure 15. A typical suspension position dependent internal friction measurement of YIG specimens. The solid line refers to equation 6.

specimen internal friction Q_s^{-1}, data shown in this study were obtained by averaging the Q_s^{-1} values which computed from 6 to 10 data pairs. The Q_s^{-1} for this specimen therefore was taken as the 27.11×10^{-5} which was the mean of the five computed Q_s^{-1} values. The typical suspension position dependent measurements of internal friction is in figure 15.

2.6 Internal Friction Calibration Procedures

The measured internal friction, Q_m^{-1} was sensitive to the suspension angle between the threads and the specimen normal plane. The suspension threads were usually normal to the specimen surface. However, the measured internal friction decreased as a function of the angle between the threads and the normal plane of the specimen (figure 16). For example, the measured internal friction at the suspension angle of 17.5 degrees was only 80 percent of the internal friction which measured at a 0 degree suspension angle. Therefore, in order to obtain good repeatibility of the internal friction measurement, suspending the threads normal to the specimen was critical.

Because the internal friction is sensitive to suspension position and suspension angle, the repeatibility was measured to obtain the uncertainty of the experimental measurements. The internal friction of a YIG specimen was measured 10 times at a single suspension position, D = 0.8 cm (D is the distance between the suspension position and the near end of the specimen). The YIG specimen was first unloaded and then reloaded on the suspension threads of the elasticity apparatus. For each internal friction measurement the

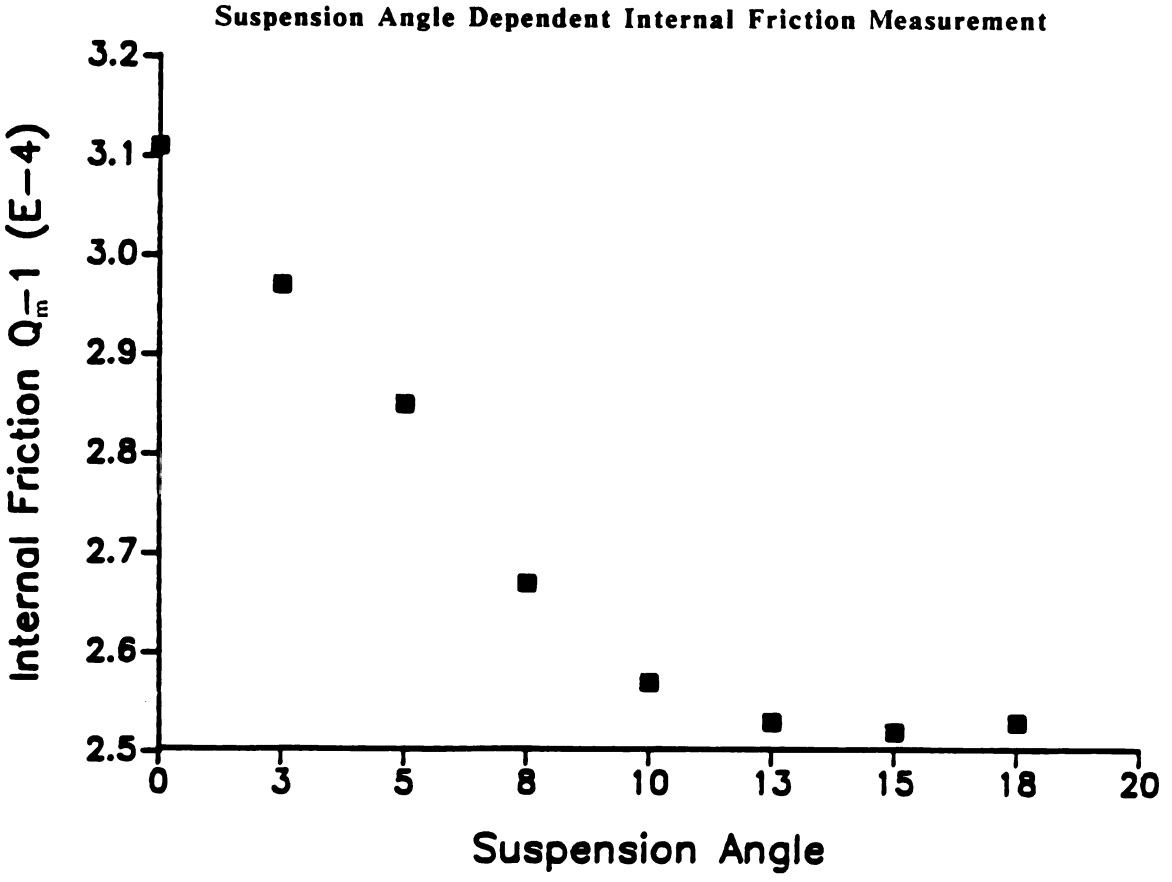

Figure 16. The suspension angle dependence of internal friction measurement.

suspension angle was adjusted to zero degrees and the suspension threads were relocated at D = 0.8 cm from the end of the specimen. The ratio of the driving voltage trigger pickup voltage was constant for each of the 10 internal friction measurements. For each trial, five data points were taken and averaged to obtain the measured internal friction. The measured internal friction of the 10 trials versus trial number is shown in figure 17. The mean internal friction of the 10 trials was $3.01 \pm 0.27 \times 10^{-4}$. Thus, the standard deviation of the 10 trials was 9.0 percent of the mean value of the internal friction.

The movement of the suspension threads on the needles of both drive and pickup transducers also may influence the internal friction measurements. Therefore, the internal friction of the YIG specimen G2E was measured at suspension position, D = 0.4 cm for another 10 trials by the same method as the previous test except suspension threads were glued to the transducers. The mean internal friction of these 10 trials, for which the needles were glued during the measurements, was $1.00 \pm 0.04 \times 10^{-4}$ (figure 18). The coefficient of variation of the 10 trials was 4.0 percent, which is smaller than the standard deviation of the trails in which the suspension threads were not glued to the transducers.

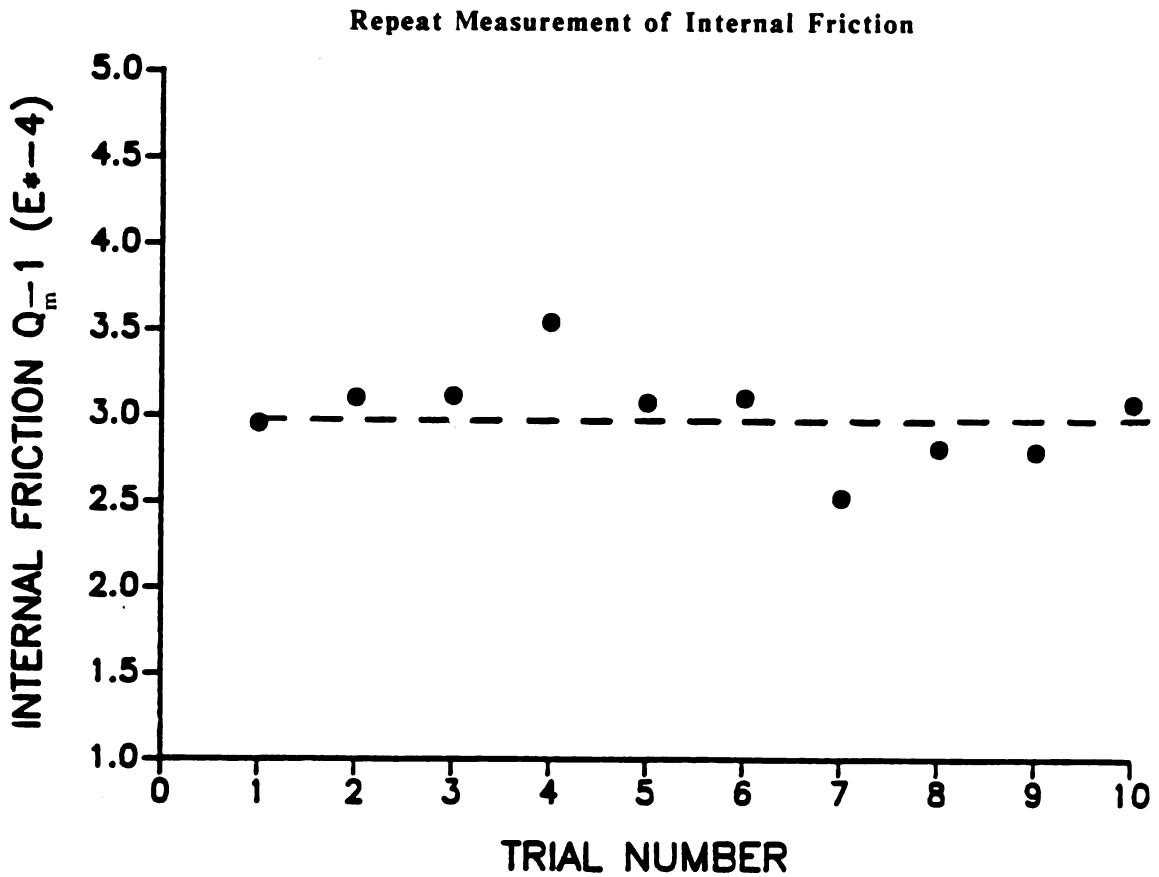

Figure 17. The repeat measurements of internal friction at D = 0.8 cm. No glue was applied to the tranducers. The dash line is the mean value of the measurements (D is the distance between the suspension position and the end of the specimen).

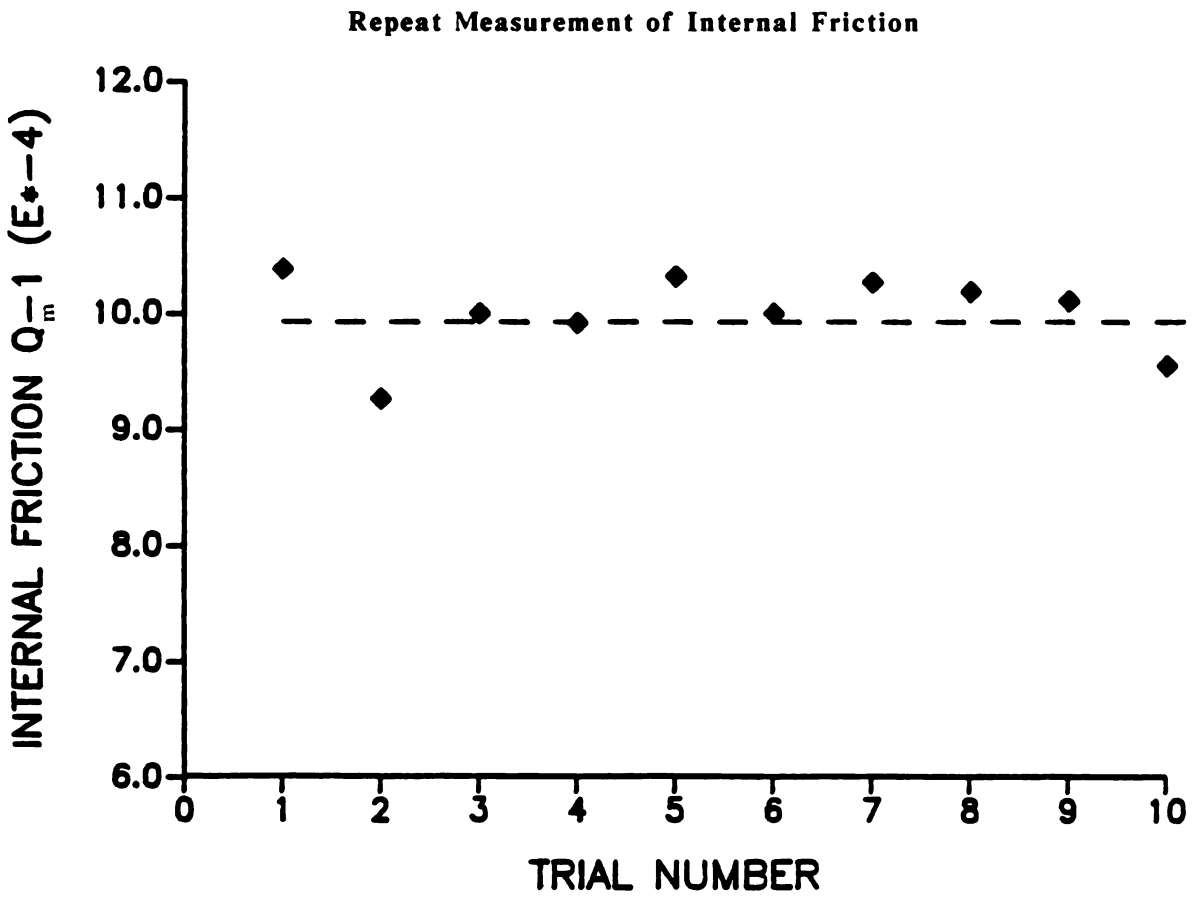

Figure 18. The repeat measurements of internal friction at D = 0.4 cm. The tranducers were glued with the threads. The dash line is the mean value of the measurements (D is the distance between the suspension position and the end of the specimen).

2.7 Control Tests to Determine the Effects of Prolonged Heating of the Specimens and Specimen-Fixture Impacts Occurring During Movement of Pneumatic Arm.

Two "control tests" were utilized to determine the extent of other possible contributions to internal friction from (1) physical property changes during the long cumulative heating time, typically hundreds of hours, in the furnace, and (2) the cyclic mechanical vibrations caused by the thermal shock apparatus during the shock process.

A YIG specimen of the same dimensions as the thermally shocked YIG specimens was taken as the "control bar." The internal friction was measured before and after heating the specimen for a time equivalent to the total cumulative time at temperature for a thermally shocked specimen that has undergone 2500 thermal cycles. The effective heating time of a YIG specimen which experienced 2500 thermal cycles is about 90 hours based on the calculation proposed above. In order to avoid thermal shock damage, the specimen was isothermally heated in an approximate heating rate of 10 degrees Celsius per minute in an electric resistant furnace to a steady state temperature for a preselected time interval of 2, 9, 21, 32.5, 54.5, 77 and 90 hours, then the specimen was allowed to cool isothermally in the furnace. It took 12 to 14 hours to isothermally cool the furnace from 280 degrees Celsius to room temperature. The Q^{-1} measurement was performed at least two hours after removal of the YIG specimen from

the furnace to avoid any involvement of time-dependent crack healing which might cause the Q^{-1} measurements to be difficult to interpret. An assumption was made that the possible microstructural and mechanical changes in the specimen were predominant at the highest anneal temperature. For a typical thermal shock cycle a YIG specimen remains at 280 degrees Celsius for about 2 minutes.

The internal friction of the specimen G3C decreased about 50 percent after the first several hours of annealing at 280 degrees Celsius. YIG specimens G2C and G2E were annealed at 280 degrees Celsius for two hours and then isothermally cooled to room temperature at the cooling rate similar to that experienced by the "heating control bar." Following the 280 degrees Celsius anneal the internal friction of both YIG specimens G2C and G2E decreased by about 30 to 50 percent compared to the internal friction prior to the anneal. The internal friction decrease upon annealing might be explained by the release of residual stress of some kind existing in the YIG specimens. Furthermore, the Q_s^{-1} measured after cumulative annealing times of 2, 9, 21, 32.5, 54.5, 77, and 90 hours are nearly the same (figure 19). The mean of the Q_s^{-1} was $12.02 \pm 1.25 \times 10^{-5}$. The coefficient of variation of the measured internal friction was about 10.5 percent. This heating control test indicates that the residual stress of the specimen should be removed before shock testing and that the contribution of internal friction change ΔQ^{-1} due to long cumulative heating time in the furnace could be ignored.

Another extraneous source of internal friction might be the cyclic mechanical collision between the tested YIG specimen and the

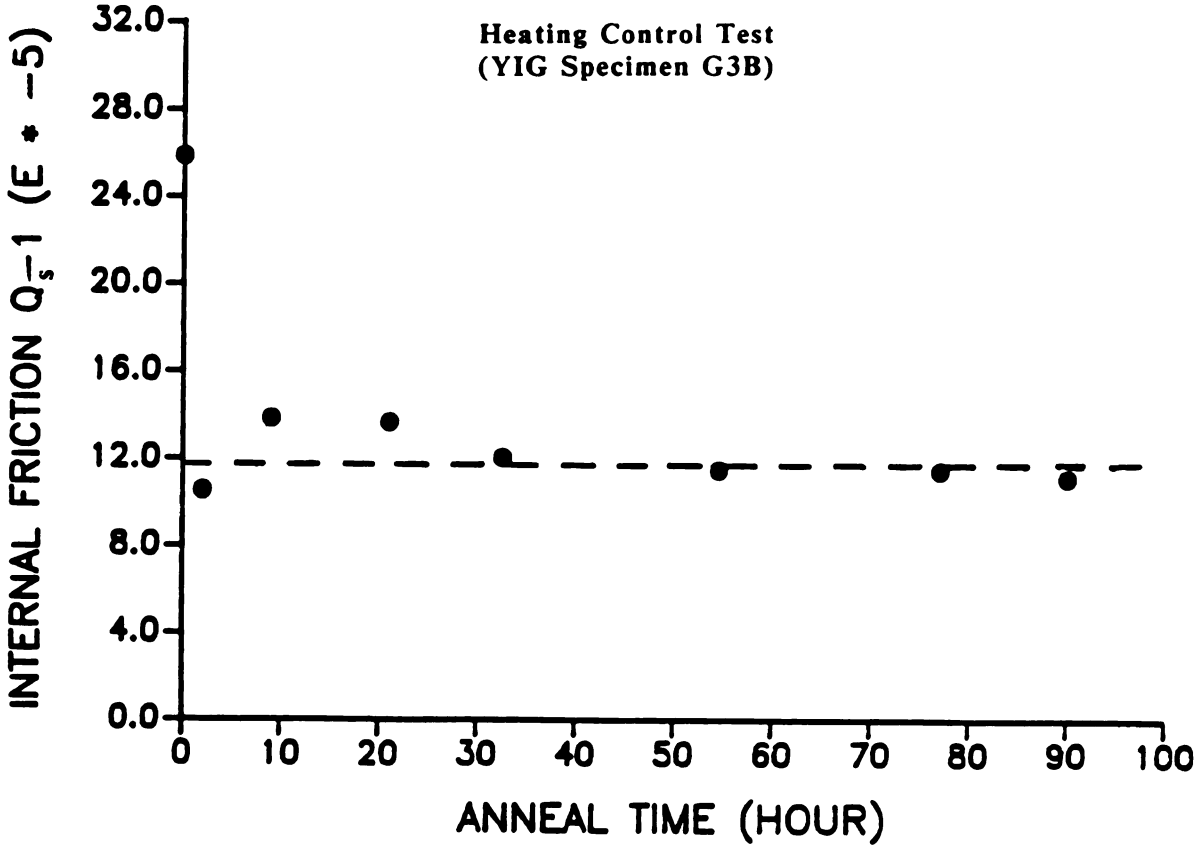

Figure 19. Internal friction measurements for a YIG specimen which experienced cumulative heating up to 90 hours at 280 degrees Celsius. The dash line is the mean value of the measurements

inside wall of the fused silica boat (figure 9B) that occurs during every cyclic mechanical extension and retraction of the pressure driven mechanical arm. (The YIG specimen may collide with the fused silica boat due to the residual momentum.) In order to determine whether the cyclic mechanical vibrations between the specimen and fused silica boat changed Q_m^{-1}, another equivalent-sized YIG specimen was taken as a "vibration control bar." The "vibration control bar" was placed in a fused silica boat identical to that used for thermal shock testing. The mechanical arm was then extended and retracted at room temperature, with the silica boat and specimen in place. The internal friction changes versus equivalent vibration cycles is plotted in figure 20. Instead of using the 25 minutes extension-retraction cycle employed in the thermal shock test, a 16 second extension-retraction cycle was used in the vibration damage test. The pushing and drawing speeds of the mechanical arm were the same as in a typical shock cycle. It was assumed that the time between extension-retraction cycles would not affect the outcome of the "vibration control" experiment, as long as sufficient time was allowed between specimen movements for the specimen and system vibrations to be extinguished.

The YIG "vibration control bar" was annealed at 800 degrees Celsius for two hours prior to the vibration test. The internal friction decreased about 30 percent after the anneal. The internal friction was measured from 0 cycles (before the test) to a maximum of 3000 cycles. The mean of the Q_s^{-1} measurements was 10.5×10^{-5} with a standard deviation of 0.7×10^{-5}. The coefficient of variation of

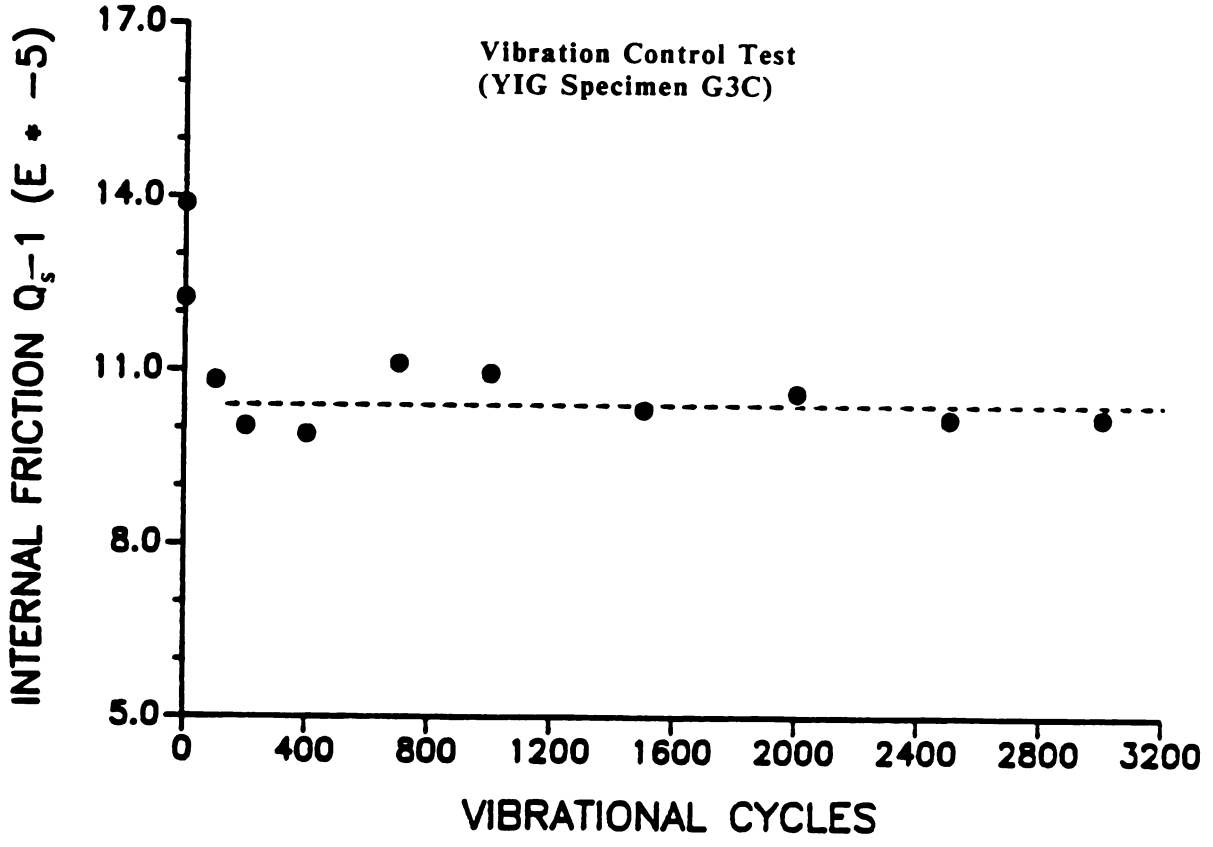

Figure 20. Internal friction measurement for a YIG specimen which experienced vibration cycles up to 3000 times without thermal shock at room temperature. The dash line is the mean value of the measurements

internal friction measured was thus about 7 percent. The cyclic mechanical vibrations between the YIG specimen and fused silica boat induced by extension and retraction of the mechanical arm was not significant.

3: RESULTS AND DISCUSSION

This study uses ΔQ^{-1} and ΔE to assess the damage induced by repeated thermal shock damage. Based on models by Budiansky and O'Connell [54], and Salganik [55], the elastic modulus decrement can be related to the crack damage parameter which is the product of the number of cracks and the third moment of the mean crack size. However, no simple model is available to assess internal friction change in terms of the crack damage parameter.

3.1 The Measurement of Temperature Versus Time During a Thermal Shock Procedure

Thermal shock severity is often expressed in terms of ΔT, which is the difference between the temperature of the specimen at the moment the quenching process begins (for example, when the specimen is removed from the furnace) and the final temperature of the specimen in the quenching fluid. In the current thermal shock literature the details of the heat transfer phenomena between the specimen and quenching fluid are typically not characterized.

The heating and cooling rate of the specimen during the thermal shock process is nearly universally ignored in both experimental and theoretical studies of thermal shock damage. Characterizing the thermal shock severity in terms of the temperature change, ΔT, is oversimplified. For example, common experience tells us that a hot glass coffee pot, when plunged into ice water, will very likely

shatter explosively. If the same pot were slowly cooled to the temperature of ice water, no damage would result even though ΔT was the same in both cases. In order to begin to characterize the rate effect, temperature versus time for the heating and cooling processes was measured.

In this study, the experimental heating and cooling curves obtained by heating the YIG specimens in an electric resistance furnace (figures 10-13) can be expressed as

$$T(t) = (T_{MAX.} - T_{R.T.})\ (1 - e^{-ht}) + T_{R.T.} \qquad \text{(Heating)} \qquad (8)$$

$$T(t) = (T_{R.T.} - T_{MAX.})\ (1 - e^{-q(t-ti)}) + T_{MAX.} \qquad \text{(Cooling)} \qquad (9)$$

where $T(t)$ = the surface temperature of a specimen at time t,

$T_{max.}$ = the highest (steady state) surface temperature,

$T_{R.T.}$ = room temperature,

t_i = the time when the specimen was begun to be quenched.

h, q = the parameters related to T_{max}, and the heat transfer coefficients of quenching media and the geometry of specimen.

Twenty-two time-surface temperature data pairs were taken from heating and cooling curves of thermally shocked YIG specimens quenched into static air, forced air, oil and water. A least-squares best fit of the time-temperature data to equations (8) and (9) resulted in correlation coefficients of 0.98 or greater (table 1). The heating and cooling data for a 90 percent alumina refractory in a thermal

Table 1. Heat transfer parameters h and q for thermally shocked YIG specimens and the 90 percent alumina refractory in different quenching media.

Material	Quenching Medium	Maximum Temperature (° C)	Minimum Temperature (° C)	h Parameter (sec^{-1})	q Parameter (sec^{-1})
1. YIG	Forced air	300	27	0.42	0.92
2. YIG	Static air	300	27	0.24	0.33
3. YIG	Oil	200	24	0.32	19.82
4. YIG	Water	200	24	0.32	42.96
5. 90 % Alumina	Forced air	1000	150-185	0.37	0.37

shock ribbon test [21] can be compared with the present study. The alumina refractory sample was heated directly by flame on its 0.228 m by 0.076 m hot surface. Cooling commenced when the burner was shut off and the specimen was subsequently exposured to moving air. The temperature was measured on both the hot-face and the cold-face. The heat transfer parameters of the ribbon test of 90 percent alumina were extracted from the least-squares best fit of equations (8) and (9) for 25 temperature-time data pairs, obtained from Semeler and Hawisher [21]. The heating parameters are not influenced much by the different furnaces or the different maximum temperatures employed in this study and the study by Semeler and Hawisher [21]. On the other hand, the quenching medium was the determining factor for thermal shock damage. The cooling factor q for water is twice as large as that of oil, and q for water is about 40 to 100 times larger than that of air.

3.2 Review of Thermal Shock Studies in Ceramics

In general, thermal shock damage decreases the resonance frequencies of ceramic materials, and decreases the number of mechanical vibration cycles of a fixed (V_1/V_2) free decay measurement. The decrease of resonance frequencies represents a reduction of elastic modulus and the decrease of vibration cycles of a free decay measurement reflects an increase of internal friction.

When subjected to thermal shock, the internal friction of alumina and silicon nitride specimens gradually increases as they experience a more severe shock environment [22 and 23] (figures 21 and 22). The

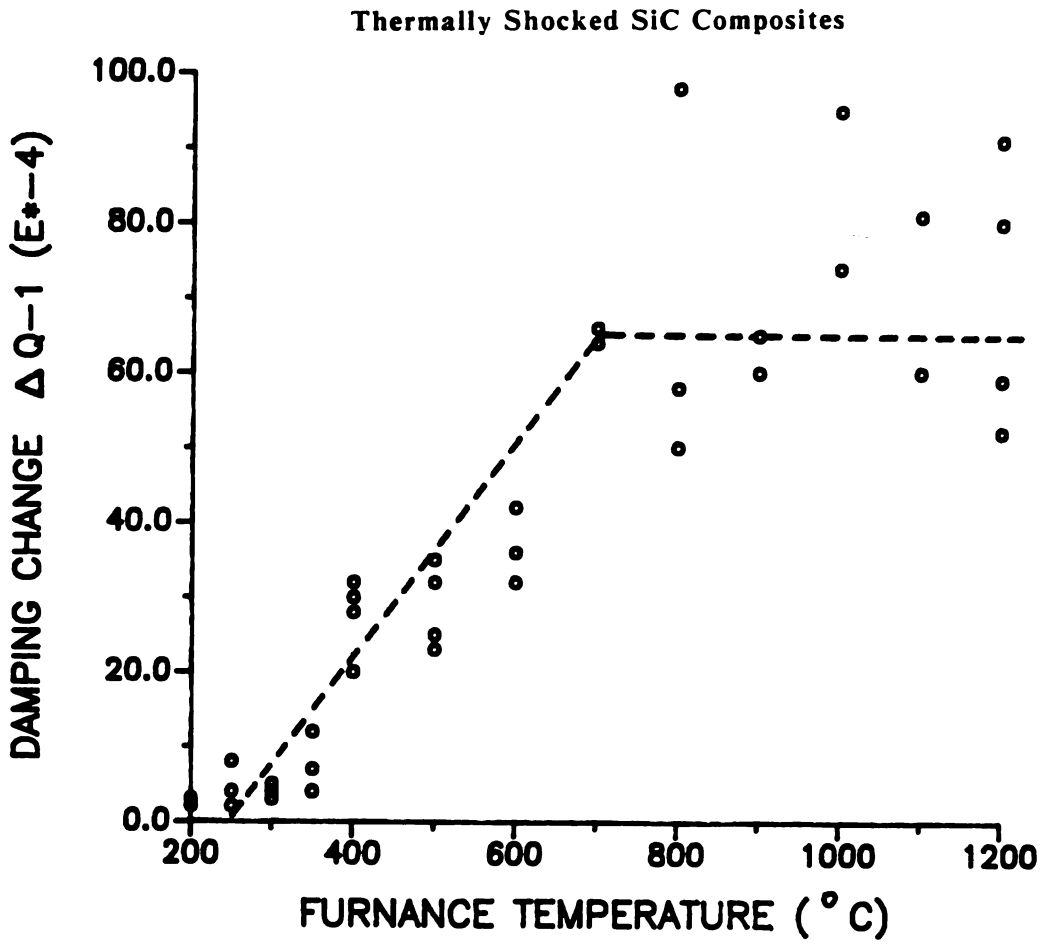

Figure 21A. Change in internal friction with increasing severity of thermal shock for RX-B SiC composite materials which were formed by slip casting technique (after Coppola and Bradt, 1973, [23]).

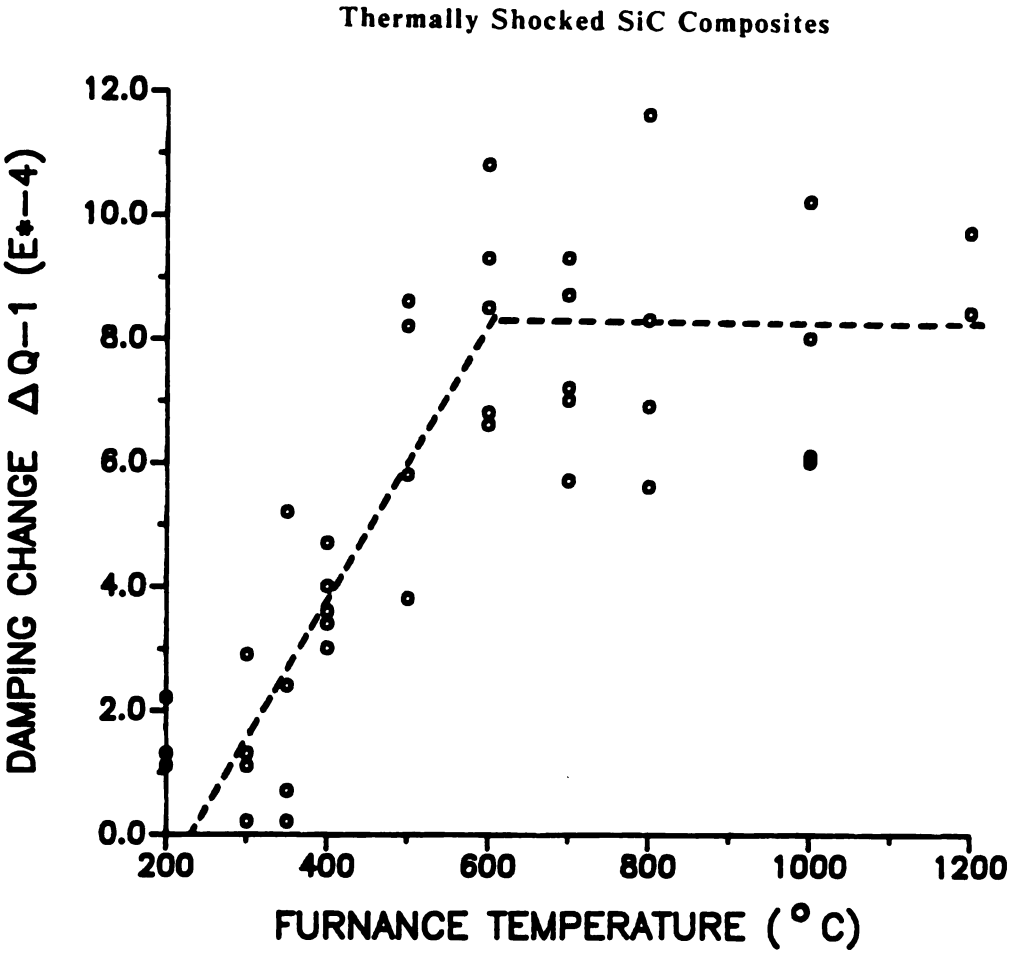

Figure 21B. Change in internal friction with increasing severity of thermal shock for RX-C SiC composite materials which were formed by similar method as the formation of RX-B SiC specimens but at a lower sintering temperature (after Coppola and Bradt, 1973, [23]).

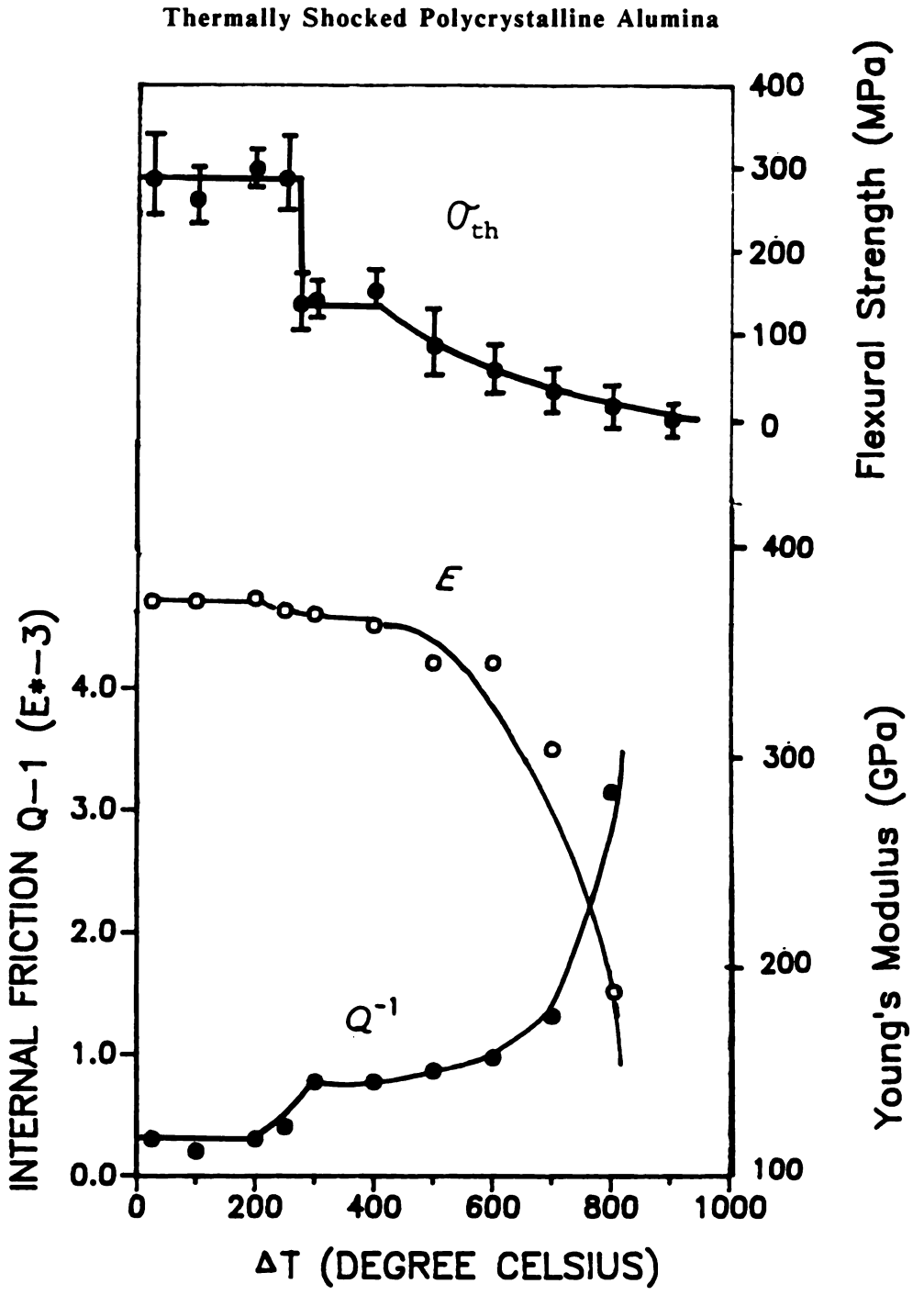

Figure 22. Change in internal friction, Q^{-1}, Young's modulus, E, and retained strength, σ_{th}, with increasing severity for thermally shocked polycrystalline alumina (after Matsushita et al., 1984, [22]).

Young's modulus, on the other hand, slowly decreases [22] (figure 22). The internal friction is more sensitive to thermal shock damage than is the Young's modulus [23, 56 and 57].

Coppola and Bradt [23] reported that the ΔQ^{-1} of brine quenched SiC composites increased linearly as the thermal shock temperature difference (ΔT) ranged from 25 to 700 degrees Celsius. The RX-B SiC specimens used in figure 21A were high temperature sintered by slip casting technique. The RX-C SiC specimens used in figure 21B made as the similar method as RX-B SiC but at a low sintering temperature. A steady state internal friction was found for ΔT in the range from 700 to 1200 degrees Celsius (figures 21A and 21B).

On the other hand, Matsushita et al. [22] found that the ΔQ^{-1} of water quenched polycrystalline Al_2O_3 increased continuously without reaching a steady state as the shock severity (ΔT) increased (figure 22). These two reports appear to be contradictory in regard to the trend of internal friction as a function of increasing shock severity, ΔT. The apparent contradiction may be explained:

1) Measurements of Q^{-1} by the sonic resonance method are suspension position dependent due to apparatus damping effects [47]. If the effect of apparatus damping is not accounted for, the error in the internal friction might be an order of magnitude [47]. Neither group (Coppola and Bradt, Matsushita et al.) [22 and 23] mentions the correction for the suspension position. Coppola and Bradt used the forced resonant method with an acoustic spectrometer to measure internal friction. Matsushita et al. used the free decay method on electrostatically driven carbon-coated specimens. The equations they

used are different

$$Q^{-1} = 0.5773 \cdot \Delta f/f_r \qquad \text{(by Coppola and Bradt)} \qquad (10)$$

$$Q^{-1} = \ln(V_0/V_2) \,/\, (\pi \cdot f_r \cdot t) \qquad \text{(by Matsushita et al.)} \qquad (11)$$

where the product of the vibration frequency (f_r) and time (t) is equal to N in equation (5).

The internal friction calculated by the free decay method and the forced resonant method were experimentally shown not to be consistent (table 2). The internal friction measured by the forced resonant method is larger than that measured by the free decay method. Furthermore, the carbon coating on the specimen (by Matsushita et al.) may influence the "real damping factors" by the coating thickness and position.

2) The measured internal friction of the YIG specimens in this study varied from one specimen to another, even if the specimens are cut from a single piece of uniform YIG material. The highest and lowest internal friction measured for the pre-shocked Gd-doped YIG were 32×10^{-5} and 21×10^{-5}, respectively. Differences for internal friction values for each specimen will be discussed in section 3.3. In figures 21A and 21B (Coppola and Bradt), the scatter of the Q^{-1} data was equal to or greater than 50 percent of the average magnitude of Q^{-1}. The trend proposed by Coppola and Bradt in regard to figures 21A and 21B is therefore not entirely convincing. Furthermore, Matsushita et al. display a continuous increase of ΔQ^{-1} versus ΔT.

Table 2. Comparison of the internal friction values measured by the free decay method and forced resonant method.

	Method	Internal Friction
1a.	Free Decay Method	1.16×10^{-3}
1b.	Forced Resonant Method	2.63×10^{-3}
1c.	Internal Friction Calculated*	1.69×10^{-3}
2a.	Free Decay Method	1.44×10^{-3}
2b.	Forced Resonant Method	2.26×10^{-3}
2c.	Internal Friction Calculated*	1.52×10^{-3}

* The calculation of internal friction was based on the free decay envelope obtained from an electronic storage oscilloscope.

However, the plot of the Matsushita et al. data does not supply statistical data, such as the number of test specimens or error bars representing, for example, the standard deviation about the mean for each internal friction data point.

3) The dependence of grain size and porosity of a specimen to thermal shock damage can not be overlooked. According to Matsushita et al. [22], when isolated (low density) cracks initiate due to thermal shock, the Q^{-1} increases by mechanical loss in pores and the stress concentration at the ends of cracks. As the cracks propagate and combine with each other to form large cracks, the Q^{-1} may increase significantly because of the mechanical loss to the slip at large crack surfaces [22]. Marlowe [58] and Dole et al. [59] indicated that the internal friction was affected by the volume fraction porosity and grain size of the test materials. Both papers fail to state grain size and average porosity of their test materials. Thus the thermal shock damage versus ΔT for Bradt and Coppola's SiC composite specimens may be very different from that of Matsushita et al.'s alumina specimens.

To the author's knowledge, only a few researchers have employed Young's modulus to evaluate repeated thermal shock damage [21].

3.3 Cyclic Thermal Shock in Polycrystalline YIG

YIG specimen G2A was thermally shocked up to 2500 cycles by quenching into forced air at a ΔT equal to 265 degrees Celsius. The measured Young's modulus versus cumulative number of the thermal shock cycles is shown in figure 23. There was no clear trend in the change

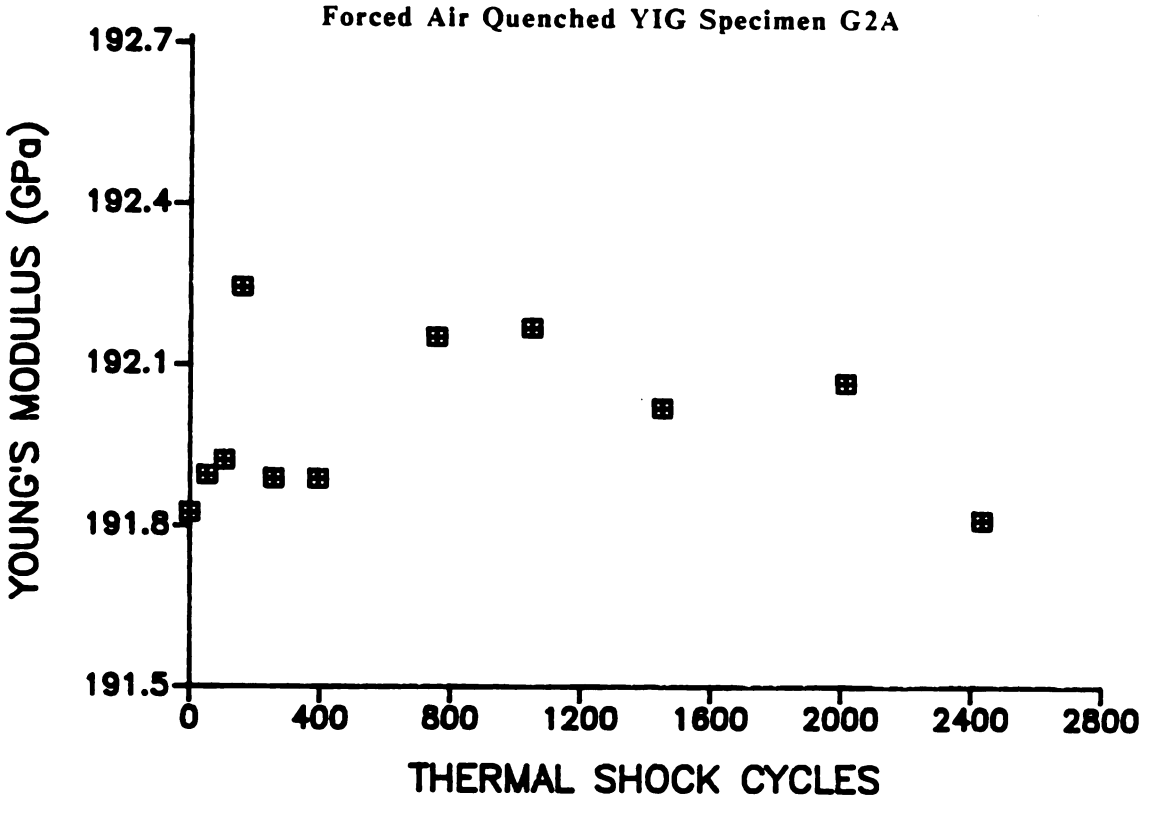

Figure 23. Young's modulus measurements for cyclic thermally shocked YIG specimen G2A (ΔT = 265 degrees Celsius).

of Young's modulus versus the shock cycles. The change of Young's modulus was relatively small, since the difference between the highest and lowest measured Young's modulus to the pre-shocked Young's modulus value, E_0, was only 0.15 percent of E_0.

The uncertainty of the Young's modulus measurement by sonic resonant method in this study is then about 0.05 percent. Therefore, 0.15 percent of E_0 change of Young's modulus due to thermal shock was not significant. This up and down type of Young's modulus change of YIG due to cyclic thermal shock observed in the present study was similar to the Young's modulus change of SiC subject to increasing thermal shock temperature [23]. However, the internal friction of the Gd-doped specimen G2A changed significantly due to the shock damage (figure 24). The specimen internal friction of specimen G2A (not annealed) decreased for the initial 260 shock cycles. Then, the internal friction of specimen G2A increased gradually for a cumulative number of shock cycles up to 400, then the internal friction reached a plateau from shock cycles 400 to 1400. The internal friction increased again after shock cycled greater than 1400. The ΔQ^{-1} after 2500 thermal shock cycles is about 200 percent larger than the internal friction of the unshocked specimen. For 160 thermal cycles at a ΔT of 265 degrees Celsius, Q^{-1} decreased to 60 percent of the pre-shock value of Q^{-1}. This phenomenon is likely due to the residual stress in the test specimen. Polariscope measurements of residual stress in as-received borosilicate glass used for thermal shock testing [39] found considerable residual stress prior to thermal shock testing. However, no connection between the residual stress and the

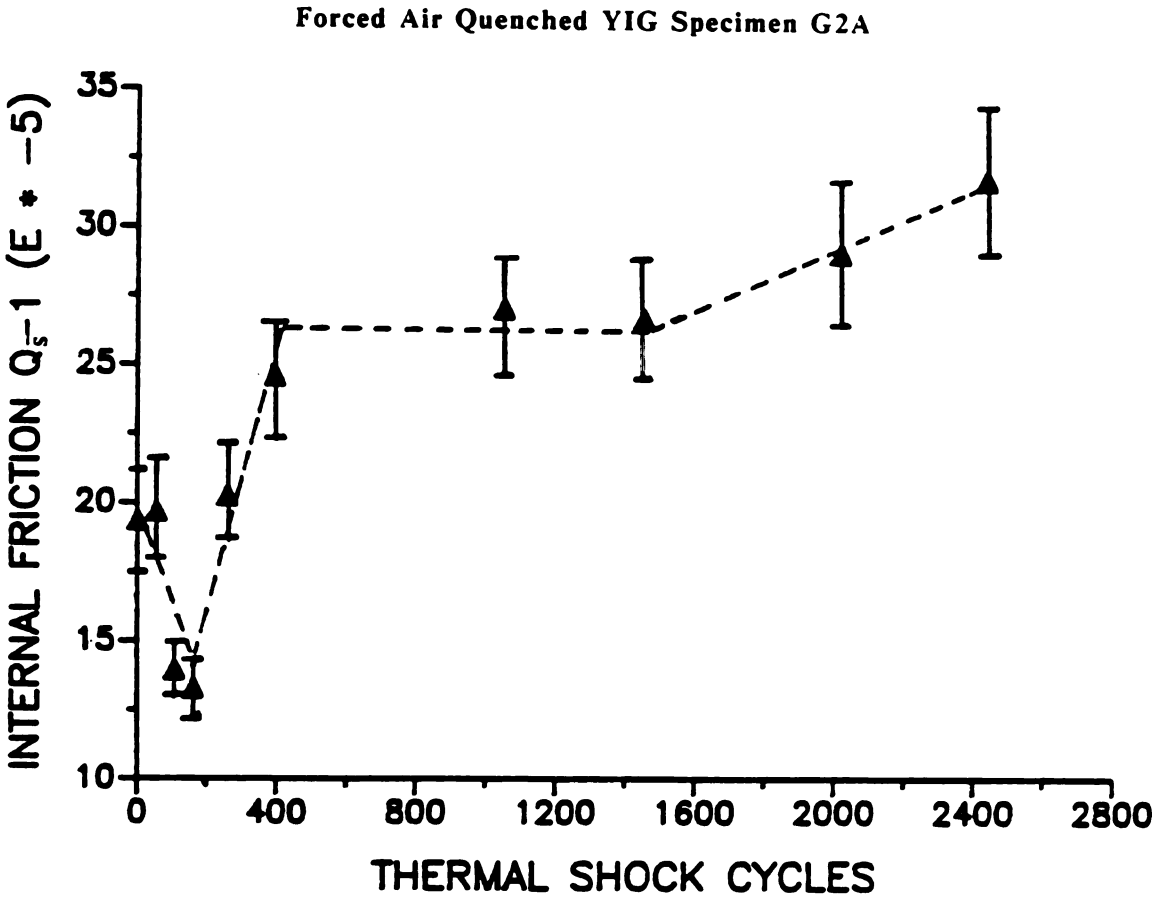

Figure 24. Internal friction measurements for cyclic thermally shocked YIG specimen G2A (ΔT = 265 degrees Celsius).

Young's modulus and Q^{-1} was reported in this paper [39].

The hardness (H) and fracture toughness (K_{IC}) for YIG unshocked specimens were measured (see Appendix B). The residual stress of an as-received YIG specimen was measured by indentation technique [60]. The residual stress σ_R is

$$\sigma_R = \frac{K_{IC}}{2(c'/\pi)^{1/2}} \cdot \left[\left(\frac{c^0}{c'}\right)^{3/2} - 1\right] \qquad (12)$$

Where σ_R = residual stress,

K_{IC} = critical stress-intensity factor taken from the indentation test on the fully annealed specimen.

c^0 = radical crack length taken from the indentation test on the as-received specimen.

c' = radical crack length taken from the indentation test on the fully annealed specimen.

The mean radial crack length for the as-received specimen and the annealed specimen was 81.1 microns and 95.9 microns, respectively. The mean radial crack length for each case was obtained by 10 to 15 indentations with load of 9.8 N, loading speed of 70 microns per second, load time of 10 seconds. The calculated residual stress of the as-received YIG specimen is about 24 Mpa based on the assumption that the annealed specimen is free of residual stress. In order to remove residual stresses, YIG specimens were annealed in air for two hours in an electrically heated furnace at 1250 degrees Kelvin (two thirds of the melting temperature of YIG, 1600 degrees Celsius [61]). Following the isothermal anneal, specimens were furnace cooled at a

rate of approximately 50 degrees Celsius per hour to room temperature. The Q_s^{-1} was measured for three YIG specimen before and after annealing. The internal Q_s^{-1} friction decreased from 30 to 50 percent of the Q_s^{-1} before the specimen was annealed.

The effect of annealing upon the internal fraction may be seen by comparing figures 24 and 25. In figure 24, YIG specimen G2A was not annealed prior to thermal shock testing. In figure 25, YIG specimen G2F was annealed at 950 degrees Celsius for two hours prior to the thermal shock test. The internal friction and Young's modulus was monitored along the thermal fatigue test at ΔT = 265 degrees Celsius (figures 25 and 26). For the internal friction measurement of specimen G2F, no decrease of internal friction was observed for the first several hundred shock cycles. The internal friction of specimen G2F increase from 8×10^{-5} to 17×10^{-5} when experiencing 300 thermal shocks by forced air quench. The internal friction had a fixed value in the range of 300 to 1000 shock cycles, then increased again after the specimen experience more than 1000 thermal cycles. This may indicate that the crack damage of the specimen increase as it experience more shock cycles, and that a quasi-static region exists for which the crack damage does not grow.

YIG specimen G2E was annealed at 950 degrees Celsius for 2 hours prior to thermal shock by forced air at a temperature difference, ΔT of 465 degrees Celsius. The Young's modulus and internal friction were measured by methods identical to those used for YIG specimen G2E. The changes of Young's modulus and internal friction versus thermal shock cycles are shown in figures 27 and 28. The measured Young's

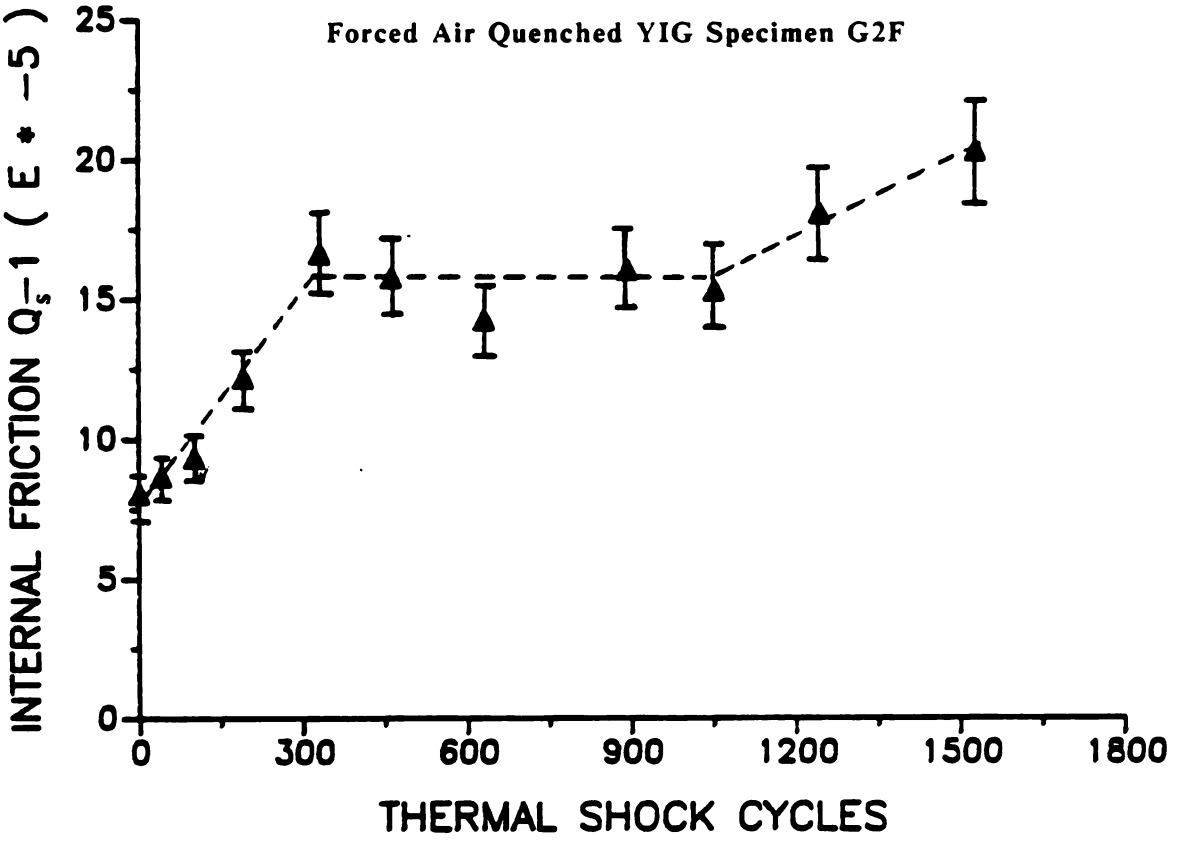

Figure 25. Internal friction measurements for YIG specimen G2F which experienced cyclic thermal shocked up to 1550 cycles (ΔT = 265 degrees Celsius).

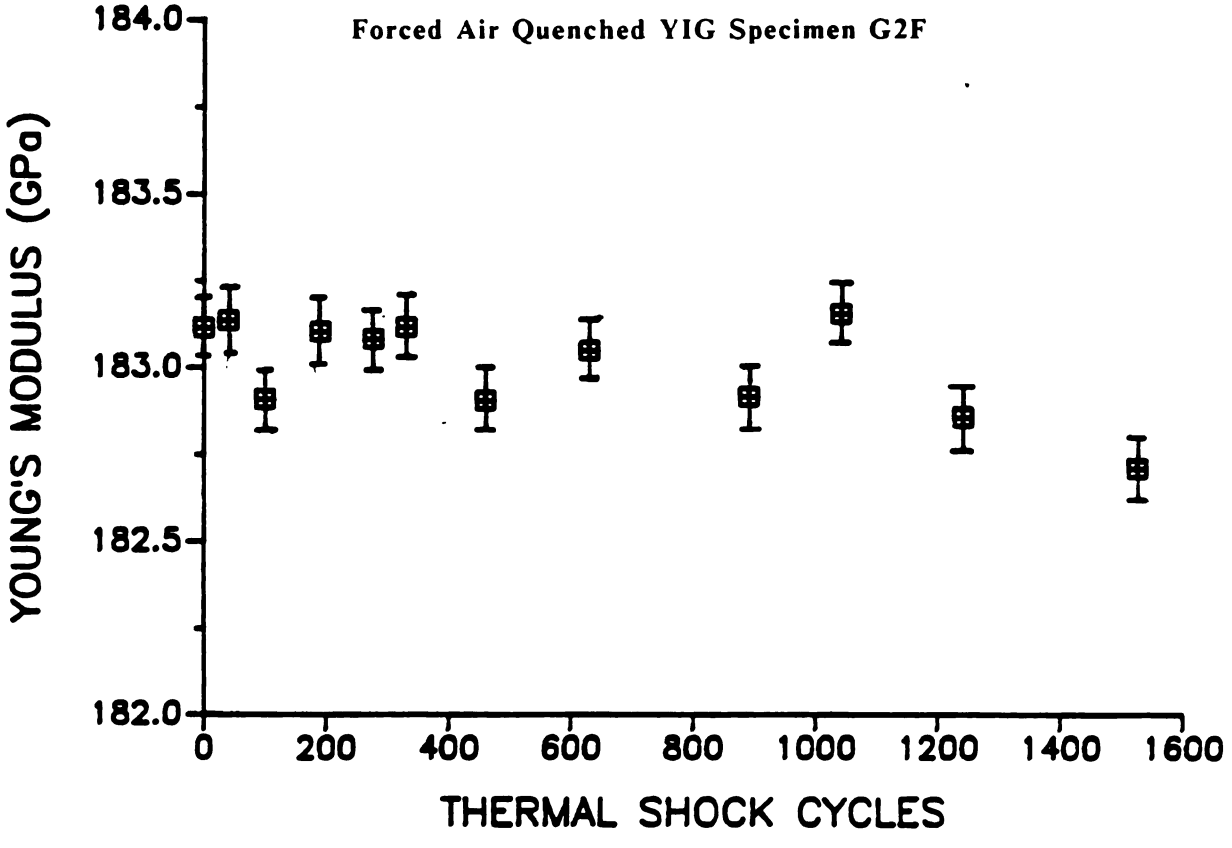

Figure 26. Young's modulus measurements for YIG specimen G2F which experienced cyclic thermal shocked up to 1550 cycles (ΔT = 265 degrees Celsius).

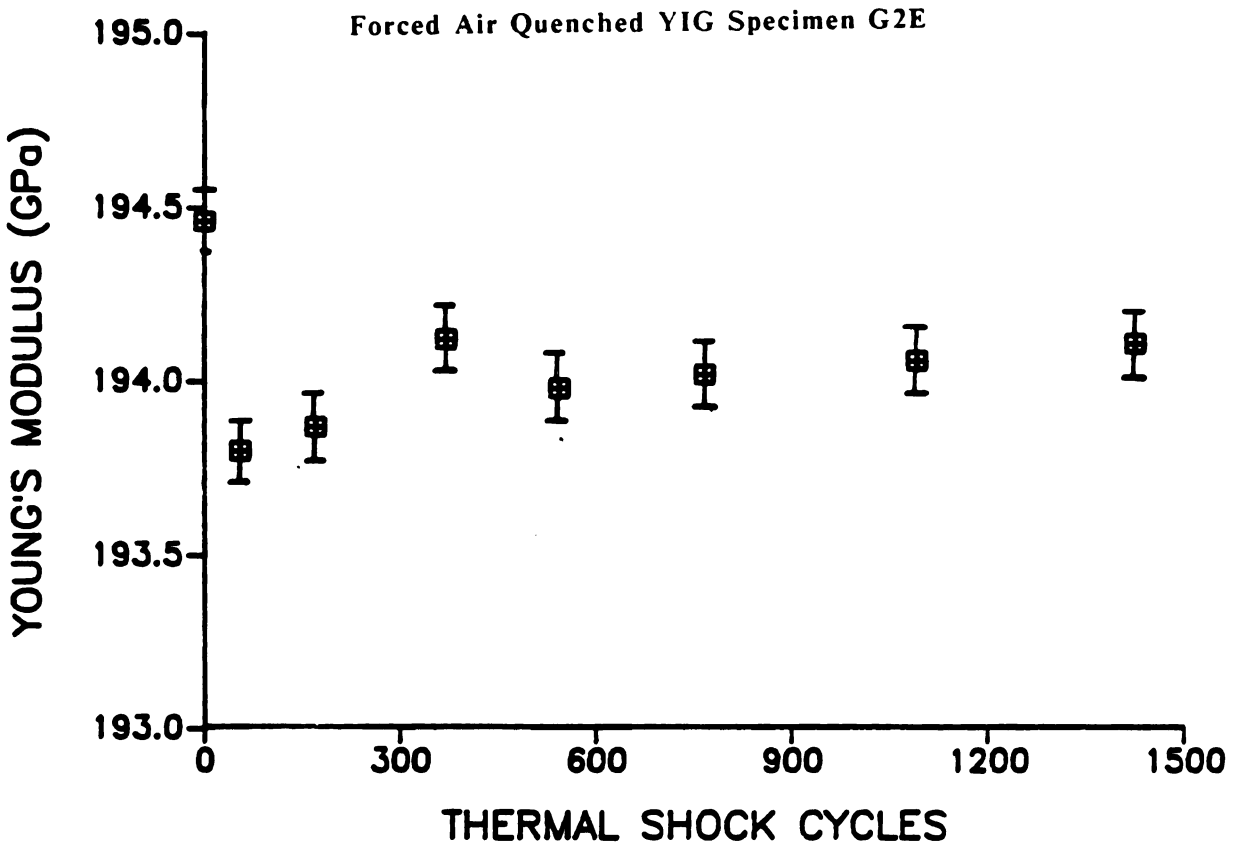

Figure 27. Young's modulus measurements for cyclic thermally shocked YIG specimen G2E (ΔT = 465 degrees Celsius).

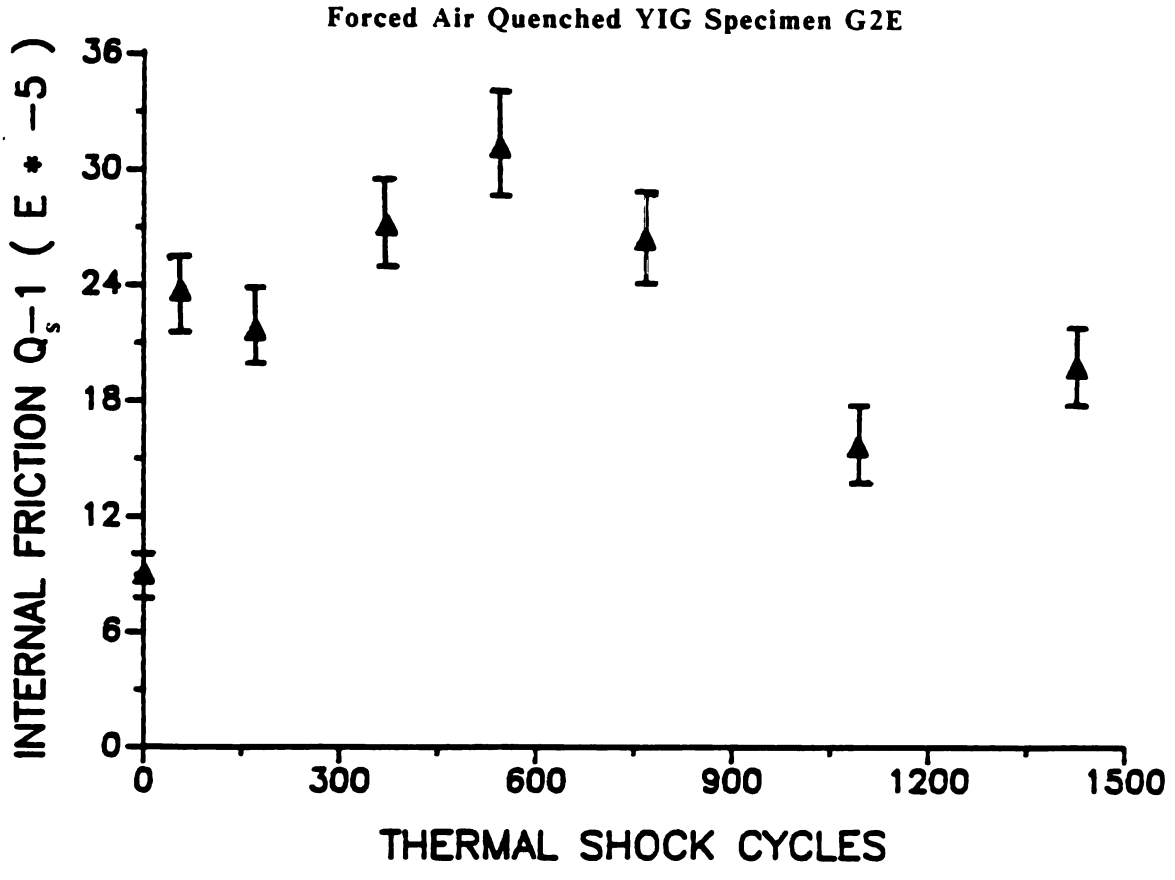

Figure 28. Internal friction measurements for cyclic thermally shocked YIG specimen G2E (ΔT = 465 degrees Celsius).

modulus decreased after cyclic thermal shock, with a maximum change of 0.4 percent E_0. On the other hand, the ΔQ^{-1} was about 200 percent higher than the internal friction of the pre-shock specimen. The decrease of internal friction after 600 thermal shock cycles may be caused by the involvement of time-dependent internal friction measurements if the time-dependent crack healing occurs in the air shocked specimen. All of the internal friction measured for specimen G2E was done after the specimen was taken out of the thermal fatigue apparatus and set at room temperature for two hours. The internal friction was measured during the third hour after the thermal fatigue test. The reason to do so is to avoid the possible time-dependent internal friction measurement. However, if the time-dependent internal friction measurement does occur and is still effective after the second hour, the internal friction measurement for specimen G2E may not reflect the actual crack damage level. More work is needed to explain this internal friction decrease.

The ΔE and ΔQ^{-1} for YIG specimens G2A and G2F, which experienced cyclic thermal shock at shock severity, ΔT, of 465 degrees Celsius and 265 degrees Celsius, respectively, showed the following behavior: (1) The Young's modulus did not change significantly for the cyclic thermally shocked YIG, even for ΔT = 465 degrees Celsius. 2) The internal friction of the higher ΔT increased faster. For example, the internal friction of specimen G2A which experienced ΔT = 265 degrees Celsius increased to 3.0×10^{-4} after 2500 thermal shock cycles. However, it took about 500 thermal shock cycles for the G2E specimen which experienced ΔT = 465 degrees Celsius to reach the same internal

friction value. 3) The change of internal friction is so sensitive that it could be a powerful technique to assess the crack damage due to cyclic thermal shock.

3.4 Time-Dependent Elastic Modulus Recovery

3.4.1 Microcracking Induced Young's Modulus Decrement

The relation between microcracking and the effective macroscopic elastic moduli of ceramics and geological materials* has been established in numerous experimental and theoretical studies [54, 55 and 62-73]. For example, the decrement in Young's modulus that accompanies microcracking can be expressed in an equation of the form [54 and 55]

$$E = E_0 [1-f(\upsilon)Na^3] \qquad (13)$$

where E - the effective Young's modulus for the microcracked body,

E_0 - the modulus for the non-microcracked (undamaged) body,

N - the number density of microcracks of mean radius a,

$f(\upsilon)$ - a function of Poisson's ratio υ.

The product Na^3 is called the crack density or the crack damage parameter, which shall be denoted here as j.

---

* The overall, macroscopic elastic moduli for a body decreases as cracks or voids are introduced, while the localized moduli remain constant for a fixed temperature and stress state.

Expressions similar to equation (13), which also depend on the crack damage parameter, j, have been developed for microcrack populations that are not randomly distributed, but rather have some preferred spatial orientation [71-73].

While many of the microcracking-elastic modulus studies have involved microcracking due to thermal expansion mismatch between crystallographic phases or due to thermal expansion anisotropy in a single phase ceramic [65-70], few studies have utilized elasticity or internal friction data as indicators of microcrack damage resulting from thermal shock [21, 22 and 30].

A study of the thermal shock of slagging coal gasifier refractory bricks [30] showed a drop in elastic modulus that coincided with a drop in residual strength.

Polycrystalline alumina, thermally shocked via a single quench into a water bath, exhibited a decreasing Young's modulus with increasing temperature difference, ΔT, of thermal shock [22]. Although these studies do qualitatively correlate a decrement in modulus with thermal shock damage, the studies failed to utilize the considerable information potentially available from analyzing the changes in elastic modulus in terms of the damage parameter, j, in equation (13) above.

3.4.2 Time-Dependent Young's Modulus Recovery Measurement

In this study, the elastic moduli of thermally shocked polycrystalline yttrium iron garnet (YIG) were measured for a total of

14 specimens. An unexpected, time-dependent recovery in elastic modulus was observed for thermally shocked specimens with low levels, $\Delta E \approx 0.01\ E_0$, of microcrack damage.

Prior to the first thermal shock treatment for specimens in this study, the undamaged Young's and shear moduli, E_0 and G_0 respectively, were measured for each of the YIG specimens. Following thermal quenching into a room temperature water bath, the Young's and shear moduli measurements were repeated. For a temperature difference, ΔT, of 165 degrees Celsius between the furnace temperature and the temperature of the water bath, a thermal shock damage induced decrement in modulus, ΔE, of about $0.01E_0$ was observed.

At these low levels of thermal shock damage ($\Delta E = 0.01E_0$) the value of the elastic modulus decrement was found to decrease with time, so that for time intervals on the order of a few hours after the thermal shock, the elastic and shear moduli had recovered to their pre-shocked values. Examples of the recovery in Young's modulus are shown in figures 29-32.

Equation (14), which was derived from modulus-microcracking theory [54 and 55] and the assumption of a linear crack healing (closure) rate, analytically describes the recovery of the elastic modulus as a function of time, t.

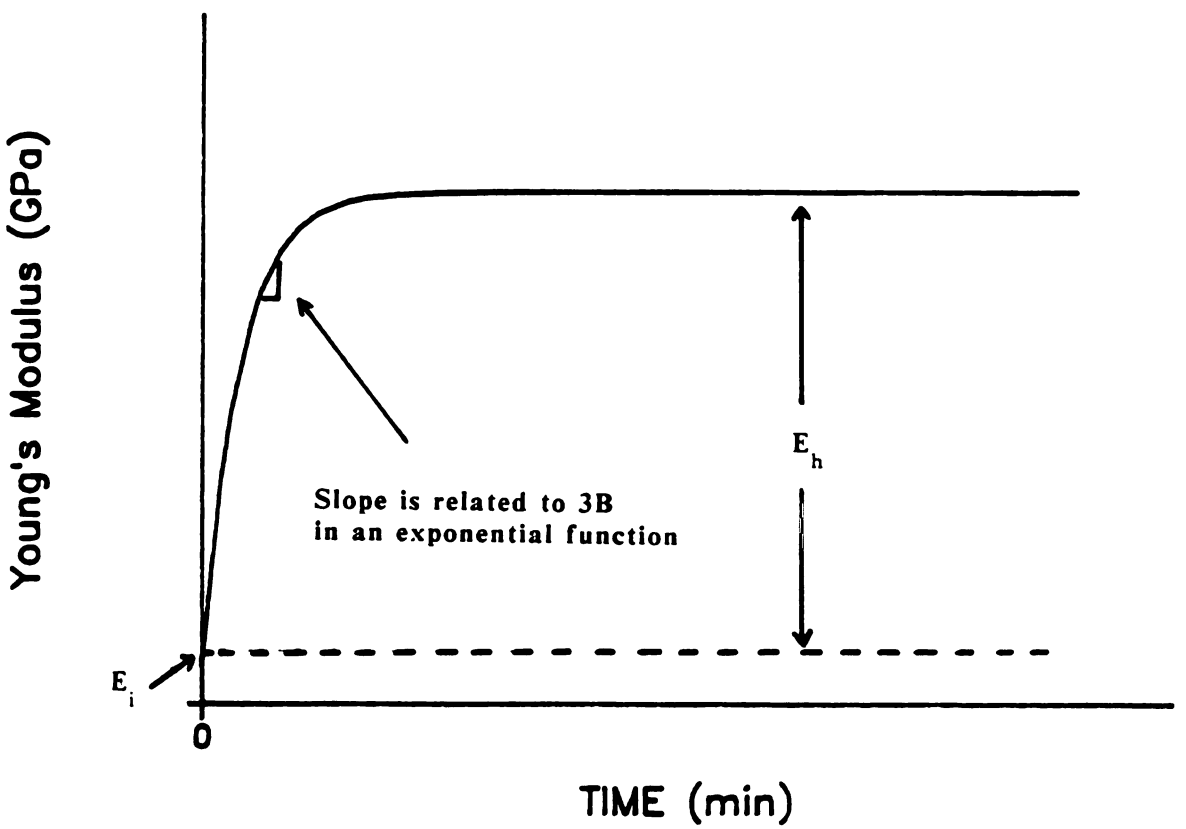

Figure 29. Schematic of the time-dependent Young's modulus recovery.

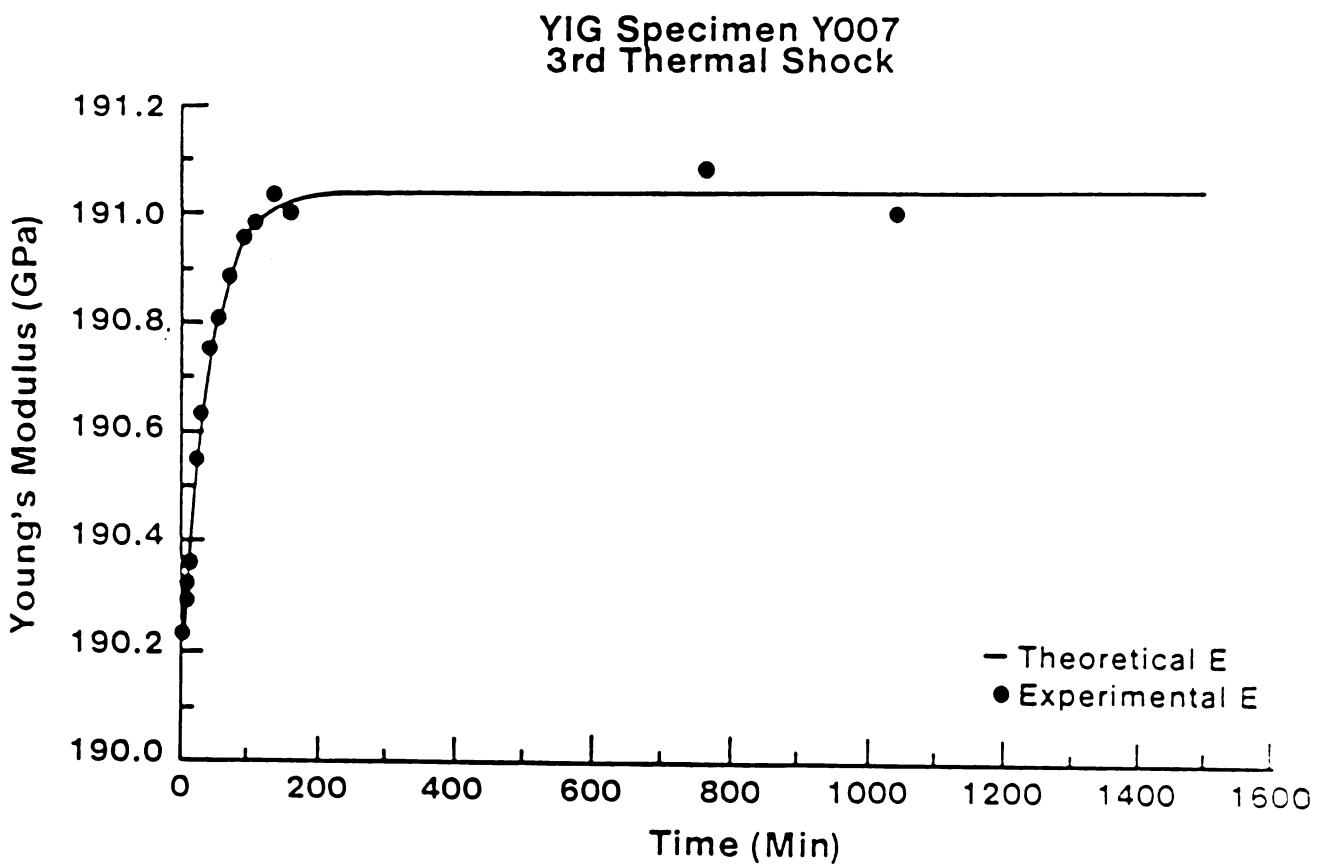

Figure 30. Young's modulus versus time for the third thermal shock cycle of yttrium iron garnet (YIG) specimen Y007. The solid line indicates the least-squares best fit of the data to equation 14.

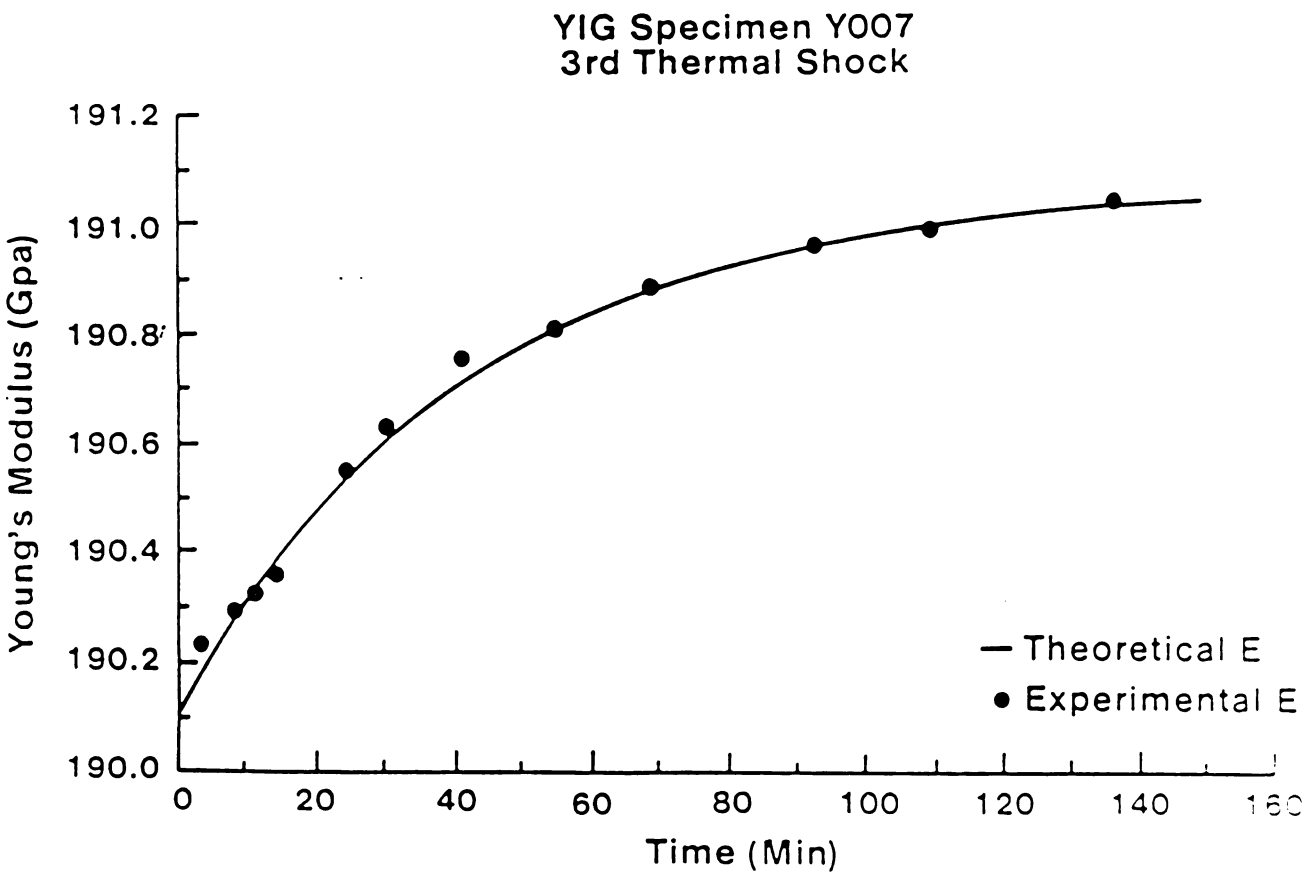

Figure 31. Young's modulus versus time behavior for the time regime up to about 160 minutes of elapsed time following the third thermal shock of specimen Y007. This figure shows the details of the short-time regime fitting to equation 14, where the entire set of data for the third shock of specimen Y007 is given in figure 30.

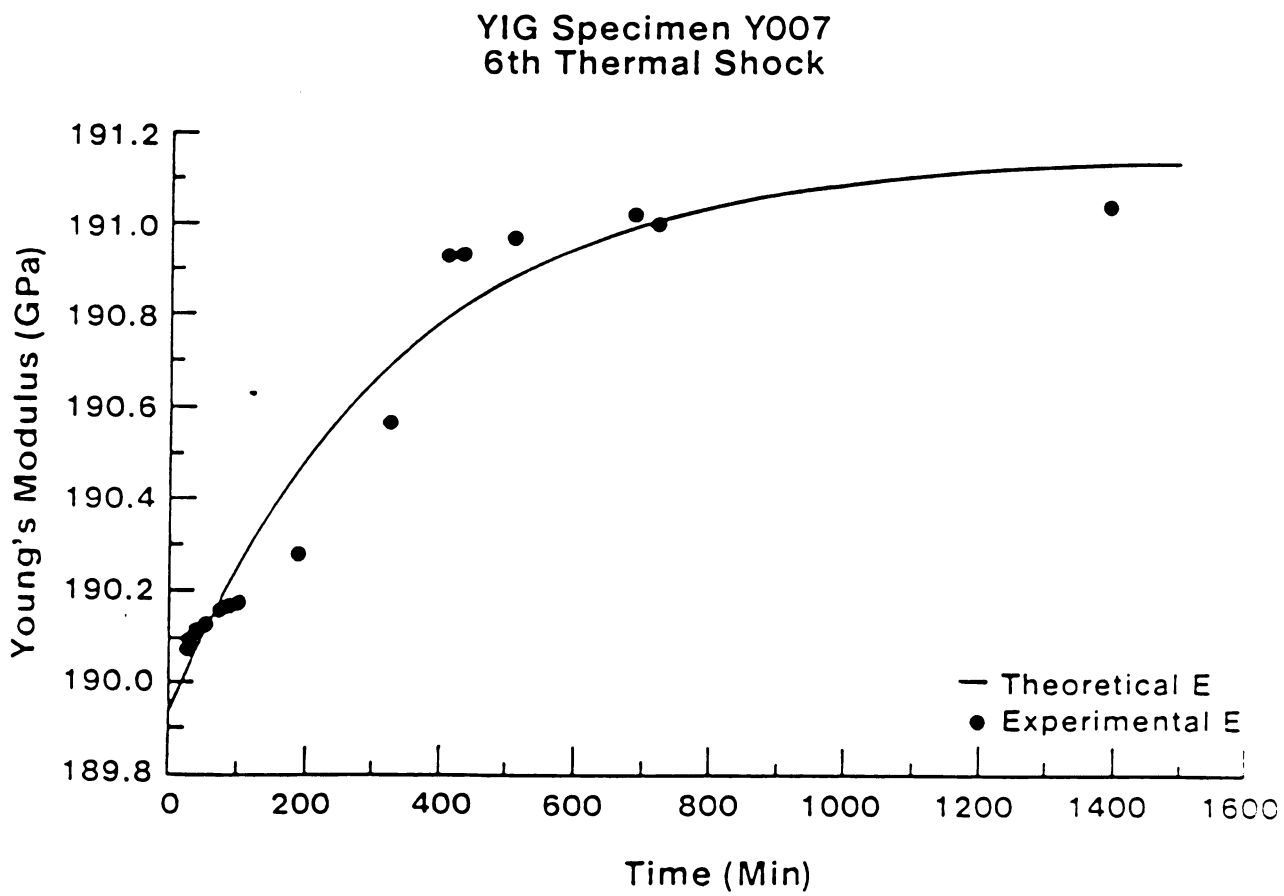

Figure 32. Young's modulus versus time behavior of the sixth thermal shock of specimen Y007. Comparison with figure 30 demonstrates a decreased healing rate with an increasing thermal shock cycle number.

$$E(t) = E_i + E_h \{1 - \exp(-3Bt)\} \qquad (14)$$

where E_i = the Young's modulus at time t = 0, which corresponds to the value of E immediately following the thermal quench.

E_h = the increase in Young's modulus from the time t = 0 until the modulus reaches a steady state value.

The elastic modulus versus time data for the lightly shocked YIG specimens was fitted to equation (14) via a non-linear least-squares fitting program. The least squares fitted form of equation (14) is shown as solid curves in figures 30-32. In each case, equation (14) was found to describe the time dependence of the data quite well, with a typical correlation coefficient of 0.98 or greater.

The physical mechanism giving rise to the observed modulus recovery has not been elucidated yet. However, control experiments were performed to determine whether the effect was related to the specimen or to the measuring system.

A YIG specimen which had never been thermally shocked and a specimen that had already undergone seven thermal shock cycles were "quenched" into a water bath with threads attached for each case, where ΔT was set to zero (that is, specimens at room temperature were placed into a water bath at room temperature). All other aspects of the experimental procedure were identical to the thermal shock tests for nonzero ΔT. For the previously unshocked YIG specimen, the measured elastic moduli did not change as a function of time. Thus, for an undamaged YIG specimen, the process of immersing the specimen

and support threads in water did not induce a time-dependent change in elastic modulus. The previously shocked YIG specimen exhibited a modulus increase of 0.2 GPa for the zero ΔT treatment compared to changes of up to 1.1 Gpa for nonzero ΔT treatments. These experiments indicate that the time-dependent factor in the elastic moduli was not due to the effect of the wetting of the specimens or the suspension threads.

In addition to the zero ΔT experiments on the YIG specimens, thermal shock trials were done on a polycrystalline copper specimen with dimensions of $7.9 \times 1.9 \times 0.17$ cm. (No microcracking was anticipated for the copper specimen, since copper is ductile.) Using an identical thermal shocking procedure such as that used on the YIG specimens, the copper specimen was quenched with ΔT values of zero, 170 degrees Celsius and 175 degrees Celsius. In each case the Young's modulus was independent of time, as would be expected in the absence of thermal shock induced damage. The copper specimen results thus also indicate that wetting of the specimens and the suspension threads have little affect on the time-dependent modulus.

In order to determine if the glue by which support threads were attached to the specimens had an effect on the measured moduli, the following experiments were performed. YIG specimens which had not been thermally fatigued were thermally shocked with ΔT = 165, 185, 205, 245 degrees Celsius, but without glue applied on the specimens or the threads. Then, the specimens were quickly attached to the threads and the elastic moduli were measured. The modulus recovery with time also was observed in each case with correlation coefficient ≥ 0.96.

Both the time dependence and the magnitude of the elastic modulus recovery were essentially the same for the glued specimens and the specimens to which glue was never applied.

These control experiments indicate that the time dependent changes in the elastic moduli are in fact related to time dependent changes in the thermal shock damage state of the YIG specimens.

As specimens were thermally cycled repeatedly, it was found that the time constant 3B in equation (14) varied as a function of the thermal shock cycle number (figure 33). For specimens that had their edges beveled, 3B tended to decrease in a nearly linear manner for the second through the eighth or ninth thermal shock. (As 3B decreases, a longer time is needed for the modulus to recover to its pre-shocked value.) For the initial thermal shock, at $\Delta T \geq 165$ degrees Celsius, a drop in modulus was not observed following the thermal shock, so that the modulus prior to the thermal shock and the modulus after the initial thermal shock were essentially identical. This could indicate that either the time constant 3B was very large for the initial thermal shock on the edge-beveled specimens, or that in fact no thermal shock damage did occur for the first thermal shock of the beveled specimens. For the absolute value of the time constants, 3B, sufficiently large, the elastic modulus might fully recover during the 4 minutes that typically elapsed from the instant of thermal shock until the modulus measurement. For specimens with untreated edges (edges not beveled), the value of time constant 3B also generally (but not always) decreased with cycle number (figure 33).

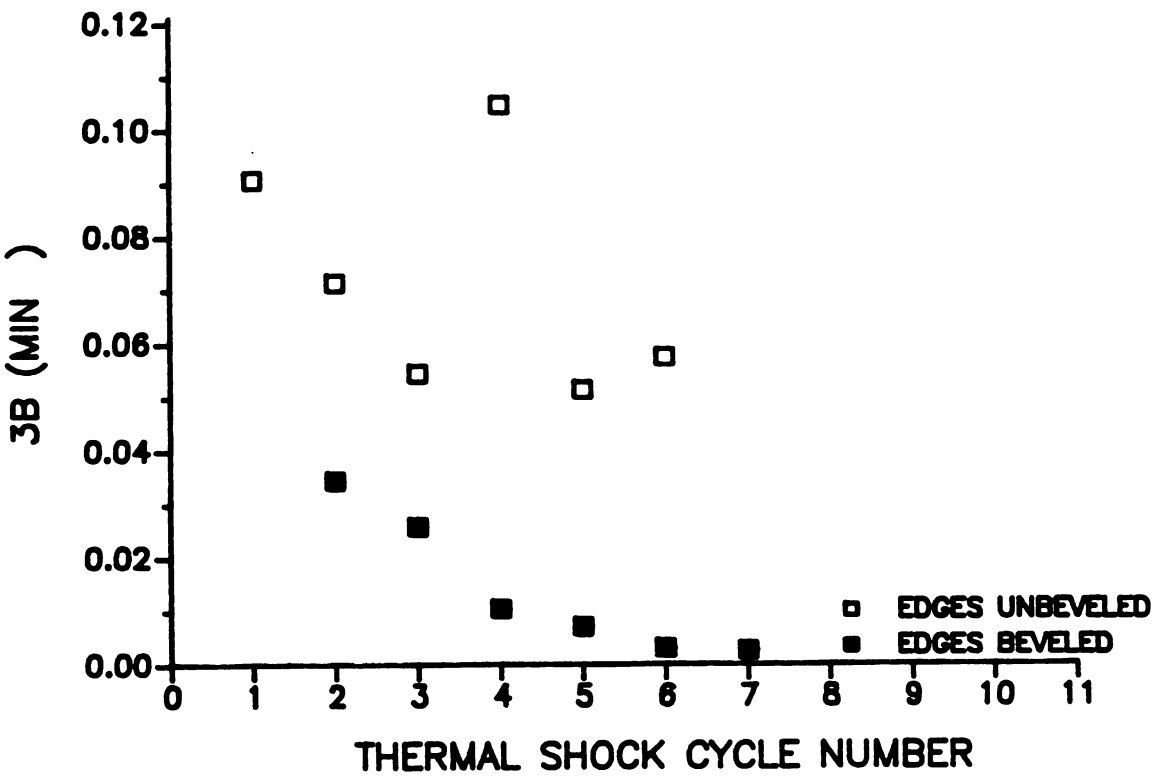

Figure 33. Time constant 3B (from equation 14) as a function of thermal shock cycle number for two YIG specimens, one specimen having unbeveled edges and one having beveled edges.

3.4.3 Modulus Recovery Mechanism

To the author's knowledge, a time-dependent recovery in the elastic modulus of a thermally shocked material has not been reported previously. It must be emphasized that the majority of thermal shock studies utilize residual fracture strength to characterize thermal shock damage. The Young's modulus recovery effect observed in this study involving specimens with relatively low levels of thermal shock damage likely would be hidden in the scatter of the fracture data. However, other researchers have noted crack healing in ceramic materials, at room temperature, even when the crack faces have been exposed to air or distilled water. For example, when studying the adhesion of mica sheets in room air, Bailey [74] noted that, "a greatly reduced value of adhesion was obtained if the sheets had been in contact for less than about 20 seconds. This reduction could be as great as 50 percent. If the specimens were left together longer than this, the full value for adhesion was always observed, even if they had been separated for as long as 10 minutes." Crack healing also has been observed in NaCl and LiF [75 and 76], KCl and NaF [76], glass [77 and 78], Ge and Si [79 and 80].

Quantitative studies of crack closure and crack reopening forces have been performed on a number of glassy materials including soda-lime-silica glass [81 and 82], vitreous silica [81 and 82], borosilicate glass [82], and glassy epoxy resin [82]. Although these studies involve quasistatic mechanical loading instead of thermal loading, the results are sufficiently interesting to be discussed here

in some detail. Stavrinidis and Holloway [81] used a double torsion apparatus to propagate and repropagate cracks in their glassy specimens, while Michalske and Fuller [82] used double-cleavage drilled-compression specimens in their study. In both studies [81 and 82], a mechanical load was initially applied to the specimen in order to propagate the crack, and the load was subsequently reduced to permit crack closure. A mechanical load was then reapplied to repropagate the crack. For each of the materials in both studies [81 and 82], a small crack closure force was observed that corresponded to a strain energy release rate of about 0.15 joules per square meter (thus at low quasistatic load levels, the cracks tended to "pull" themselves closed). The strain energy release rate for crack repropagation under a reapplied load was found to be as high as 1.7 joules per square meter for soda-lime-silica glass, for example, which is about 20 percent of the magnitude of the strain energy release rate needed to propagate a crack in virgin glass [82]. Both Stavrinidis and Holloway [81] and Michalske and Fuller [82] found that crack closure forces increased with the relative humidity of the ambient environment. Michalske and Fuller present a model based on hydrogen bonding across the crack surfaces that fits the data quite well for a range of relative humidity from nearly zero to 100 percent. Michalske and Fuller also propose that once the crack surfaces have closed, the relatively high crack repropagation energies stem from developing cationic bridging or siloxane bridging across the crack surfaces [82].

The modulus recovery in thermally shocked YIG specimens observed in this study likely has a similar origin to the crack healing

observed by Stavrinidis and Holloway and [81] Michalske and Fuller [82] in their quasistatic loading of oxide glasses and epoxy. Appendix A contains a further discussion and a derivation of the modulus-recovery relationship given in equation (14). The dependence of the modulus recovery (crack healing) rate upon the thermal cycle number (figure 33) may relate to a chemical reaction product, such as a hydrate, that is formed upon the initial exposure of the freshly cracked surfaces of the YIG specimens to water vapor (or the water in the quenching bath). Fresh crack faces are known to be very reactive chemically, even at room temperature [81 and 82]. One of the two crack closure mechanisms might result in the observed modulus recovery: a hydrate may form that helps to "heal" the crack, or water molecules in a nearly closed crack diffuse out of the crack in time allowing at least partial crack closure. The composition of the possible hydrate form is still not clear. However, a 1 to 3 M NaOH solvent has been used for growing single crystals of YIG [83]. The YIG crystal growth process was under high pressure, 200 to 1350 atm, and moderately high temperature, 400 to 750 degrees Celsius [83]. This indicates at least that YIG powders may form hydrate in a base solution. However, the microscopic reaction may not be the same as the macroscopic reactions. For example, glass is very "inert" (extremely low solubility) to water, however, the fracture strength of glass rapidly decrease due to the atomic interactions between the water molecules and highly stressed silicon-oxygen bonds at crack tips in silica glass [84 and 85]. This phenomena is known as crack-tip water corrosion [84 and 85]. Therefore, the formation of YIG hydrate

on the crack surfaces is not necessarily the same as the reaction between the powders and solution. The author will like to take the mechanism investigation of crack healing mechanism as further studies.

3.4.4 Comparison of the Strength and the Young's Modulus of Crack Healed Specimens

The retained strengths of the repeated thermally shocked YIG specimen were measured by three point bend method in air at room temperature. Strength degradations were observed for all tested YIG specimens when Young's moduli had recovered to essentially their value prior to the first thermal shock. The retained strength was about 50 to 70 percent of the pre-shocked strength. The reason that the strength degradations were not reflected by the Young's modulus measured for thermally shock specimens could be that the properties measured by the techniques are intrinsically different since the sonic modulus is a very low strain experiment and fracture tests involve strain-to-failure.

For brittle materials, such as ceramics, the strength measured by bending methods may reflect only the critical flaw in the specimen. The cracks which propagate during a thermal shock may develop into macrocracks and cause fracture to the specimen when subjected to a bending stress. The retained strength in most of the thermal shock literature [2-7,24-26] was measured by three or four point bending methods.

On the other hand, the modulus measured is related to the forces

between atoms and the atomic binding energy of a sample. The change of elasticity reflects the entire spectrum of the flaw density and flaw size in a specimen. If cracks are assumed to act as a second phase in the test specimen, the overall modu phase in the test the "rule of mixtures" which can be expressed as [86]

$$E_{tot} = E_1 V_1 + E_2 V_2 \qquad (15)$$
$$= E_1 V_1 + E_2 (1 - V_1)$$

where E_{tot} - the overall modulus for two phases

E_1 - modulus of phase I

E_2 - modulus of phase II

V_1 - Volume fraction of phase I

V_2 - Volume fraction of phase II, $(V_1 + V_2 = 1)$

Let us label the YIG matrix as phase I, and the hydrate form as phase II. The volume fraction of the hydrate phase, which is proportional to crack displacements, will be extremely small compared to the matrix. In addition, the hydrate phase was supposed relatively low in strength compared to YIG specimen. Thus, it is reasonable to assume $E_2 = 0.0001\ E_1$, and $V_2 = 0.0001\ V_1$. The E_{tot} calculated according to Equation (14) is $0.9999\ E_1$ which means the change of Young's modulus (ΔE) is only $10^{-4}\ E_1$. Such a small change of Young's modulus is not measurable experimentally. Therefore, for the model of the "hydrate filled" cracks, the shock damage reflected by degradation of strength will not be detected by Young's modulus measurements, particularly for the modulus recovered specimen. However, this does not mean that

modulus measurement is limited or impractical in assessing thermal shock damage. Elasticity measurement can be used to evaluate the crack damage parameter. The elastic modulus also can characterize repeated thermal shock damage [56], especially for homogeneous low level damage.

3.4.5 Factors Affecting the Elastic Modulus Recovery Rate

Stavrinidis and Holloway [81] and Michalske and Fuller [82] found that water played the central role in the crack healing for several glassy materials at room temperature. The proposed Young's modulus recovery mechanism for thermally shocked YIG specimens was a "hydrate phase" formed on the fresh crack surfaces (details are given in Section 3.3.3). The hydrate phase may function as an adhesive compound, such as a glue, whose adhesion is time dependent according to its reaction rate with the YIG crack surfaces. The hydrate phase will reach its full strength after a period of setting time. The response of the crack surfaces to this adhesive reaction was assumed to be the result of the time-dependent crack closures for the YIG specimens. This model reasonably explains the observed time-dependent Young's modulus recovery phenomenon.

However, the fracture test of three thermally shocked YIG specimens shows that the strength decreases up to 50 percent of the preshocked strength value even though the elastic modulus was almost 100 percent recovered. The hydrate phase is therefore relatively weak, and the thermal shock induced cracks were reopened in the

fracture test. Similarly, the cracks are likely to reopen for a subsequent thermal shock cycle. Since the healing rate is usually slower after repeated thermal shock cycling, the author will assume a cracking healing model to explain this decreasing healing rate. The thermal shock induced hydrate phase working as an adhesive compound may lose its adhesion for a crack reopening process, and the binding between the crack surface and the hydrate phase may be separated. It is then the newly formed "hydrate phase", which is active in adhesion, that helps the healing process. However, the diffusion of the reactants, such as water, through the "dirty" hydrate layers to produce the active hydrate phase becomes slower due to the accumulation of hydrate phase. More accumulation of the hydrate phase will make the diffusion slower. The slow diffusion rate of the reactant may decrease the crack healing rate, which may in term decrease the modulus recovery rate.

Another cause for the slowing of the modulus recovery rate with repeat cycling may be the hindrance of crack closure between differently orientated cracks. The directions of the thermal shock induced thermal stress on the YIG specimens may vary from one thermal shock cycle to another based on how the specimens are shocked. For example, the induced thermal stress may be quite different for each thermal shock due to the various directions that the specimen may immerse into a liquid bath. The author might not always have immersed the YIG specimens into the water bath in the same direction for every thermal shock cycle in this study, and the different direction of the induced thermal stress may cause different crack orientations. The

thermal shock induced residual stress in glass slides was observed in different orientation [87]. Thus, the possible crack orientations may increase for each additional thermal shock cycle due to the various direction of induced thermal stress. Since the possible crack orientations are increased by every repetitive thermal cycling, the crack closure in one orientation may hinder the crack closure in different orientations. The possibility that the differently oriented cracks close at the same moment may be a factor which determines the healing rate. In general, the increase in possible crack orientations and the accumulation of the hydrate phase in them may make the modulus recovery rate slower.

Furthermore, the decreasing healing rate for the increasing thermal shock cycles on the edge beveled specimens was not seen on the edge unbeveled specimens. The basic difference between the edge beveled and edge unbeveled specimens is that the edge unbeveled specimens usually include many edge flaws, and the edge beveled specimens may eliminated some of the edge flaws [88]. The critical flaws in a ceramic specimen are often edge flaws induced by the cutting process [89]. Chipping and cracking are the two main features that the cutting process usually produce, no matter how carefully the cutting proceeds. The edge flaws are assumed to play an important role in the cracking-healing mechanism. Let us first consider the crack opening for the thermally shocked specimens. The cracks opened in a repeated thermal shock involve the opening of newly formed cracks and the reopening or extension of cracks generated by previous thermal shock cycles. The crack healing observed in the present study likely

includes the closure of both new and old cracks. The crack healing of a YIG specimen after its first thermal shock is mainly the closure of the newly formed cracks. For the YIG specimens with beveled edges, the observed healing rate, da/dt, for the first thermal shock was larger than the healing rate observed for the specimen that was repeatedly thermally shocked. Therefore, the healing rate of thermally shocked specimens depends on the contributions from the closure rate of both the new and the old cracks. According to equation (A7) in the Appendix section, the healing rate, da/dt, is proportional to the the average crack length, a, with no influence due to the crack density.

For the edge beveled specimens, thermal shock may cause the reopening of the old cracks and new cracks induced by surface flaws. On the other hand, the cracks opened in unbeveled specimens subjected to repeated thermal shock may include the old cracks and many large and long newly formed cracks which are induced by the edge flaws. The edge flaws are usually easier to propagate than the surface flaws when the specimen was subjected to thermal shock. The comparison of the drop of Young's modulus shows that the damage level of an unbeveled specimen is usually larger than those of a beveled specimen. This could be explained by comparing the stress intensity factor, K_I, for the specimens with edge flaws and surface flaws. The resistance to crack growth for a ceramic material can be approximated in terms of stress field near a crack tip [83]. The higher stress intensity factor will result in easier crack propagation. In order to compare the stress intensity factor, K_I, of the edge flaws and surface flaws,

an ideal orientation of the crack with a simple opening mode is considered. With the crack length, a, the stress intensity factor of the edge crack, K_I, could be treated as a semicircular corner crack [90] subject to a uniaxial tensile stress, σ, perpendicular to the crack surface. The calculated K_I is 0.799 $\sigma\sqrt{\pi a}$. If one applies 1.5 as the flaw shape parameter [90] and using the same crack length, a the stress intensity factor of the surface crack is 0.577 $\sigma\sqrt{\pi a}$, where σ is the remote normal stress acting on the specimen and a is the crack length. This simplified comparison shows that the K_I of the specimen with an edge flaw is much larger than the K_I of the specimen with the same size surface flaw. Thus, the edge flaws have smaller resistance to crack propagation, and grow more easily. Based on the previous arguments of the healing rate dependence, the newly formed edge-flaw-induced cracks are assumed to heal faster than the old cracks (see Appendix D). Thus, after several thermal shock cycles, the edge flaws induced new cracks in an edge unbeveled specimen may significantly influence the healing rate. For example, the total healing rate may be larger than the healing rate predicted by. Figure 34 shows the influence of the newly formed cracks on the total cracking healing rate. Therefore, the decreasing trend of the healing rate, 3B, for an edge beveled specimen may not be observed for an edge unbeveled specimen.

Since the change in internal friction is very sensitive to cracking, Q^{-1} and E were measured for a Gd-doped YIG specimen before- and after- the edges were beveled to investigate the details of the influence of the edge flaws on Q^{-1} and E. The internal friction

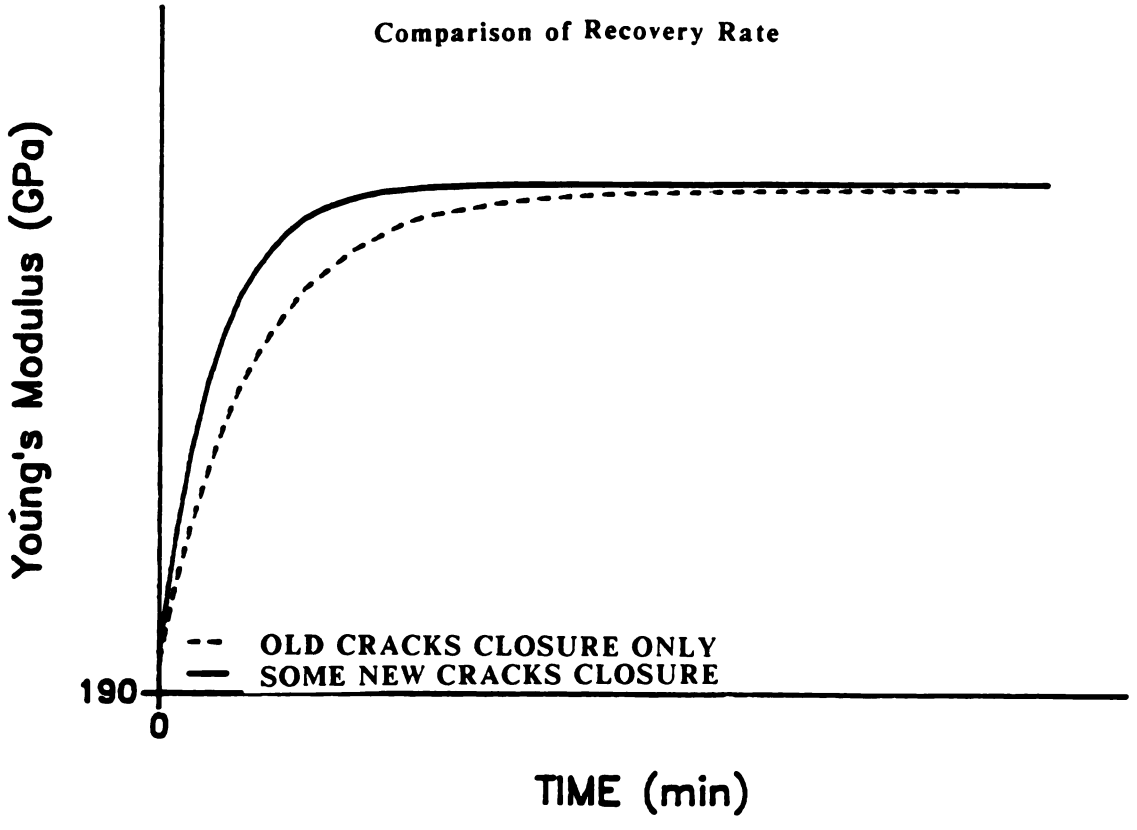

Figure 34. Comparison of the Young's modulus versus time relationship for (1) closure of the old cracks only, (2) closure of both old and new cracks.

decreased considerably after the YIG specimen was edge-beveled. The reduction of edge flaws by carefully polishing the specimen may be the reason that the internal friction decreases for the YIG specimen. On the other hand, Young's modulus did not change for the edge beveled specimens. Striking differences between the beveled and the unbeveled specimens include the rate at which crack healing occurred, the magnitude of the drop in modulus due to thermal shock, and the fact that the initial thermal shock for the unbeveled specimen did show an observable time-dependent recovery in the elastic moduli.

3.5 Details of Quenching Experiments

The thermal shock quench media used by several researchers include water [4,17, 20-30], air [21,30 and 36], oil [38], liquid nitrogen [39] and liquid metals [38].

Water is the most common quench medium. As a quench medium water has several advantages: 1) good heat transfer coefficient ($h \approx 1.0$ $cal/sec \cdot cm^2 \cdot °C$), 2) both liquid water and vapor water are harmless (nontoxic), 3) specimens can be dried easily, 4) the fluid bath temperature is easy to control, particularly in the temperature range from zero to 100 degrees Celsius, 5) availability and economy.

However, any possible chemical reactions between the specimen and water needs to be understood to ensure reliable thermal shock characterization by water quench. Water can induce slow crack growth in brittle materials thereby reducing the specimen fracture strength and changing the elastic modulus and internal friction. For example,

the residual strength of shocked borosilicate glass measured while immersed in distilled water [39] is only about 50 percent of that measured in inert surroundings (liquid nitrogen). Most retained strength measurements are done in air so that trace amounts of water existing in the air or on the surface of the shocked ceramic specimens can potentially degrade residual strength. Furthermore, water may react with freshly opened cracks to form a hydrate phase or phases during a shock process. The hydrate presumably can influence crack closure and crack reopening during repeated thermal cycling.

For thermal shock experiments where a high heat-transfer coefficient is required, liquid metals (such as liquid sodium and mercury) have been used [38]. The heat-transfer coefficients of liquid metals may be larger by two orders of magnitude than the heat transfer coefficient of water [38]. Therefore the thermal stress induced by quenching in a liquid metal is usually larger than the thermal stress induced by a water quench. However, in practice, due to the difficulties and high cost of operation, quenching via liquid metal media is typically used only in a laboratory procedure.

Some researchers [39] have used a liquid nitrogen quenching bath. Liquid nitrogen at 77 degrees Kelvin as a quench medium provides a greater ΔT in thermal shock tests than does the water quench. Ashizuka, Easler and Bradt [39] commented that by using liquid nitrogen as the quench medium to shock borosilicate glass, the retained strength measured in liquid nitrogen represented the true strength degradation due to thermal shock. Slow crack growth which may occur in borosilicate glass during the strength measurement in the

presence of water is assumed not to occur during liquid nitrogen quenching.

Although the liquid nitrogen quench test offers greater ΔT in a thermal shock, the heat transfer phenomena between the shocked specimen and liquid nitrogen is complicated. When the hot specimen surfaces reach the liquid nitrogen bath, liquid nitrogen vaporizes immediately and forms gas bubbles. These nitrogen gas bubbles (produced around the specimen surfaces) become heat transfer barriers which significantly reduce the heat transfer efficiency between the specimen surface and the liquid nitrogen during the quench process. The sizes and concentration of such gas bubbles, and the time intervals over which the bubbles exist are difficult to measure. The shock damage parameter in liquid nitrogen is therefore difficult to estimate. Unless the production of gas nitrogen bubbles (and the bubbles' subsequent effect on the heat transfer properties) is well determined, the evaluated shock damage parameter may not be reliable. Thus, the thermal shock damage may be different for a different quench medium.

Air quenching [21,30 and 36] also is used for thermal shock testing. An excellent correlation between experimental results and calculated damage resistance parameter R'''' has been reported for the ribbon test for several commercial refractories. The ribbon test has drawn the interest of several researchers [21 and 30], so that it may be established as a new standard laboratory-scale thermal shock test for refractory materials. The specimen sizes typically used in a ribbon test are 22.8 cm by 2.54 cm as the area of hot face which is

directly heated by gas flame up to 1000 degrees Celsius. Specimen thicknesses of 2.54 cm, 5.72 cm and 11.43 cm provide different ΔT between the hot face and the cold face of the specimen. Thus the different specimen thicknesses induce differing thermal stress levels which can result in differing levels of thermal shock damage. Repeated thermal shock tests of refractory materials have utilized ribbon tests [21 and 30]. The damage parameters measured for specimens of different geometries are the retained Young's modulus versus thermal shock resistance parameter R''''. The general trend observed in ribbon tests is a decrease in the Young's modulus as a function of increasing numbers of shock cycles [21]. In particular, the Young's modulus of alumina refractories remained essentially constant for the fifth through the thirty-sixth thermal shock cycles [21]. For the first five shocks, the Young's modulus was measured after every shock because the change of modulus was relatively high. The modulus was measured later at intervals of several thermal shocks since the Young's modulus changed slowly after the first five shocks. Furthermore, since the maximum temperature of these ribbon tests [21] is very high (1000 degrees Celsius) crack healing may occur during the typical heating cycle. It should be noted, however, that Semler and Hawisher [21] do not discuss crack healing or suggest crack healing effects in any way. Thus, the crack propagation rate may be in equilibrium with the crack healing rate for each shock cycle after the fifth shock cycle.

Refractories usually have a relatively high volume fraction porosity, which in turn provides a high density of Griffith flaws.

Crack extensions due to cyclic thermal shock are likely arrested by these pre-existing pores during the repetitive cycling in the ribbon test. Unless higher thermal stress is provided, crack growth may not proceed. The fifth thermal shock in these ribbon tests may be considered as the stage that the crack arrest occurs when the refractories were subjected to repeated thermal loading. The assumption of crack arrest is consistent with the observed constant value of Young's modulus for the fifth through the thirty-sixth thermal cycle for the alumina refractory specimens [21].

The significance of studying different quench media can be derived into two aspects : (1) mechanics, and (2) material science (chemistry). The mechanics aspect mainly involves the calculation of thermal stress. For relatively low rates of surface-heat-transfer coefficients, such as air and oil, the maximum thermal stress can be expressed by [86].

$$\sigma_{max} = 0.31\ \beta = 0.31\ r_m h/k \qquad (16)$$

where β = Biot's modulus

r_m = half-thickness (radius of the specimen)

h = surface-heat-coefficient

k = thermal conductivity

For a severe thermal shock, such as might be experienced if the specimen is subjected to high rates of cooling via quenching in water or liquid metal, the maximum thermal stress can be expressed by [86].

$$\sigma_{max} = \frac{E\alpha\Delta T}{(1-\nu)} f(\beta) \qquad (17)$$

where $f(\beta)$ is Biot's factor.

The materials science aspect of the selection of the quench medium may be related to, for example, the time-dependent elastic modulus recovery of polycrystalline YIG shocked into water. The proposed crack healing mechanism for YIG is that a hydrate may form to help "heal" the crack, or water molecules in a nearly closed crack diffuse out of the crack in time allowing at least partial crack closure. In this study, oil quench was used to investigate this "hydrate-closure" mechanism. An oil quench medium helps to minimize chemical reaction, such as oxidation and hydration between the hot test specimen and quench medium. A YIG specimen, Y016LU, which had been thermally shocked in water once and shown elastic modulus recovery, was annealed at 950 degrees Celsius for 11 hours. Specimen Y016LU was then thermally shocked in oil at ΔT = 175 degrees Celsius. No time-dependent elastic modulus recovery was observed for the first three shocks. The measured flexural resonant frequency after each thermal shock of specimen Y016LU was about 2480.0 ± 1.5 Hz. This Y016LU specimen was then thermally shocked at a higher ΔT = 265 degrees Celsius in oil. The flexural resonant frequency decrease for 15 Hz, which corresponds the decrease of Young's modulus of 2.2 Gpa. The Young's modulus was not fully recovered for this thermal shock (figure 35). This YIG specimen was continued to be shocked for three times at ΔT = 265 degrees Celsius in oil. The Young's modulus measured after each of the three thermal shocks showed partial time-dependent modulus

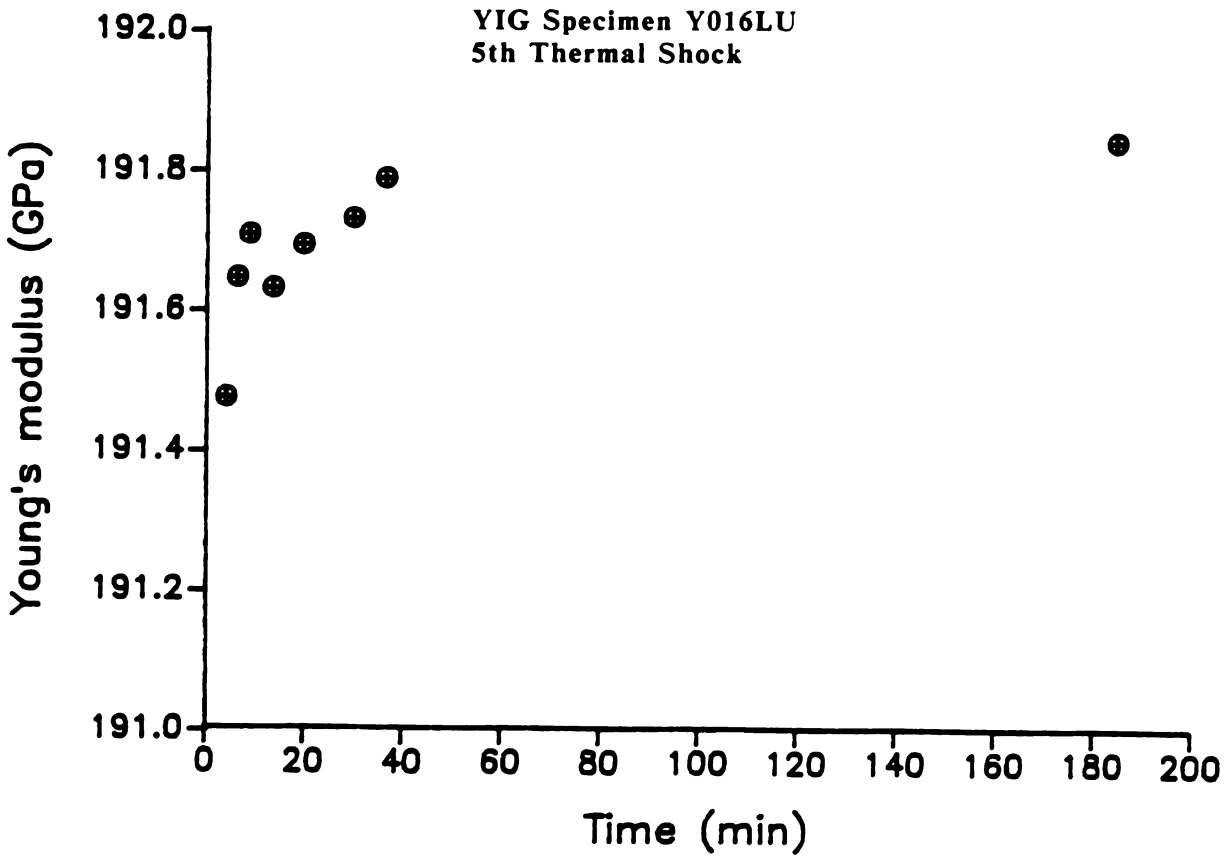

Figure 35. Young's modulus versus time for the fifth thermal shock cycle of yttrium iron garnet (YIG) specimen Y016LU. The specimen was quenched in oil (ΔT = 265 degrees Celsius).

recovery relationship. However a time-dependent elastic modulus recovery was observed for a Gd-doped YIG specimen following a thermal shock in an oil bath (see figures 36-39). Data for Young's modulus versus time were fit using equation (14), which was also used for the modulus-time recovery for the water-quenched specimens. For the oil quench, the modulus recovery-time data fit equation (14) with a correlation coefficient equal to or greater than 0.97. The healing parameter 3B for the oil quenched specimens was usually smaller than that of water quench when the same number of shock cycles were compared. However, the Young's modulus dropped below the first measured value ($E_t = 0$) within about 14 to 18 hours after the third thermal shock (figure 37).

In this oil quench test, no glue was applied to the specimen and the oil was carefully removed from the specimen surface by a paper towel. This helps to rule out the possibility that the glue may affect either the observed elastic modulus recovery or the decrease of elastic modulus following the recovery. However, the thin oil film that remains on the specimen surface could possibly cause a time-dependent effect. One YIG specimen, Y016LU, was immersed in oil without thermal shock for 30 seconds and then monitored by sonic resonant technique to investigate whether the oil film causes any time-dependent modulus recovery. The procedure to clean the oil from the specimen (Y016LU) surface after taking the specimen out of the oil bath was identical to the procedure that used for a thermally shocked specimen. However, the control specimen did not experience a thermal shock. The flexural resonant frequency changed 1.4 Hz within 800

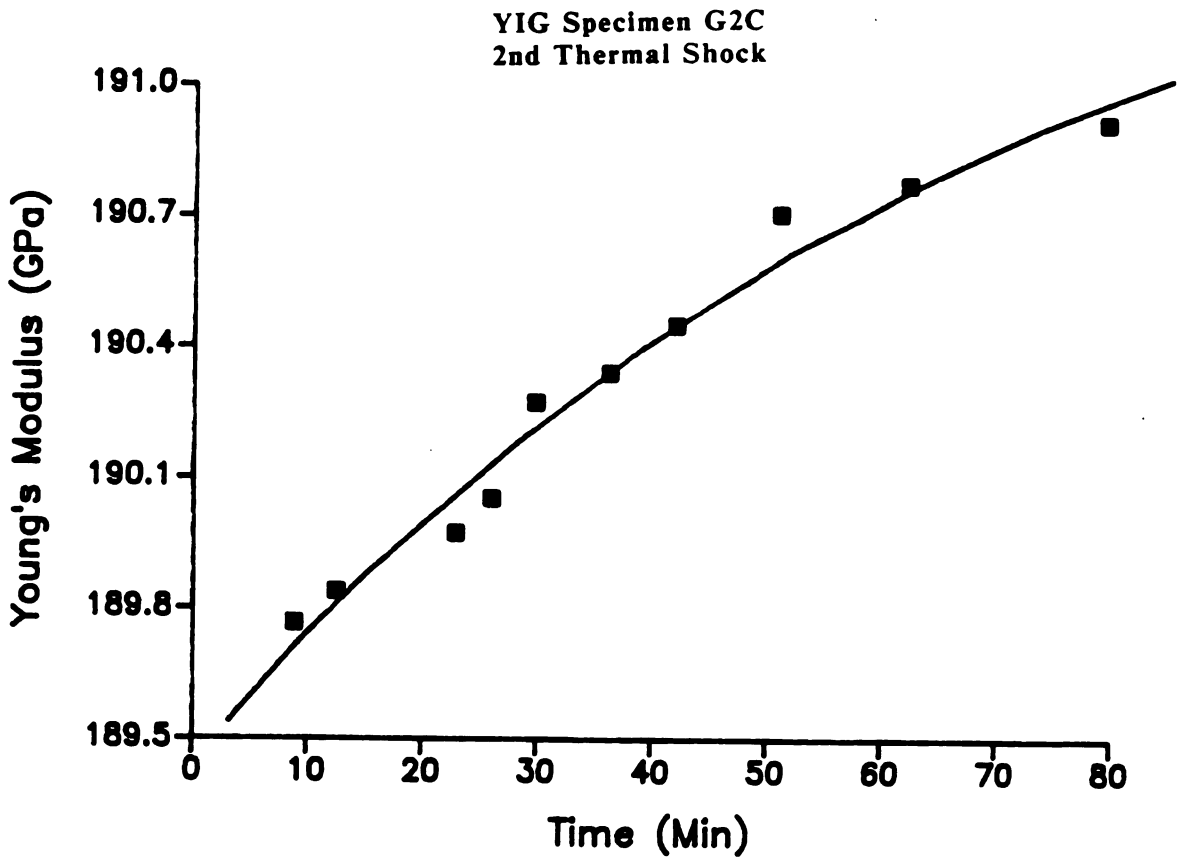

Figure 36. Young's modulus versus time for the second thermal shock cycle of yttrium iron garnet (YIG) specimen G2C in oil bath (ΔT = 265 degrees Celsius).

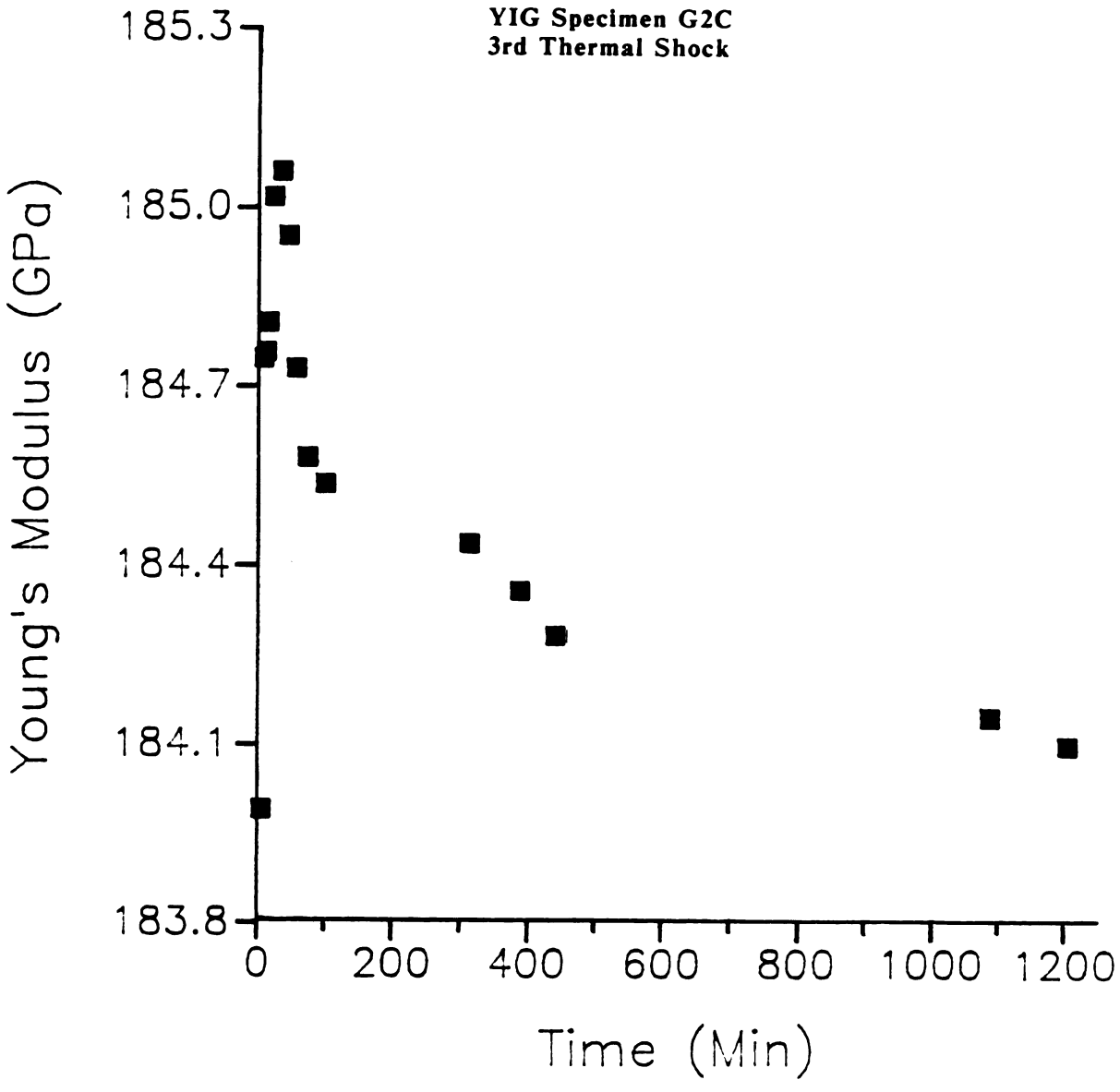

Figure 37. Young's modulus versus time for the third thermal shock cycle of yttrium iron garnet (YIG) specimen G2C in oil bath (ΔT = 265 degrees Celsius).

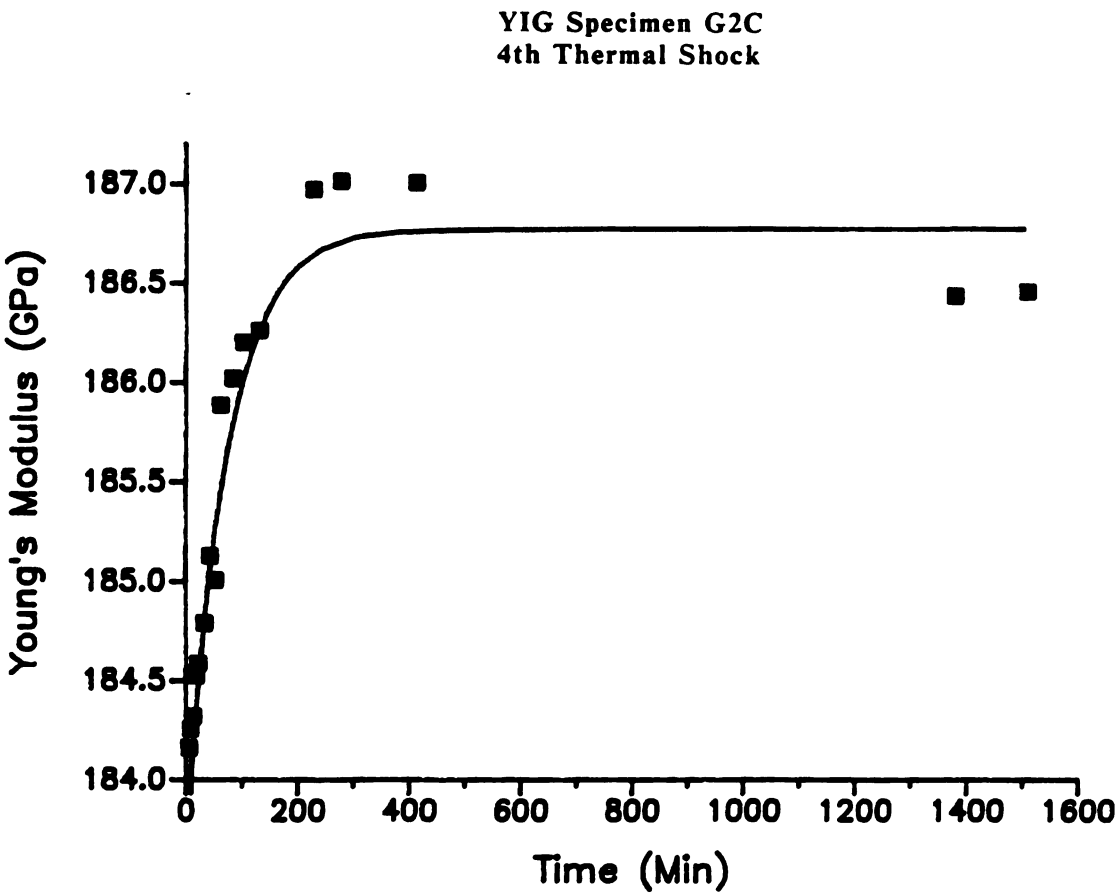

Figure 38. Young's modulus versus time behavior of the fourth thermal shock of specimen G2D in oil bath (ΔT = 265 degrees Celsius).

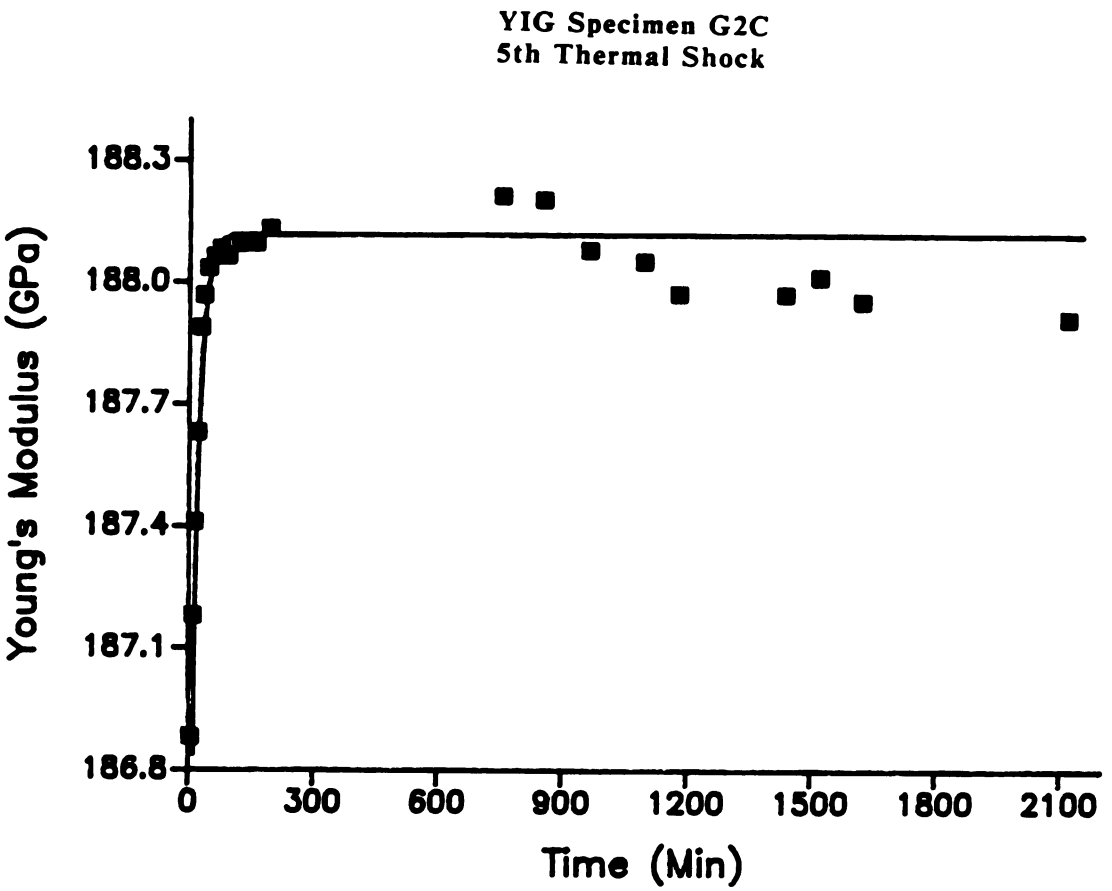

Figure 39. Young's modulus versus time behavior of the fifth thermal shock of specimen G2D in oil bath (ΔT = 265 degrees Celsius).

minutes. This indicated that the oil film on the surface does not significantly affect the time-dependent Young's modulus recovery for a specimen which experienced thermal shock in oil bath. The recovery and subsequent drop of Young's modulus in an oil quench test may be interpreted as two competing reactions that proceed after the specimens are subjected to a thermal shock in an oil bath. The time-dependent elastic recovery by a hydrate phase formed on the crack surfaces may be nullified by time-dependent oil diffusion into crack tips. The quenching oil could "kill" the hydrate and allow the closed cracks to reopen. In the oil quench tests, the difference that the Young's modulus recovery was not observed for no doped YIG specimen and it was observed for Gd-doped YIG specimen is still not fully understood.

One YIG specimen was thermally shocked in forced air with temperature differences of 250 and 450 degrees Celsius. The Young's modulus of the shocked specimen was measured in 4 to 6 minutes following the experimental procedures used for water and oil bath quench time-dependent elastic modulus recovery experiments. No obvious time effect for Young's modulus was observed for either of two air quenches. Further investigation of time-dependent effect in modulus of air quenched YIG specimens is needed.

A magnesium aluminate spinel specimen having dimensions 6.38 cm × 1.14 cm × 0.3 cm was thermally shocked in water to determine if ceramic materials other than YIG exhibit a time-dependent modulus change subsequent to thermal shock damage. Spinel specimen, S001, was glued with threads when the Young's modulus was monitored. Spinel exhibit time-dependent elastic recovery following a thermal shock

using a water quench at ΔT = 255 degrees Celsius (figure 40). Therefore, ceramic materials with two different compositions, YIG and spinel shows time-dependent elastic modulus recovery.

Since Michalske and Fuller [82] reported that the environmental relative humidity affected the crack closure of glass specimens, the humidity dependence of the Young's modulus recovery of YIG specimens was investigated. One YIG specimen, Y015LU, was thermally shocked in water at ΔT = 165 degrees Celsius and then the Young's modulus was measured in vacuum. A time-dependent Young's modulus recovery was observed in a vacuum environment (vacuum pressure was about 10^{-2} to 10^{-3} torr) after each thermal shock (figures 41-43). The observed crack healing behavior in vacuum was not fit as well as that specimen tested in air. However these results indicated that the relative humidity does not affect the crack closure rate. Thus, the possibility that the modulus recovery is caused by the evaporation of the water which drawn into the microcracks by capillary action during thermal shock is relatively small.

In order to have a better understanding of the time-dependent Young's modulus recovery for different treatments in this study, the specimens and their thermal shock treatments and the fitting parameters are summarized (table 3).

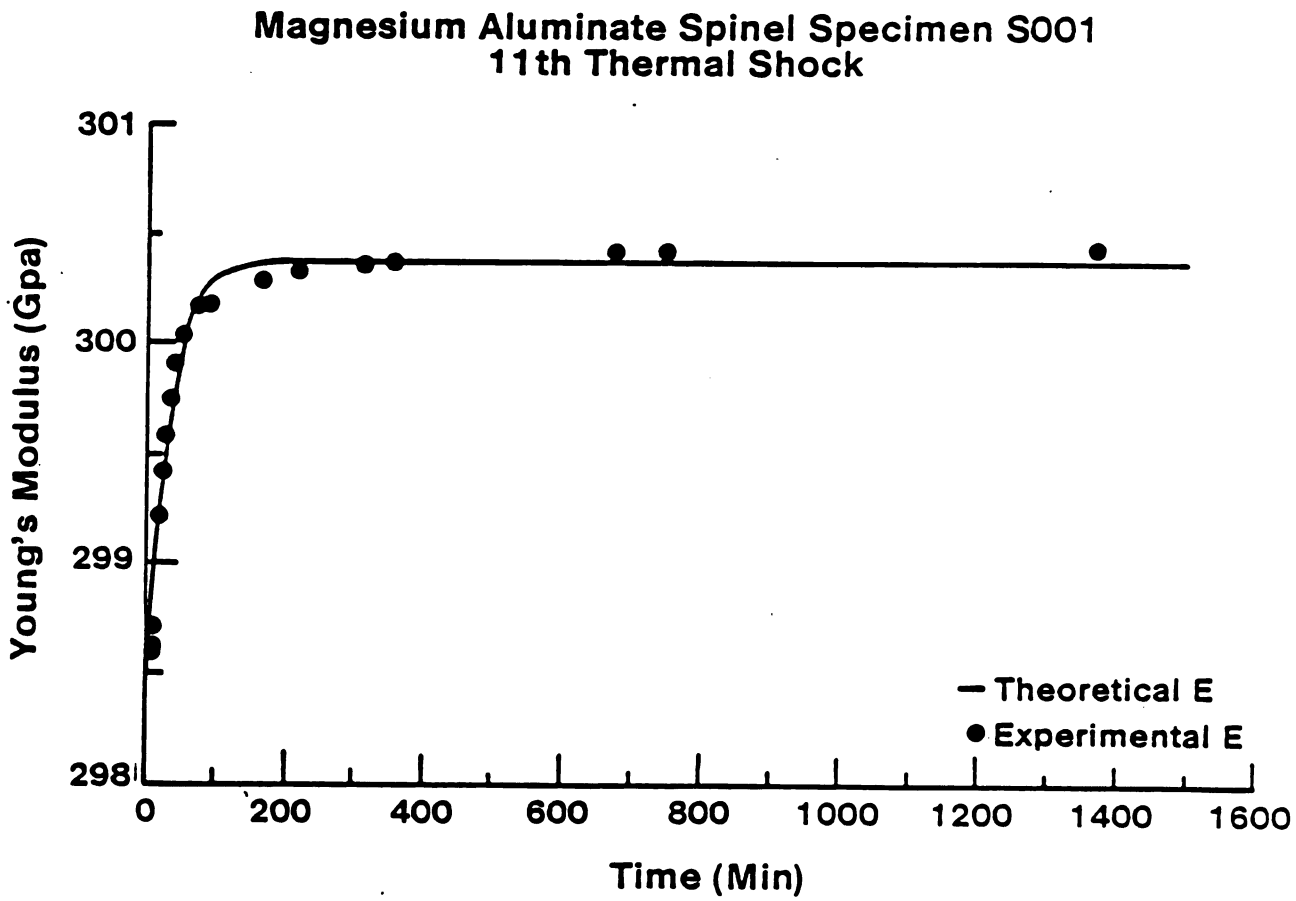

Figure 40. Young's modulus versus time behavior of the eleventh thermal shock of spinel specimen S001 (ΔT = 255 degrees Celsius).

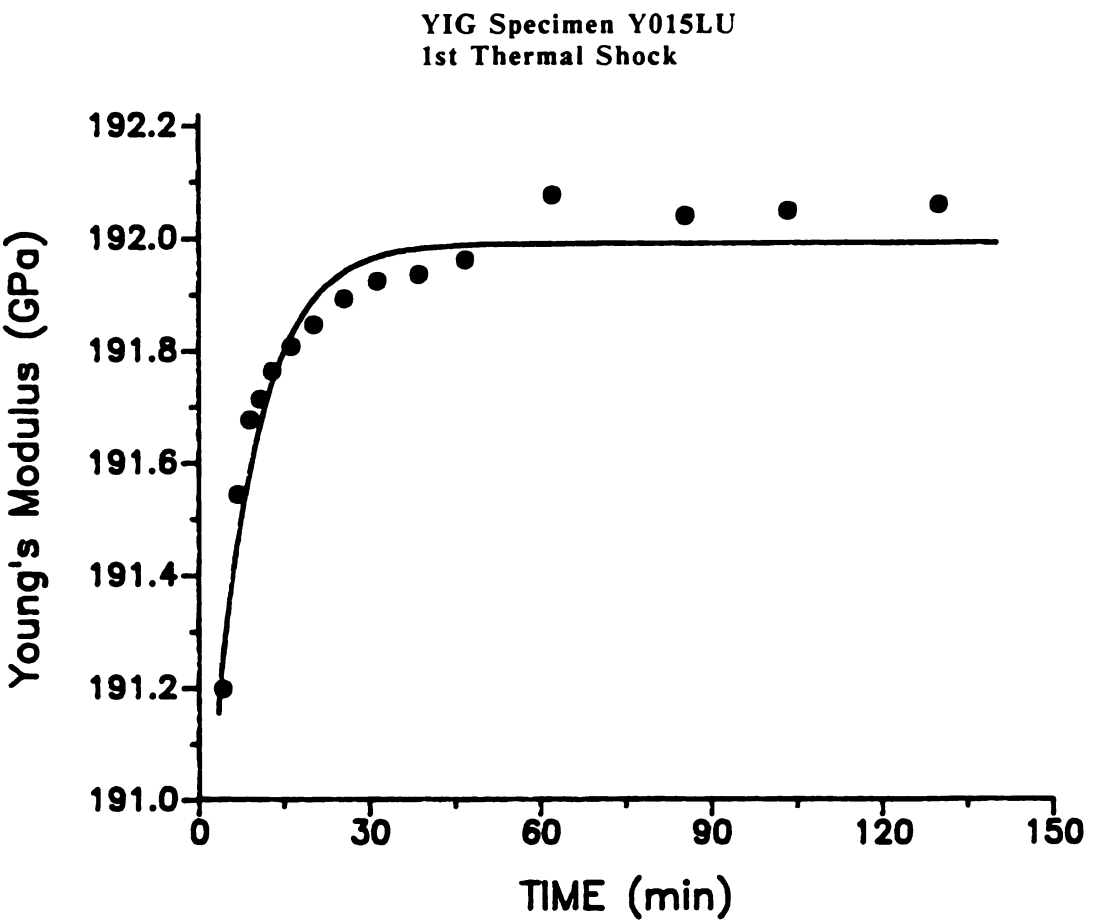

Figure 41. Young's modulus versus time for the first thermal shock cycle of yttrium iron garnet (YIG) specimen Y015LU. The Young's modulus was measured in a vacuum. The solid line indicates the least-squares best fit of the data to equation 14 (ΔT = 165 degrees Celsius).

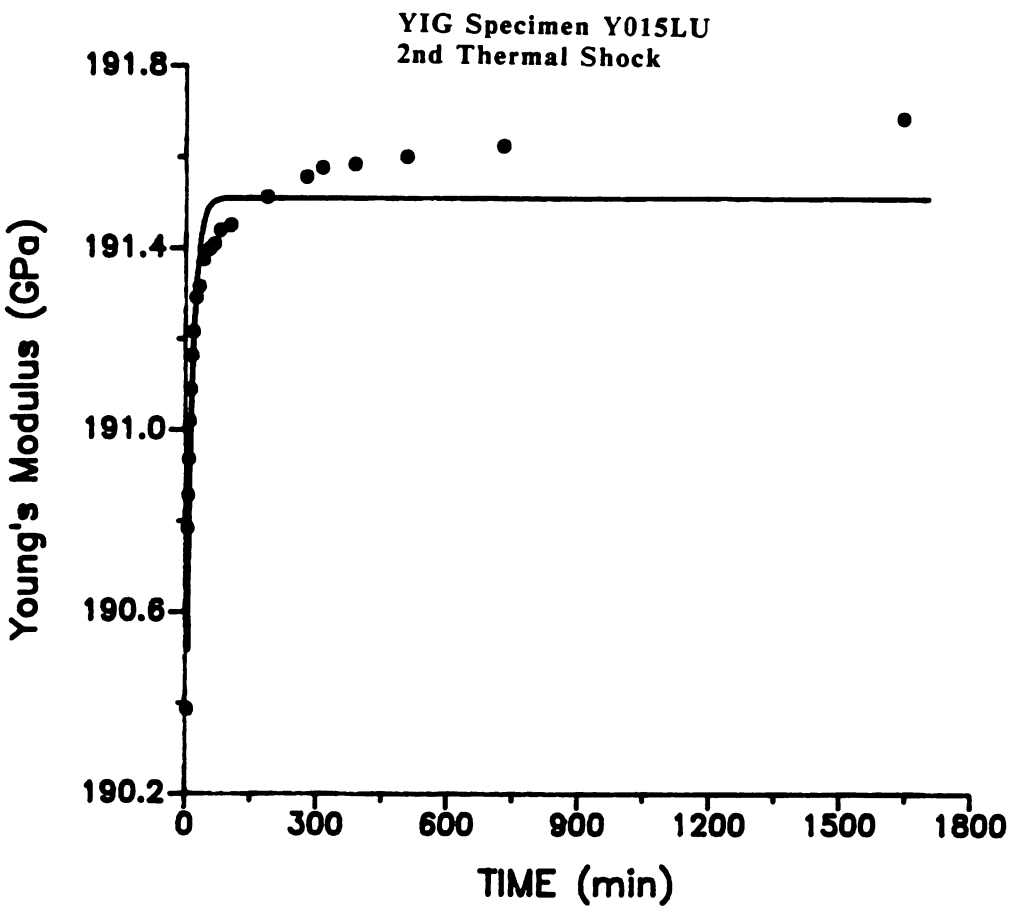

Figure 42. Young's modulus versus time for the second thermal shock cycle of yttrium iron garnet (YIG) specimen Y015LU. The Young's modulus was measured in a vacuum. The solid line indicates the least-squares best fit of the data to equation 14 (ΔT = 165 degrees Celsius).

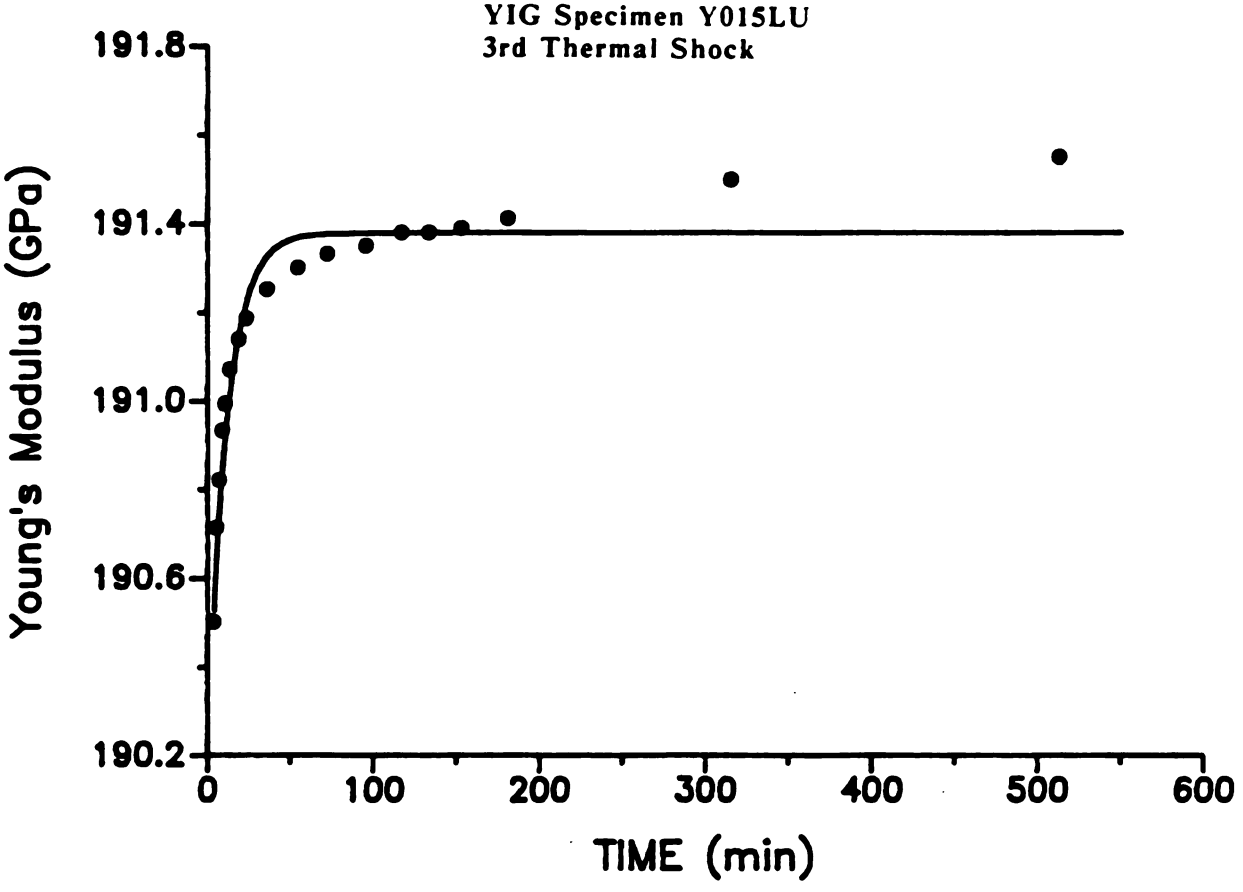

Figure 43. Young's modulus versus time for the third thermal shock cycle of yttrium iron garnet (YIG) specimen Y015LU. The Young's modulus was measured in a vacuum. The solid line indicates the least-squares best fit of the data to equation 14 (ΔT = 165 degrees Celsius).

Table 3. Summary of the number of thermal cycles, temperature difference ΔT, and the fitting parmeters E_i, E_h, and 3B for equation 14 for all the specimens for which modulus recovery was measured in this study.

Material	Specimen Label	No. of Cycles	ΔT (°C)	E_i (Gpa)	E_h (Gpa)	3B (1/sec)	R
YIG	Y005FP	0	0	191.88	-	-	-
		1	165	-	-	-	-
		2	165	190.00	1.2693	0.0483	0.994
(Water quenched)		3	165	189.34	1.8689	0.0621	0.989
		4	165	189.25	1.5868	0.1816	0.994
		5	165	189.53	1.0748	0.1046	0.979
		6	165	189.62	1.2045	0.0562	0.976
YIG	Y006FP	0	0	191.58	-	-	-
(Water quenched)		8	165	185.40	0.9767	0.0161	0.987
YIG	Y007FP	0	0	192.47	-	-	-
		1	165	-	-	-	-
		2	165	189.76	1.1655	0.0344	0.983
		3	165	190.11	0.9268	0.0258	0.996
(Water quenched)		4	165	189.63	1.1328	0.0104	0.981
		5	165	189.27	0.9675	0.0071	0.991
		6	165	189.93	1.2104	0.0030	0.974
		7	165	189.99	0.8959	0.0026	0.954
YIG	Y008FP	0	0	193.07	-	-	-
(Water quenched)		1	165	187.72	0.4676	0.0230	0.986
(macrocrack observed)		2	165	181.06	1.8640	0.1149	0.969

Table 3. (continued)

Material	Specimen Label	No. of Cycles	ΔT (°C)	E_i (Gpa)	E_h (Gpa)	3B (1/sec)	R
YIG	Y009FU	0	0	193.38	-	-	-
(Water quenched)		1	165	187.83	4.0076	0.3114	0.988
YIG	Y010FU	0	0	193.32	-	-	-
		1	165	192,31	0,6803	0.0906	0.962
		2	165	192.58	0.6104	0.0713	0.983
(Water quenched)		3	165	194.48	1.1392	0.0544	0.977
		4	165	191.52	1.1389	0.1047	0.973
		5	165	191.42	1.0990	0.0514	0.981
		6	165	190.94	1.3330	0.0575	0.969
YIG	Y011LU	0	0	193.55	-	-	-
(Water quenched)		1	165	188.78	0.9607	0.1154	0.984
YIG	Y012LU	0	0	192.33	-	-	-
(Water quenched)		1	185	188.67	0.9867	0.0620	0.982
		2	200→Liq N_2	189.37	0.3516	0.0198	0.992
YIG	Y013LU	0	0	194.07	-	-	-
(Water quenched)		1	205	189.55	1.0414	0.0988	0.974
YIG	Y014LU	0	0	193.50	-	-	-
(Water quenched)		1	245	189.92	-	-	0.962

Table 3. (Continued)

Material	Specimen Label	No. of Cycles	ΔT (°C)	E_i (Gpa)	E_h (Gpa)	3B (1/sec)	R
Spinel	S001FU	10	245	299.63	1.1990	0.0326	0.988
(Water quenched)		11	255	297.81	2.5223	0.0428	0.993
Gd-doped G2C		0	0	192.51	-	-	-
YIG		1	265	192.30	-	-	-
		2	265	189.46	2.2675	0.0138	0.987
(Oil quenched)		3	265	183.99	-	-	-
		4	265	183.83	2.9600	0.0138	0.981
		5	265	186.40	1.7300	0.0597	0.994
YIG	Y015LU	0	0	192.22	-	-	-
(Water quenched)		1	165	190.78	1.2200	0.1250	0.969
(Measured in		2	165	190.26	1.2600	0.0795	0.966
vacuum)		3	165	190.29	1.1000	0.0860	0.974

Note 1: The quench medium used in all the thermal shock experiments was water at 35 degrees Celsius except that liquid nitrogen was used at the second thermal shock of Y012LU specimen, and oil was used for all the thermal shock cycles of the Gd-doped G2C specimen.

Note 2: Specimens Y005FP, Y006FP, Y007FP, Y008FP were edge beveled. All the others were unbeveled.

Note 3: The Young's modulus was measured in air except that the Y015LU specimen was measured in a vacuum enviroment.

Note 4: R is the correlation coefficient of the least-squares best fit.

4. CONCLUSIONS

The conclusions of this study can be divided into two major parts: 1) the characterization of thermal fatigue by non-destructive techniques, 2) the time-dependent elastic modulus recovery.

First of all, the thermal fatigue of polycrystalline yttrium iron garnet (YIG) was characterized by non-destructive techniques. After 2500 thermal shock cycles the Young's modulus of a YIG specimen only changed by 0.3 percent relative to of the pre-shocked Young's modulus value. The increase of the internal friction due to 2500 thermal cycles was as high as 300 percent of the pre-shock internal friction value. The internal friction is therefore much more sensitive than the Young's modulus to specimen damage due to thermal fatigue. For YIG specimen annealed prior to the repeated thermal shock test the internal friction change showed three regions. The internal friction gradually increased in the first region, then remained at a plateau for the second region. In the third region the internal friction again increased. In order to obtain reliable internal friction measurements, the suspension position dependence and the suspension angle dependence need to be considered. The changes in internal fraction induced by repeated thermal shock were found to be affected by annealing the specimens prior to initiate the series of thermal shock. These effect are likely related to the release of residual stress during annealing.

Secondly, the studies on time-dependent elastic modulus recovery

indicated that a possible hydrate phase may play the major role in the crack healing (closure) process. The time-dependent crack closure may be associated with the time-dependent adhesive reaction between the hydrate phase and the crack surfaces.

The healing rate of the specimens with unbeveled edges was usually larger than the healing rate of the specimen with beveled edges. The calculated K_I for a specimen with a semicircular corner crack (edge flaw) is larger than the calucated K_I for a specimen with a surface flaw (section 3.4.5). Thus, the edge flaw has lower resistance to crack propagation and can grow more easily. The higher crack healing rate of the edge unbelved specimen may indicate that the edge-flaw-induced cracks are longer than the surface-flaw-induced cracks.

The crack healing rate usually decreased as the specimen experienced more thermal shock cycles. The accumulation of the hydrate phase in cracks may slow modulus recovery. However, the closure of the newly formed cracks may affect the observed healing rate (Appendix D).

The Young's modulus measured in vacuum for water quenched YIG specimen increased as a function of time. For sufficiently long times, the elastic modulus asympoptically approached the pre-shock values (figures 42 and 43). The Young's modulus of the oil quenched YIG specimen at the third cycles shown a initial increase and then a decrease after a period of time. The occurrence of a maximum in the Young's modulus may be caused by the diffusion of the oil molecules reopening the healed cracks. More investigation is needed to fully understand this mechanism.

Appendices

APPENDIX A: DERIVATION OF TIME-DEPENDENT MODULUS

From equation (13) in section 3.4.2 of this study,

$$dE/dj = -E\,[f(\upsilon)] \qquad \text{(A1)}$$

where E is the Young's modulus, υ is Poisson's ratio, and j is the crack damage parameter. From the definition of the damage parameter, j,

$$dj/da = 3Na^2 = 3j/a \qquad \text{(A2)}$$

where a is the crack length. Furthermore, let us define the crack healing (closure) rate as

$$da/dt = -g(a). \qquad \text{(A3)}$$

By the chain rule for derivatives, the time rate of change of Young's modulus, E, may be written as

$$dE/dt = (dE/dj)\,(dj/da)\,(da/dt). \qquad \text{(A4)}$$

Using equations (A1), (A2), and (A3) equation (A4) may be rewritten as

$$dE/dt = 3E_0 [f(\upsilon)]j \{g(a)/a\}. \quad \text{(A5)}$$

But, from equation (13), it is seen that

$$E = -[E_0 f(\upsilon)j] + E_0. \quad \text{(A6)}$$

In order to make further progress, we shall assume a linear crack healing rate, such that

$$-g(a) = -Ba = da/dt \quad \text{(A7)}$$

where B is a non-negative constant. If one considers the time dependence of crack length, a, then equation (A7) corresponds to an exponential time dependence of crack length.

Given the assumption represented by equation (A7), equation (A5) can then be expressed in terms of the following nonhomogeneous, linear, first order differential equation:

$$dE(t)/dt + 3BE(t) = 3BE_0. \quad \text{(A8)}$$

Solving equation (A8) then yields

$$E(t) = E_i + E_h \{1 - \exp(-3Bt)\} \quad \text{(A9)}$$

where E_i is the Young's modulus at time t = 0, which corresponds to

the value of E immediately following the thermal quench. E_h is the increase in Young's modulus from the time t = 0 until the modulus reaches a steady state value. Note that equation (A9) is identical to equation (14), the modulus recovery equation presented in the Results and Discussion section 3.4.

Equation (A3) was a critical assumption in the derivation of equation (14), which agrees very well with the experimentally observed elastic modulus recovery. Equation (A3) describes a crack closure rate that is identical (in its mathematical form) to a first order chemical reaction rate equation. If the crack closure rate were simply proportional to a chemical reaction rate on the crack surfaces, then this crack closure rate could be a consequence of the first-order rate of a chemical reaction on the crack surfaces. The chemical reactions involved in the modulus-recovery of YIG may be analogous to the chemical reactions proposed by Stavrinidis and Holloway [A1] and by Michalske and Fuller [A2] to account for the observed crack healing in a variety of oxide glasses and in a glassy epoxy.

Such crack closure mechanisms should be studied further in order to determine the crack closure kinetics of any chemical reactions that may occur at the crack surfaces.

References of Appendix A

A1. B. Stavrinidis and D. G. Holloway, Phys. Chem. Glasses, 24: 19-25 (1983).

A2. T. A. Michalske and E. R. Fuller, Jr., J. Am. Ceram. Soc., 68: 586-590 (1985).

APPENDIX B: CHARACTERIZATION OF SOME MECHANICAL PROPERTIES OF POLYCRYSTALLINE YTTRIUM IRON GARNET (YIG) BY NON-DESTRUCTIVE TECHNIQUES

Yttrium Iron Garnet ($5Fe_2O_3.3Y_2O_3$, commonly referred to as YIG) is one of a group of ferrimagnetic garnets discovered [B1-B2] in 1956-57. Both the single crystal and polycrystalline forms of YIG can resonate at microwave frequencies when magnetized [B3]. The importance of YIG is that it shows one of the lowest resonance linewidths ever observed in ferrimagnets [B4]. YIG is presently used as an electronic resonator and Faraday rotator, gyrator, and filter in microwave circuitry [B3-B4].

Most of the material properties known for YIG have been determined for the single crystal form. In particular, the mechanical properties of polycrystalline YIG are not well characterized. Non-destructive techniques have been employed in this study to characterize the hardness, fracture toughness, Young's modulus, shear modulus, and Poisson's ratio of polycrystalline YIG.

The elasticity was measured by sonic resonance technique [B5-B9]. The flexural and torsional resonance frequencies of the prismatic specimens were used to calculate the Young's and shear moduli, according to theory developed by Pickett [B7] and Hasselman [B8]. Table B1 lists the mean value and coefficient of variation for the elastic modulus data and Poisson's ratio data for 15 YIG specimens.

Table B1. Mean values and coefficients of variation of Young's modulus, E, shear modulus, G, and Poisson's ratio, υ, for polycrystalline YIG specimens.

Property	Average Value	Coefficient of Variation*	Number of Specimens
1. E	192.61 GPa	1.0 %	15
2. G	75.42 GPa	0.9 %	15
3. υ	0.277	2.4 %	15

* Coefficient of Variation = Standard Deviation/Average Value

Single crystal elasticity data may be used to calculate the expected bounds for the Young's modulus E_0 and the shear modulus G_0 of theoretically dense polycrystalline bodies. Voigt [B10] and Reuss [B11] calculated the effective elastic modulus of a polycrystalline body using the concept that an aggregrate of randomly oriented crystals may be replaced by an equivalent isotropic and homogeneous elastic body. Voigt assumed that when a polycrystalline specimen is subjected to a gross uniform strain, the crystals would be in a state of uniform strain. Reuss assumed that all crystals in a polycrystalline body were in a state of uniform stress. The Voigt and Reuss bounds are considered to be upper and lower bounds of the true elastic constants for polycrystalline bodies. Hashin and Strikman [B12] developed improved bounds for crystals of cubic lattice symmetry by using variational principles which considered the anisotropic and nonhomogeneous conditions in polycrystals. A relatively accurate estimate of the elastic modulus of a polycrystalline body can be obtained from the arithmetic average of Hashin-Strikman bounds [B12] or Voigt-Reuss bounds [B13] using the modului of the corresponding single crystal. Since each of the bounds are calculated from single crystal data, these aggregate bounds may be used to estimate the elastic moduli of polycrystalline specimens in the zero porosity limit.

The Voigt, Reuss, Hashin and Strikman bounds calculated from measurements on single crystal YIG* are listed in Table B2 [B14]. In fact, the Young's modulus, shear modulus and Poisson's ratio of the

---

* Since YIG exhibits a cubic atomic lattice symmetry, the Hashin and Strikman bounds do apply.

Table B2. The Voigt, Reuss, Hashin and Strikman bounds calculated from measurements on single crystal YIG [B14].

	Property/bound	Young's modulus	shear modulus	Poisson's ratio
1.	Voigt	200.6 GPa	77.4 GPa	0.295
2.	Hashin	200.6 GPa	77.4 GPa	0.295
3.	Strikman	200.5 GPa	77.4 GPa	0.295
4.	Reuss	200.6 GPa	77.4 GPa	0.295

four different bounds are almost the same for YIG. The arithmetic means of both the Voigt-Reuss bounds and of the Hashin-Strikman bounds are 200.6 GPa for E_0, the Young's modulus and 77.4 GPa, for G_0, the shear modulus.

The measured elastic constants, E and G, for polycrystalline YIG (Table B1) are slightly lower than the mean of Hashin-Strikman bounds and the Voigt-Reuss bounds calculated from single crystal data [B14]. This reduction in the measured elastic moduli for the polycrystalline YIG specimens presumably is caused, at least in part, by porosity of the YIG specimens (See Figure B1 and B2).

Six frequently used elastic moduli-porosity relationships [B15-B33] are listed in Table B3. The elastic modulus versus porosity data obtained for the 15 polycrystalline YIG specimens included in this study were fit to equation B6(a) and B6(b) via a least-squares best fit procedure. The fitting parameters obtained are listed in Table B4.

For the 15 polycrystalline YIG specimens included in this study, the least-squares best fit of Young's modulus versus porosity data to equation (B6a) is satisfactory with the χ^2 value of 0.018. The shear modulus-porosity fit to equation (B6b) is relatively scattered with a χ^2 value of 0.036.

For zero porosity, Wang's model (equations B6a and B6b) gives E_0 = 197.05 GPa and G_0 = 77.46 GPa (Table B4) as the estimated moduli of nonporous YIG specimen, which agrees within 1.8 percent with the E_0 and G_0 from single crystal data (Table B2). Table B4 summarizes the regression parameters for the modulus-porosity relations listed in

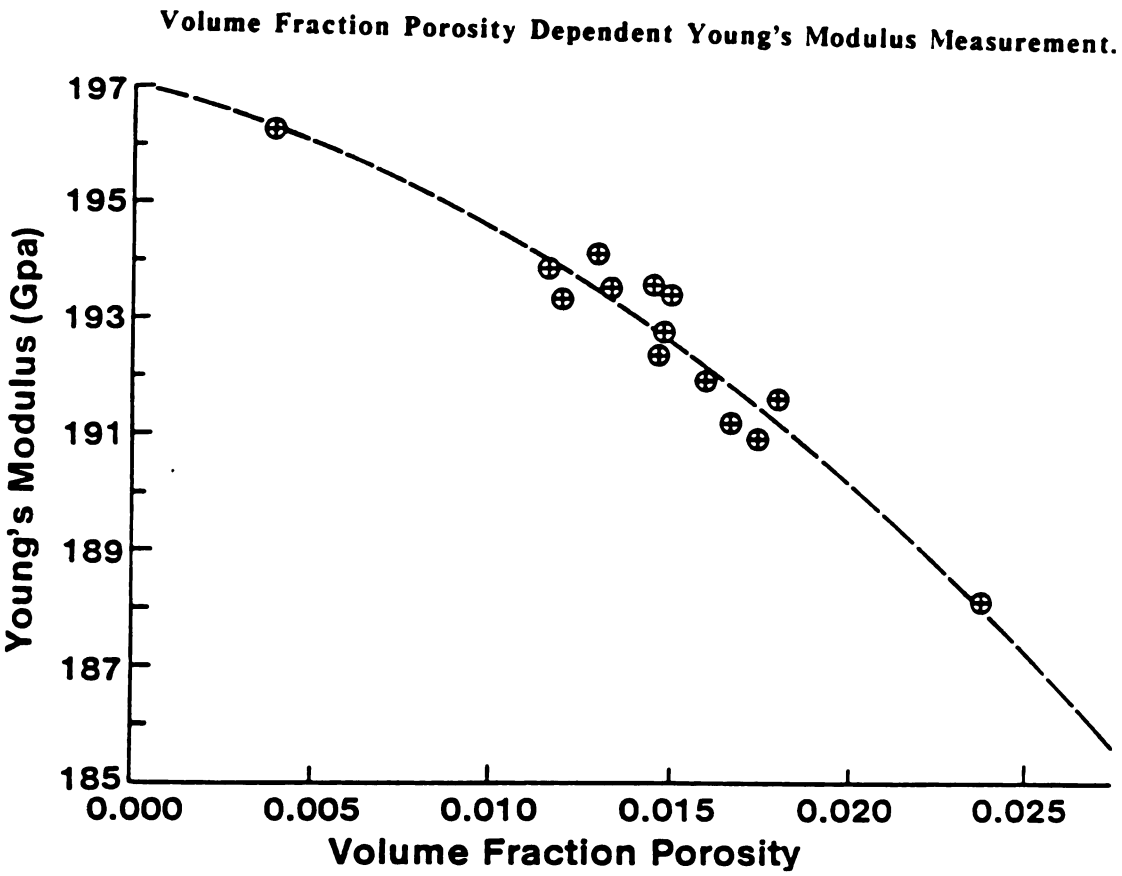

Figure B1. Young's modulus versus volume fraction porosity for 15 YIG specimens. The dotted line represents a least-squares best fit of the data to equation (B6a).

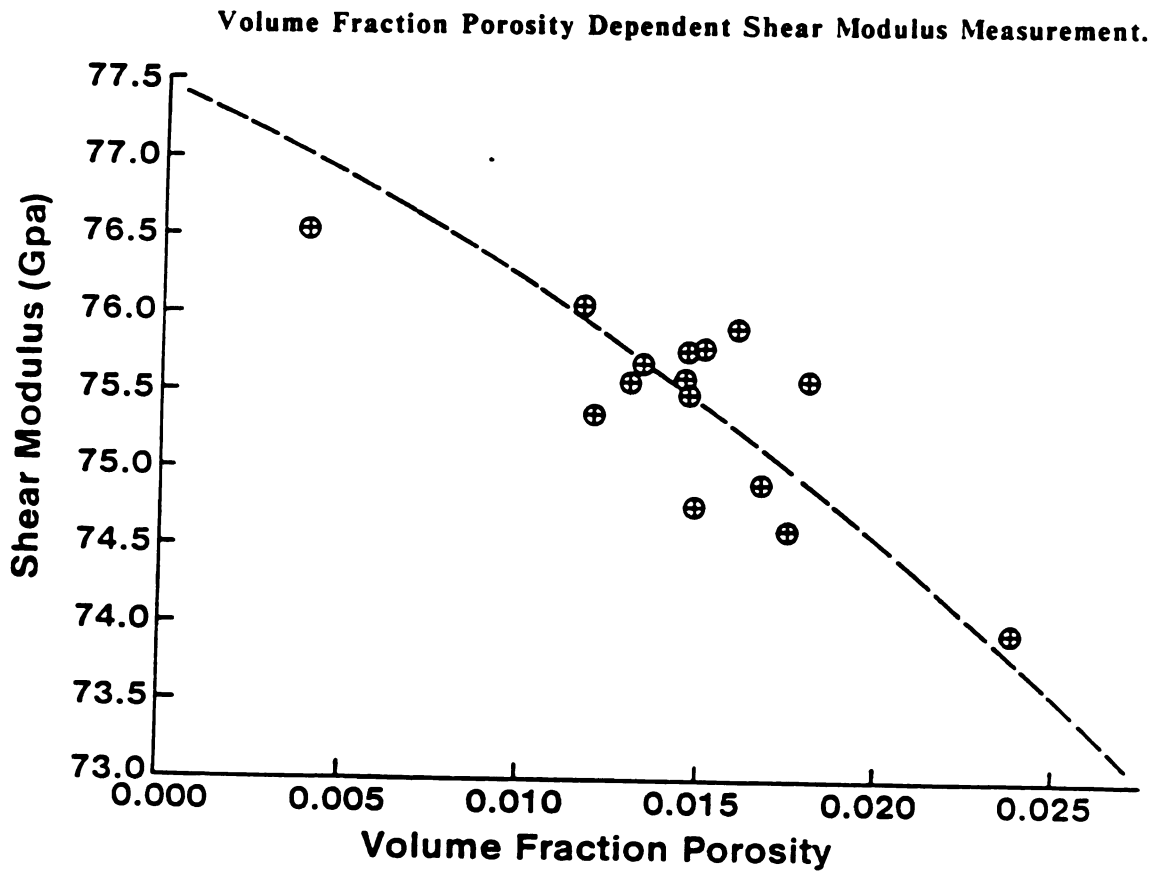

Figure B2. Shear modulus versus volume fraction porosity for 15 YIG specimens. The dotted line represents a least-squares best fit of the data to equation (B6b).

Table B3. Survey of six elastic modulus-porosity relationships in materials studied.

Equation	Materials and porosity ranges		References
B1a $E = E_0 \exp(-xp)$*	ZrO_2	$.05 < p < .20$	B17
	HfO_2	$.04 < p < .24$	B18
	$MgAl_2O_4$	$.05 < p < .25$	B19
B2a $E = E_0(1 - wp)$	Y_2O_3	$.006 < p < .31$	B20
	Dy_2O_3, Er_2O_3	$.03 < p < .22$	B21
	Sc_2O_3, Tm_2O_3	$.02 < p < .24$	B22
	Yb_2O_3	$.058 < p < .271$	B23
	Gd_2O_3	$.023 < p < .367$	B24
B3a $E = E_0(1 - ep + fp^2)$	ThO_2	$.03 < p < .39$	B25
	Al_2O_3	$0 < p < .50$	B26
	Si_3N_4	$0 < p < .44$	B27
B4a $E = E_0[1 + Ap/(1 - (A + 1)p)]$**	B_4C	$0 < p < .15$	B28
B5a $E = E_0(1 - ap)^n$	Gypsum	$.11 < p < .70$	B29
	Si_3N_4 (MgO doped)	$0 < p < .44$	B30
	ThO_2	$.037 < p < .334$	B31
B6a $E = E_0 \exp(-bp - cp^2)$	Al_2O_3	$.05 < p < .32$	B32
	YIG	$.004 < p < .024$	present study

* Equation 1a was proposed by Spriggs [B31].
** Equation 4a was derived by Hasselman [B22] from the theoretical work of Hashin [B33].

Table B4. **Summary of the test data parameters of regression lines for the Young's and shear modulus measured for the YIG specimens.**

Equation	Young's modulus (.004 < p < .024)			Shear Modulus (.004 < p < .024)		
	E_0(Gpa)	Parameters	χ^2	G_0(Gpa)	Parameters	χ^2
B1a $E = E_0 \exp(-xp)$	198.80	x = 2.17	0.027	78.19	y = 2.41	0.045
B1b $G = G_0 \exp(-yp)$						
B2a $E = E_0(1 - wp)$	198.74	w = 2.11	0.027	78.13	v = 2.31	0.044
B2b $G = G_0(1 - vp)$						
B3a $E = E_0(1 - ep + fp^2)$	197.05	e = 0.76	0.018	77.66	e' = 1.62	0.038
B3b $G = G_0(1 - e'p + f'p^2)$		f = -49.65			f' = -19.69	
B4a $E = E_0[1 + Ap/(1 - (A + 1)p)]$	198.79	A = -2.16	0.027	78.21	A' = -2.43	0.045
B4b $G = G_0[1 + A'p/(1 - (A' + 1)p)]$						
B5a $E = E_0(1 - ap)^n$	198.76	a = 1.903	0.027	78.17	a' = 1.0	0.044
B5b $G = G_0(1 - a'p)^{n'}$		n = 1.11			n' = 2.385	
B6a $E = E_0 \exp(-bp - cp^2)$	197.05	b = 0.728	0.018	77.46	b' = 1.31	0.036
B6b $G = G_0 \exp(-b'p - c'p^2)$		c = 52.87			c' = 31.01	

Table B3.

It should be noted that the least-squares procedure can determine whether or not a model adequately fits, in this case, the elastic modulus versus porosity data for the polycrystalline YIG in the present study. Other physical models not included in this study may be equally good or even superior over a given range of porosity. The present set of data is quite limited, in that the volume fraction porosity ranges from only about 0.004 to 0.024, so that extrapolations far outside this porosity range may be questionable. For example, in Table B4, equations (B3a) and (B3b) fit the data nearly as well as Wang's equations (B6a) and (B6b). However, the extrapolation of moduli to zero porosity in equations (B3a) and (B3b) occurs at volume fraction porosity less than 18 percent which is thought to be unphysical*. Thus equations (B3a) and (B3b), applied to the present YIG data, demonstrate the danger of extrapolating regression equations far outside the data range over which the regression was performed.

The hardness and fracture toughness of the polycrystalline YIG specimens were determined by the microhardness indentation method. The crack length and indentation diagonal dimensions were used to determine the hardness, H, and fracture toughness, K_{IC}, values.

The hardness was calculated by dividing the load by the contact area using [B34]

$$H = 0.47\ P\ /\ a^2 \qquad \text{(B7)}$$

---

* Modulus-porosity models typically do not predict a vanishingly small modulus until a volume fraction porosity of roughly 0.40 is reached.

where P is the peak indentation load and 2a is the pyramid diagonal of the indent impression.

Vickers indentation loads ranging from 0.5 N to 9.8 N were used on the YIG specimens in this study. Serious chipping occurred for loads larger than 9.8 N. A loading time of 10 seconds was employed for all indentations, with an indentor loading speed of 70 microns per second. The loading speed and load time were selected in order to minimize chipping of the indented specimens. The indent diagonals and the radial crack lengths were measured with a calibrated optical microscope equipped with a digital length read out [Semimacro Hardness Tester Series No.5987, Buehler Ltd., Lake Bluff, IL].

K_{IC} was calculated from the expression of Evans and Charles [B35] and modified by Lawn et al. [B36] as follows

$$K_{IC} = A\ (E/H)^{1/2}(P/C^{3/2}) \qquad (B8)$$

where P is the peak indentation load, A is a calibration constant of 0.017 ± 0.001 [B34], and C is the radial crack length as measured from the center of the indentation.

The first step in the fracture toughness testing was to determine whether a function of crack length, C, versus applied normal load, P, predicted by equation (B8) was valid for the YIG specimens included in this study and for the particular range of loads actually employed in the experimentation. A plot of log C versus log P gave a slope of 1.38 ± 0.03, with correlation coefficient 0.999 (Figure B3).

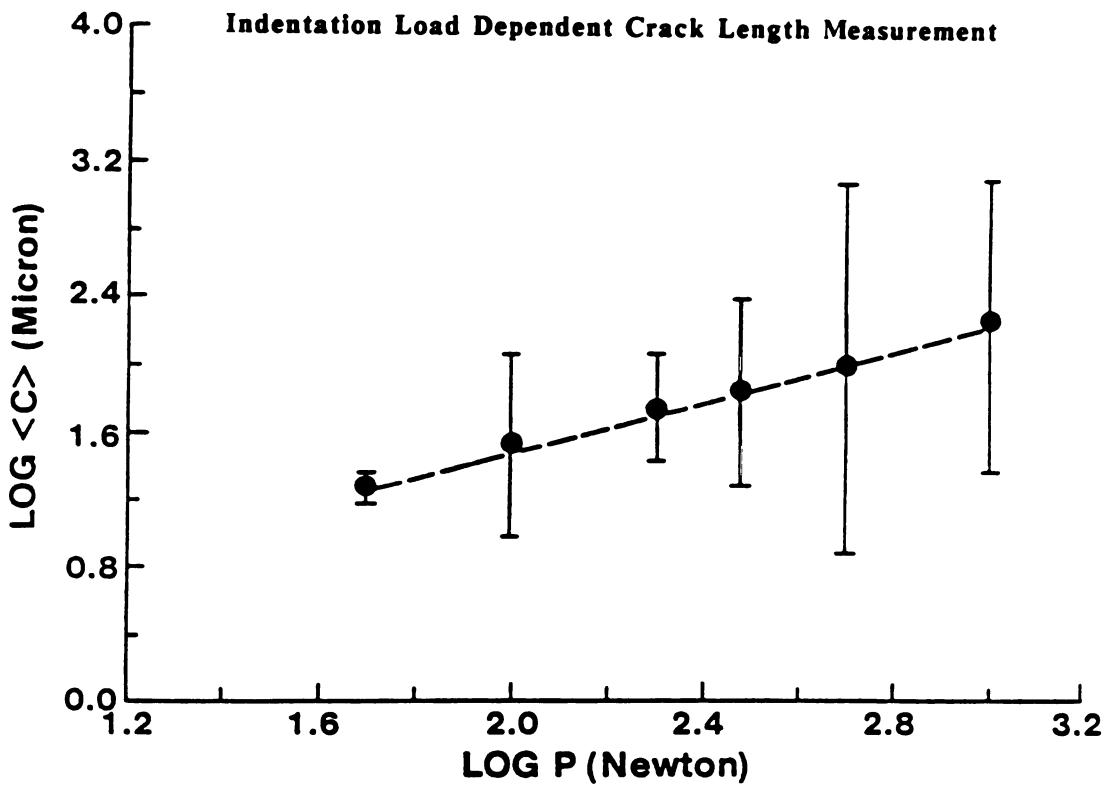

Figure B3. A log-log plot of the mean crack length <C> versus the load P for loads ranging from 0.5 N to 9.8 N. The dotted line represents a least-squares best fit of the data for six indentation load levels. The error bars represent the standard deviation of the measured crack lengths at a given load.

This slope is in reasonable agreement with the slope of 1.5 predicted from equation (B8).

Fifteen indentations were made to obtain a mean hardness value of 2.04 Gpa and a fracture toughness of 0.74 Mpa $m^{1/2}$ (Table B5). The mean values of hardness and fracture toughness given in Table B5 were calculated for a maximum normal load, P, of 9.8 N, which gave the lowest coefficients of variation among the loads applied in this study. The mean values of hardness and toughness for the other five indentation load levels were within ± 3 and ± 9 percent, respectively, of the hardness and toughness values listed in Table B5.

Table B5. Mean values and coefficients of variation of hardness, H, and fracture toughness, K_{IC}, for polycrystalline YIG specimens.

Property	Average Value	Coefficient of Variation*	Indentation Numbers
1. H**	2.04 GPa	5.4 %	15
2. K_{IC}**	0.74 MPa $m^{1/2}$	11.9 %	15

* Coefficient of Variation = Standard Deviation/Average Value
** Load = 9.8 Newton
Load Time = 10 Seconds
Loading Speed = 70 Microns per Second

References of Appendix B

B1. F. Bertaut and F. Forrat, C. R. Acad. Sci., (Paris) 242: 382 (1956).

B2. S. Geller and M. A. Gilleo, Acta Crystal., 10: 239 (1957).

B3. J. Helszajn, pp. 1-28, in "YIG Resonators and Filters", edited by J. Helszajn, John Wiley & Sons Ltd., New York (1985).

B4. R. F. Belt, p. 216, in "YIG Resonators and Filters", edited by J. Helszajn, John Wiley & Sons Ltd., New York (1985).

B5. F. Forster, Z. Metall., 29: 109 (1937).

B6. S. Spinner and W. E. Tefft, ASTM Proc., 61: 1221 (1961).

B7. G. Pickett, ibid, 45: 846 (1945).

B8. D. P. H. Hasselman, in "Tables for the Computation of Shear Modulus and Young's Modulus of Rectangular Prisms", Carborundum Co., Niagara Falls, NY (1961).

B9. E. Schreiber, O. L. Anderson, and N. Soga, Chapter 4, in "Elastic Constants and Their Measurement", McGraw-Hill, New York (1974).

B10. W. Voigt, Lehrbuch der Kristallphysik, 962 (1928).

B11. A. Reuss, Z. angew. Math. Mech., 9: 55 (1929).

B12. Z. Hashin and S. Strikman, J. Mech. Phys. Solids, 10: 335-52 (1926).

B13. O. L. Anderson, J. Phys. Chem. Solids, 24: 909-17 (1963).

B14. G. Simmons and H. Wang, p. 188, in "Single Crystal Elastic Constants and Calculated Aggregate Properties", The M. I. T. Press, MA (1971).

B15. C. F. Smith and W. B. Crandall, J. Am. Ceram. Soc., 47 [12]: 624-27 (1964).

B16. S. L. Dole, O. Hunter, Jr., and C. J. Wooge, ibid., 60 [11-12]: 488-490 (1977).

B17. D. F. Porter, J. S. Reed, and D. Lewis III, ibid., 60 [7-8]: 345-49 (1977).

B18. W. R. Manning and O. Hunter, Jr., ibid., 51 [9]: 537-38 (1968).

B19. W. R. Manning, M. O. Marlowe, and D. R. Wilder, ibid., 49 [4]: 227-28 (1966).

B20. S. L. Dole, O. Hunter, Jr., and F. W. Calderwood, ibid., 60 [3-4]: 167-68 (1977).

B21. B. R. Powell, Jr., O. Hunter, Jr., and W. R. Manning, ibid., 54 [10]: 488-90 (1971).

B22. J. A. Haglund and O. Hunter, Jr., ibid., 56 [6]: 327-30 (1973).

B23. S. Spinner, F. P. Knudsen, and L. Stone, J. Res. Natn. Bur. Std., 67C: 39 (1963).

B24. R. L. Coble and W. D. Kingery, J. Am. Ceram. Soc., 39 [11]: 377-85 (1956).

B25. G. De Portu and P. Vincenzini, p. 265, XIII Siliconf. Vol. 1 Budapest, Hungary (1981).

B26. G. W. Hollenberg and G. Walther, J. Am. Ceram. Soc., 63 [11-12]: 610-13 (1980).

B27. K. K. Phani, Am. Ceram. Soc. Bull., 65 [12]: 1584-86 (1986).

B28. K. K. Phani and S. K. Niyogi, J. Mat. Sci. Lett., 6: 511-15 (1987).

B29. K. K. Phani, J. Mater. Sci. Lett., 5: 747-50 (1986).

B30. J. C. Wang, J. Mat. Sci., 19: 801-814 (1984).

B31. R. M. Spriggs, J. Am. Ceram. Soc., 44 [12]: 628-29 (1961).

B32. D. P. H. Hasselman, J. Am. Ceram. Soc., 45 [9]: 452-53 (1962).

B33. Z. Hashin, J. Appl. Mech., 29: 143 (1962).

B34. M. C. Shaw, pp. 1-15, in "Fundamental Basis of the Hardness Test", Science of Hardness Testing and Its Research Application, A.S.M., Metals Park, OH (1973).

B35. A. G. Evans and E. A. Charles, J. Am. Ceram. Soc., 59 [7-8]: 371-72 (1976).

B36. B. R. Lawn, A. G. Evans, and D. B. Marshall, ibid., 63 [9-10]: 574-81 (1980).

APPENDIX C: DERIVATION OF THE UNCERTAINTY OF YOUNG'S MODULUS MEASUREMENT

For sonic resonance measurements, the Young's modulus can be expressed as [C1]

$$E = A\rho f_r^2 \tag{C1}$$

where A = shape factor, depending on the dimensions and geometry of the specimen.

ρ = density

f_r = flexural resonant frequency

If the Young's modulus, E_1, of a specimen is calculated as

$$E_1 = A_1\rho_1 f_r^2 \tag{C2}$$

then for a given specimen at a fixed temperature and suspension position, the uncertainty of the Young's modulus measurement is a function of the uncertainty of the flexural resonant frequency measurement, Δf_r. For the same specimen

$$\begin{aligned} E_1' &= A_1\rho_1[f_r \pm \Delta f_r]^2 \\ &= A_1\rho_1 f_r^2 [1 \pm \Delta f_r/f_r]^2 \end{aligned} \tag{C3}$$

If $\Delta f_r \ll f_r$, $(\Delta f_r/f_r) \approx 0$, equation (C3) can be simplified as

$$E_1' = A_1 \rho_1 f_r^2 [1 \pm 2 (\Delta f_r/f_r)] \quad (C4)$$

The uncertainty of Young's modulus measurement is then

$$\Delta E = E_1' - E_1 = 2 (\Delta f_r/f_r) E_1 \quad (C5)$$

For example, the pre-shocked resonant frequency of the specimen Y015LU is 2498.50 Hz, which corresponds to Young's modulus of 192.22 Gpa. If the uncertainty of the flexural resonant frequency measurement is ± 0.5 Hz, the uncertainty of the Young's modulus measurement based on equation (C5) is thus $2 \times (0.5/2498.5) \times 192.22$ Gpa, which is about $(4 \times 10^{-4}) \times 192.22$ Gpa or 0.08 Gpa.

Reference for Appendix C

C1. S. Spinner and W. E. Tefft, "A Method for Determining Mechanical Resonance Frequency and for Calculating Elastic Moduli from These Frequencies", A.S.T.M. Proc., 61: 1221 (1961)

APPENDIX D: DERIVATION OF THE HEALING RATE CONTRIBUTED FROM THE NEWLY FORMED CRACKS AND THE OLD CRACKS.

The derivation of time-dependent modulus recovery in Appendix A treated all the theraml shock induced cracks as a single population with a mean crack radius. However, the healing rate of the newly formed cracks is assumed to be greater than the healing rate of the old cracks (section 3.4.5). In order to obtain the observed healing rate contributed from both new cracks and old cracks, the crack population, the mean crack length and healing constant of each kind were defined as

property	new cracks	old cracks*	total cracks
population	N_1	N_2	N
crack length	a_1	a_2	a
healing constant	B_1	B_2	B
damage parameter	$j_1 = N_1 a_1^3$	$j_2 = N_2 a_2^3$	j

* For simplicity, all the old cracks induced by prior thermal shock cycles were treated in one population.

According to equation (13)

$$E = E_0 (1 - f(\nu)Na^3) \tag{D1}$$

where N is the total number density of cracks of mean radius a, $f(\nu)$ is a function of Poisson's ratio. Based on the above definition, N and a can be expressed as

$$N = (N_1 + N_2) \tag{D2}$$

$$a = \frac{a_1N_1 + a_2N_2}{N_1 + N_2} = \frac{a_1N_1 + a_2N_2}{N} \tag{D3}$$

Therefore, equation (13) can be rewritten as

$$E = E_0 \{1 - f(\nu)(N_1 + N_2)[(a_1N_1 + a_2N_2)/(N_1 + N_2)]^3\} \tag{D4}$$

The damage parameter, j, therefore can be defined as

$$j = (N_1 + N_2)[(a_1N_1 + a_2N_2)/(N_1 + N_2)]^3. \tag{D5}$$

The first derivative of E to j is

$$dE/dj = -E_0 f(\nu). \tag{D6}$$

shock cycles were treated in one population.

Apply equations (D2) and (D3) to equation (A2) in Appendix A, and obtain

$$dj/da = 3\,Na^2 = 3\,[(a_1N_1 + a_2N_2)]^2/(N_1 + N_2) \tag{D7}$$

Assume the linear healing rate still holds for both the crack closure of the newely formed cracks and the old cracks. Then, observed healing rate yields

$$\begin{aligned} da/dt &= (da/da_1)(da_1/dt) + (da/da_2)(da_2/dt) \\ &= (-N_1/N)(da_1/dt) + (-N_2/N)(da_2/dt) \\ &= (-N_1/N)(B_1a_1) + (-N_2/N)(B_2a_2) \end{aligned} \tag{D8}$$

By the chain rule for derivatives, the rate of change of Young's modulus dE/dt may be expressed as

$$\begin{aligned} dE/dt &= (dE/dj)(dj/da)(da/dt) \\ &= 3Ef(\nu)\cdot(a_1N_1 + a_2N_2)^2/N^2\cdot(N_1B_1a_1 + N_2B_2a_2) \end{aligned} \tag{D9}$$

On combining with euqation (D4), equation (D9) can be written as

$$dE/dt + 3E(t)(N_1B_1a_1 + N_2B_2a_2)/Na = 3E_0(N_1B_1a_1 + N_2B_2a_2)/Na \tag{D10}$$

The time dependent-modulus recovery resulted from both the crack closure of the new cracks and the old cracks can be obtained by solving equation (D10), and yields a non-homogeneous first order

differential equation

$$E(t) = E_i + E_h \{1 - \exp [-3(N_1B_1a_1 + N_2B_2a_2)t/Na]\} \quad (D11)$$

Where $3(N_1B_1a_1 + N_2B_2a_2)/Na$ is the observed healing rate. The author will like to give an example to show how, based on equation (D10), the healing rate of the new cracks affects the observed healing. The Young's modulus recovery for the old cracks only is

$$E(t) = E_i + E_h [1 - \exp (-3B_2t)]. \quad (D12)$$

On the other hand, if some new cracks are formed and affect the observed healing rate, let us arbitrary chose $N_1 = 0.2N$, $N_2 = 0.8N$, $B_1 = 3B_2$, $a_1 = 2a_2$, the modulus recovery based on equation (D11) will be

$$E(t) = E_i + E_h [1 - \exp (-3 \times 1.6B_2t)] \quad (D13)$$

Comparing equations (D12) and (D13), one finds that the observed healing rate increases significantly due to the rapid crack closure rate of some small population of newly formed cracks. Figure 34 empirically demonstrats this relationship.

List of References

References

1. B. A. Boley and J. H. Weiner, "Theory of Thermal Stress", John Wiley and Sons, Ins., New York (1960).

2. D. P. H. Hasselman, J. Am. Ceram. Soc., 52: 600 (1969).

3. D. P. H. Hasselman, Int. J. Fract. Mech., 7: 157 (1971).

4. T. K. Gupta, J. Am. Ceram. Soc., 55: 249 (1972).

5. J. P. Singh, J. R. Thomas, and D. P. H. Hasselman, ibid., 63: 140 (1980).

6. P. F. Becher, ibid., 64: 378 (1981).

7. M. V. Swain, pp. 355-69, in "Fracture Mechanics of Ceramics", Vol. 6, edited by R. C Bradt, A. G. Evans, D. P. H. Hasselman, and F. F. Lange, Plenum Press, New York (1983).

8. IBM Packaging Technology, IBM Journal of Research and Development, Vol 26, No.3 (1982).

9. C. A. Andersson, pp. 497-509, in "Fracture Mechanics of Ceramics", Vol 6, edited by R. C. Bradt, A. G. Evans, D. P. H. Hasselman, and F. F. Lange, Plenum Press, New York (1983).

10. K. Kokini, Am. Ceram. Soc. Bull., 65: 1493-97 (1986).

11. K. Kokini, R. W. Perkins, and C. Libove, pp. 413-30, in "Thermal Stresses in Severe Enviroments", edited by D. P. H. Hasselman and R. A. Heller, Plenum Press. New York (1980).

12. C. S. Morgan, A. J. Moorhead, and R. J. Lang, Am. Ceram. Soc. Bull., 61 [9]: 974-76 (1982).

13. W. D. Kingery, J. Am. Ceram. Soc., 38: 3-15. (1955).

14. W. D. Kingery, H. K. Bowen and D. R. Uhlmann, pp. 823-24, in "Introduction to Ceramics", 2nd ed. John Wiley & Sons, New York (1976).

15. F. J. P. Clark, H. G. Tattersall, and G. Tappin, Proc. Brit. Ceram. Soc., 6: 163-72 (1966).

16. W. R. Buessen, J. Am. Ceram. Soc., 38: 15-17 (1955).

17. C. C. Seaton and S. K. Dutta, ibid., 57 [5]: 228-29 (1974).

18. E. O. Hall, Proc. Phys. Soc. London, 643: 747 (1951).

19. N. J. Petch, J. Iron Steel Inst. London, 173: 25 (1953).

20. D. Goeuriot-Launay, G. Brayet, and F. Thevenot, J. Mat. Sci. Lett., 5: 940-42 (1986).

21. C. E. Semler, and T. H. Hawisher, Bull. Am. Ceram. Soc., 59 [7]: 732-38 (1980).

22. K. Matsushita, S. Kuratani, T. Okamoto, and M. Shimada, J. Mat. Sci. Lett., 3: 345-48 (1984).

23. J. A. Coppola, and R. C. Bradt, J. Am. Ceram. Soc., 56 [4]: 214-217 (1973).

24. J. R. G. Evans, R. Stevens, and S. R. Tan, J. Mat. Sci., 19: 4068-4076 (1984).

25. J. R. G. Evans, R. Stevens, and S. R. Tan, ibid., 19: 3692-3701 (1984).

26. C. J. Fairbanks, H. L. Lee, and D. P. H. Hasselman, J. Am. Ceram. Soc., 67: C236-C237 (1984).

27. G. R. Eusner, and W. S. Debenham, Bull. Am. Ceram. Soc., 31 [12]: 489 (1952).

28. ASTM Designation, C-38-49, ASTM Comm. C-8 (1952).

29. J. H. McKee and A. M. Adams, Trans. Brit. Ceram. Soc., 49: 386-407 (1950).

30. J. P. Singh, D. W. Diercks, and R. B. Poeppel, Am. Ceram. Soc. Bull., 64: 1373-1377 (1985).

31. E. D. Case, Personal Communication, Michigan State University, East Lansing, MI (1987).

32. D. Lewis III, pp. 489-496, in "Fracture Mechanics of Ceramics," Vol 6, edited by R. C. Bradt, A. G. Evans, D. P. H. Hasselman, and F. F. Lange, Plenum Press, New York (1983).

33. B. K. Sarkar and T. G. J. Glinn, Trans. Brit. Ceram. Soc,. 69: 1285-1287 (1970).

34. K. T. Faber, M. D. Huang, and A. G. Evans, J. Am. Ceram. Soc., 64: 296-301 (1981).

35. J. P. Singh, K. Niihara, and D. P. H. Hasselman, J. Mat. Sci., 16: 2789-2797 (1981).

36. C. S. Lee, Master Thesis, The New Mexico Technology, New Mexico, (1987).

37. A. G. Evans, and R. L. Jones, J. Am. Ceram. Soc., 61: 156 (1978).

38. H. Hencke, J. R. Thomas, JR., and D. P. H. Hasselman, ibid., 67[6]: 393-98 (1984).

39. M. Ashizuka, T. E. Easler, and R. C. Bradt, ibid., 66[8]: 542-50 (1986).

40. M. A. Gilleo and S. Geller, Phys. Rev., 110: 73 (1958).

41. R. L. Fullman, Trans. AIME, 197[3]: 447-452 (1953).

42. F. Forster, Z. Metall., 29: 109 (1937).

43. S. Spinner and W. E. Tefft, A.S.T.M. Proc., 61: 1221 (1961).

44. G. Pickett, ibid, 45: 846 (1945).

45. D. P. H. Hasselman, "Tables for the Computation of Shear Modulus and Young's Modulus of Rectangular Prisms", Carborundum Co., Niagara Falls, New York (1961).

46. E. Schreiber, O. L. Anderson, and N. Soga, Elastic Constants and Their Measurement, McGraw-Hill, New York (1974).

47. J. B. Wachtman, Jr. and W. E. Tefft, Rev. Sci. Instr., 29: 517-520 (1958).

48. S. L. Dole, O. Hunter, F. W. Calderwood, and D. J. Bray, J. Amer. Ceram. Soc., 61: 486-472 (1978).

49. C. J. Malarkey, "Effects of Microstructure on the Elastic Properties of Selected Ta_2O_5-Eu_2O_3 Compositions", M. S. Thesis, Iowa State University, Ames, IA (1977).

50. R. W. Dickson and J. B. Wachman Jr., "Polycrystalline Alumina Elasticity Standard", Standard Referance Material 718, National Bureau of Standard, Washington, D. C., (1972).

51. Annual Book of ASTM Standards, 14 [1]: E230 (1987).

52. C. Zener, p 61 in "Elasticity and Anelasticity of Metals", University of Chicago Press, IL. (1948).

53. L. Rayleigh, pp. 253-83, in "The Theory of Sound", Vol. 1, Dover Publication, New York (1976).

54. B. Budiansky and R. J. O'Connell, Int. J. Solids Struct., 12: 81 (1976).

55. R. L. Salganik, Mech. Solids, 8: 135 (1973).

56. W. J. Lee, Master Thesis, Michigan State University, East Lansing, MI (1988).

57. S. L. Dole, M. S. Thesis, Iowa State University, Ames, IA (1977).

58. M. O. Marlowe, pp.63-70, M. S. Thesis, Iowa state University, Ames, IA (1963).

59. S. L. Dole, O. Hunter, Jr., and C. J. Wooge, J. Am. Ceram. Soc., 60 [11-12]: 488-90 (1977).

60. D. B. Marshall and B. R. Lawn, J. Am. Ceramic Soc., 61 [1-2]: 21-27 (1978).

61. J. W. Nielsen and E. F. Dearborn, Phys. Chem. Solids, 5[3]: 203 (1958).

62. R. W. Davidge, J. R. McLaren, and I. Titchell, pp. 495-506, in "Fracture Mechanics of Ceramics", Vol. 5, edited by R. C. Bradt, A. G. Evans, D. P. H. Hasselman, and F. F. Lange, Plenum Press, New York (1983).

63. J. J. Cleveland and R. C. Bradt, J. Amer. Ceram. Soc., 61: 478-481 (1978).

64. E. D. Case, J. R. Smyth, and O. Hunter, Jr., pp. 507-530, in "Fracture Mechanics of Ceramics", Vol. 5, edited by R. C. Bradt, A. G. Evans, D. P. H. Hasselman, and F. F. Lange, Plenum Press, New York (1983).

65. R. R. Suchomel and O. Hunter, Jr., J. Amer. Ceram. Soc., 56: 149 (1976).

66. E. D. Case, J. R. Smyth, and O. Hunter, Jr., J. Nucl. Mater., 102: 135 (1981).

67. E. D. Case, Mater. Sci. Eng., 51: 175 (1981).

68. J. A. Kuszyk and R. C. Bradt, J. Amer. Ceram. Soc., 56: 420 (1973).

69. W. J. Buykx, ibid, 62: 326 (1979).

70. E. D. Case, J. Mater. Sci., 19: 3702 (1984).

71. A. Hoenig, Int. J. Solids Struct., 15: 137-154 (1979).

72. A. Hoenig, "Elastic Moduli of Non-Randomly Microcracked Bodies", Ph.D. Thesis, Harvard University, Cambridge, MA (1979).

73. D. L. Anderson, B. Minster, and D. Cole, J. Geophys. Res., 79: 4011-4015 (1974).

74. A. I. Bailey, J. Appl. Phys., 32: 1407-1412 (1961).

75. A. J. Forty and C. T. Forwood, Trans. Brit. Ceram. Soc., 62: 715-724 (1963).

76. M. P. Shaskol'skaya, Wang Yen-Wen, and Ku Shu-Cao, Soviet Phys. Crystall., 6: 483-490 (1962).

77. S. M. Wiederhorn and P. R. Townsend, J. Amer. Ceram. Soc., 53: 486-489 (1970).

78. V. M. Finkel and I. A. Kutkin, Soviet Phys. - Doklady, 7: 231-232 (1962).

79. D. Haneman, J. T. P. Grant, and R. U. Khokhar, Sur. Sci., 13: 119-129 (1969).

80. J. T. P. Grant and D. Haneman, Sur. Sci., 15: 117-136 (1969).

81. B. Stavrinidis and D. G. Holloway, Phys. Chem. Glasses, 24: 19-25 (1983).

82. T. A. Michalske and E. R. Fuller, Jr., J. Amer. Ceram. Soc., 68: 586-590 (1985).

83. S. Sakaguchi and S. Takahashi, pp. 142-150, in "Fine Ceramics", ed. by S. Saito, Elsevier Applied Science Publishers Ltd,. Essex, England (1985).

84. S. Hirance, p.21, in "Fine Ceramics", ed. by S. Saito, Elsevier Applied Science Publishers Ltd,. Essex, England (1985).

85. T. A. Michalske and B. C. Bunker, Scientific American, 257 [6]: 122-129 (1987).

86. W. D. Kingery, H. K. Bowen and D.R. Uhlmann, p. 774, in "Introduction to Ceramics," 2nd ed. Hohn Wiley & Sons, New York (1976).

87. C. C. Chiu, Personal Communication, Michigan State University, East Lansing, MI (1988).

88. D. B. Marshall and B. R. Lawn, pp. 221-242. in "Fracture in Ceramic Materials", ed. by A. G. Evans, Noyes Publications, NJ (1984).

89. C. H. Hsueh and A. G. Evans, pp. 215-255, in "Ceramic Containing Systems", ed. by A. G. Evans, Noyes Publications, NJ (1986).

90. R. W. Hertzberg, pp. 282-285, in "Deformation and Fracture Mechanics of Engineering Materials", 2nd ed. John Wiley & Sons, New York (1983).